
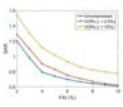


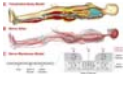

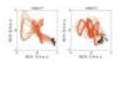



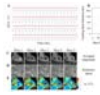
Poster: Interventional/Safety/Engineering

Exhibition Hall

Monday 9:15 - 10:15

- 1  Plasma 1  **Overcoming Limitations of Virtual Observation Points in pTx using IMPULSE**
Mihir Pendse¹ and Brian K Rutt¹
¹Stanford University, Stanford, CA, United States
- We analyze the performance of the IMPULSE pTx optimization algorithm, which allows SAR-aware pulse design without virtual observation points (VOP) compression. We compare performance of IMPULSE with conventional optimization methods using VOPs and compare different values of the overestimation parameter. We show that IMPULSE results in elimination of the time-intensive compression step without significantly increasing the time for real-time optimization. Additionally by eliminating the overestimation error from the VOP compression, IMPULSE is able to achieve better mitigation of local SAR hotspots after optimization than VOP-based methods.
-
- 2 Plasma 2  **Optical-based probe for real time assessment of RF electrical field during MRI exam**
Isabelle Saniour¹, Gwenaël Gaborit^{2,3}, Lionel Duvillaret³, Anne-Laure Perrier², and Olivier Beuf¹
¹Univ. Lyon, CREATIS ; CNRS UMR 5220 ; INSERM U1206 ; INSA-Lyon ; UJM-Saint-Etienne ; Université Lyon1, Villeurbanne, France, ²Univ. Savoie-Mont-Blanc, IMEP-LAHC, Le Bourget-du-Lac, France, ³Kapteos, Sainte-Hélène-du-Lac, France
- During MRI exam, Specific Absorption Rate (SAR) is essential to be controlled and can be evaluated by measuring either indirectly for instance the rise in temperature or directly the radiofrequency induced electrical E -field. In the current study, we proposed an optical probe based on the Pockels effect for subcentimeter resolution measurements of the E -field without altering the surrounding media. Measurements were performed at 4.7 T and 3.0 T. Results show that the probe has an excellent linear response and allow a real time estimate of the three components of the E -field produced during MRI examination.
-
- 3  Plasma 3  **Modeling of Peripheral Nervous Stimulation Thresholds in Realistic Body Models**
Mathias Davids^{1,2}, Bastien Guérin^{2,3}, Lothar R Schad¹, and Lawrence L Wald^{2,3,4}
¹Computer Assisted Clinical Medicine, Heidelberg University, Mannheim, Germany, ²Martinos Center for Biomedical Imaging, Massachusetts General Hospital, Charlestown, MA, United States, ³Harvard Medical School, Boston, MA, United States, ⁴Harvard-MIT Division of Health Sciences Technology, Cambridge, United States
- Peripheral Nervous Stimulation (PNS) has become an important limitation in MRI with the latest generation of high-performance gradient systems. We present – to our knowledge for the first time – a model to predict PNS thresholds for arbitrary coil geometries. Our model consists of an accurate body model for EM simulations, a detailed nerve atlas of the human body, and a numerical model to predict nerve responses to induced electrical fields. With this model, we were able to reproduce PNS threshold curves of two leg/arm solenoid coils that were previously evaluated experimentally. We intent to use this PNS model to design high-performance gradient coils with significantly lowered PNS capabilities.
-
- 4  Plasma 4  **Cardiac Synchronization at Ultra-High Field Using a 3-Lead ECG Trigger Device**
Daniel Stáb¹, Juergen Roessler², Kieran O'Brien³, Je Yen Su¹, Christian Hamilton-Craig⁴, and Markus Barth¹
¹The Centre for Advanced Imaging, The University of Queensland, Brisbane, Australia, ²Siemens Healthcare GmbH, Erlangen, Germany, ³Siemens Healthcare Pty Ltd, Brisbane, Australia, ⁴Richard Slaughter Centre of Excellence in CVMRI, The Prince Charles Hospital, Brisbane, Australia
- Accurate cardiac synchronization is essential in CMR. At ultra-high field, ECG triggering can be significantly impacted by the magneto-hydrodynamic (MHD) effect. Here, we investigate the performance of a conventional 3-lead ECG trigger device and a state-of-the-art trigger algorithm for cardiac ECG synchronization at 7 T. We show that by appropriate subject preparation and by including a learning phase for the R-wave detection outside of the magnetic field, reliable ECG triggering at ultra-high field is feasible despite severe distortions of the ECG signal. A quantitative analysis in 10 healthy subjects revealed a trigger sensitivity and specificity of 97.6% and 98.4%, respectively.
-
- 5 Plasma 5  **A Combined 7 Tesla MRI/NMR Probe Head for Photochemical Applications.**
Jens Groebner¹, Gernot Heitmann¹, Marcel Dommaschk¹, Lukas M. Huber², Eduard Stadler³, Reiner Umathum⁴, Frank D. Sönnichsen¹, and Rainer Herges¹
¹Otto Diels Institute for Organic Chemistry, Kiel University, Kiel, Germany, ²Molecular Imaging North Competence Center, University Medical Center Schleswig-Holstein, Kiel, Germany, ³Institute of Physical and Theoretical Chemistry, Graz University of Technology, Graz, Austria, ⁴Medical Physics in Radiology, German Cancer Research Center, Heidelberg, Germany
- The development of new photoswitchable contrast agents requires analysis with both NMR and MRI. In this work a combined probe head for *in situ* light exposure is presented which can be used on NMR and MRI systems with both 7 Tesla. A probe head with four slanted quartz rods was fabricated. A dual tuned (¹H and ²H) Helmholtz coil was integrated into the probe head. NMR and MRI experiments were performed on photoswitchable solutions (e.g. contrast agents). Results show that photoswitchable solutions can be successfully switched *in situ* and simultaneously analyzed with NMR or imaged with MRI.
-
- 6 Plasma 6 **Evaluation of cardiac magnetic resonance thermometry in patients**

6



Valery Ozenne¹, Solenn Toupin^{1,2}, Pierre Bour¹, Baudouin Denis de Senneville³, Alexis Vaussy², Matthieu Lepetit-Coiffé², Pierre Jaïs⁴, Hubert Cochet⁴, and Bruno Quesson¹

¹Electrophysiology and Heart Modeling Institute, Bordeaux, France, ²Siemens Healthcare, Paris, France, ³Mathematical Institute of Bordeaux, Bordeaux, France, ⁴Department of Cardiac Electrophysiology, Hôpital Cardiologique de Haut-Lévêque, Bordeaux, France

Recent studies have proposed to monitor radiofrequency ablation on the heart using real-time MR-thermometry. Methods rely on ECG triggering which can fail in presence of arrhythmia. This study evaluates the precision of MR-thermometry on patients (N=15) even in presence of cardiac arrhythmia. Phase images were acquired using a single-shot multi-slice echo planar imaging and temperature maps were calculated and displayed on the fly. ECG was recorded simultaneously for further analysis of cardiac rhythm and post-processing of temperature images. Stability of temperature mapping without RF-heating was evaluated in each pixel and correlated to the prevalence of arrhythmia.

7

Plasma 7



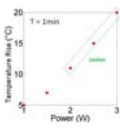
MRI-monitored Anterior Cervical Discectomy and Fusion (ACDF) surgery: Observation of intra-procedural nerve decompression during surgery
Ehud J Schmidt¹, Daniel F Kacher¹, Wei Wang¹, Mitchel B Harris², Thomas C Lee¹, Ravi Seethamraju³, Clare M Tempany¹, and Jay Zampini²

¹Radiology, Brigham and Womens Hospital, Boston, MA, United States, ²Orthopedic Surgery, Brigham and Womens Hospital, Boston, MA, United States, ³MRI, Siemens Healthcare, Boston, MA, United States

ACDF is a surgical procedure performed when herniated disks produce severe pain, or arm/hand weakness. Severe complications occur in ~9% of cases, mainly due to tissue resection adjoining the spinal canal. MRI imaging, performed at several procedure stages, can visualize the extent of resection, and the degree of nerve decompression. We performed ACDF surgery on the MRI table, using an MRI-compatible tool-set. Imaging at 3T was performed at four procedure phases. Imaging disclosed significant spine decompression immediately after disk resection, with smaller changes after osteophyte and posterior longitudinal ligament removal. MRI-monitored ACDF can revise procedure phases, leading to improved outcomes.

8

Plasma 8



Water diffusivity changes in the brain following exposure to low levels of focused ultrasound energy

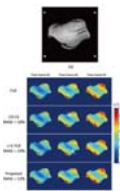
Sijia Guo¹, Jiachen Zhuo¹, Xin Lu¹, Su Xu¹, and Rao Gullapalli¹

¹Department of Diagnostic Radiology & Nuclear Medicine, University of Maryland School of Medicine, Baltimore, MD, United States

MR-guided Focused ultrasound (MRgFUS) for neuro-interventions is gaining popularity. However, the biological effects of low level exposure on the brain tissue are less understood. In this study, we used in-vivo MR diffusion kurtosis imaging (DKI) to measure water diffusion changes in vivo in rats at varying FUS exposure levels in the whole brain. Acoustic simulation and experimental data demonstrate more wide spread tissue diffusion changes and not just local changes with just a single exposure albeit for varied duration. Our results suggest that diffusion changes are mainly due to shearing forces exerted on the brain.

9

Plasma 9



Low Rank plus Sparse Compressed Sensing Reconstruction for PRF Temperature Imaging

Zhipeng Cao^{1,2}, Sumeeth V. Jonathan^{2,3}, and William A. Grissom^{1,2}

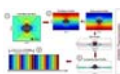
¹Biomedical Engineering, Vanderbilt University, Nashville, TN, United States, ²Institute of Imaging Science, Vanderbilt University, Nashville, TN, United States, ³Radiology, Vanderbilt University, Nashville, TN, United States

A novel compressed sensing reconstruction method based on L+S separation on complex difference image domain data is demonstrated to perform better than existing methods on major applications in RF heating monitoring and MR guided focused ultrasound intervention.

10



Plasma 10



2D Multi-Spectral Thermometry for Monitoring Focused-Ultrasound Sonications Near Metallic Hardware

Hans Weber¹, Pejman Ghanouni¹, Aurea Pascal-Tenorio², Kim Butts Pauly¹, and Brian A. Hargreaves¹

¹Radiology, Stanford University, Stanford, CA, United States, ²Comparative Medicine, Stanford University, Stanford, CA, United States

The lack of a technique for MR thermometry near metallic hardware excludes a growing patient population from MR-guided focused ultrasound treatments. In this work, we explore the temperature-induced signal change in fast two-dimensional multi-spectral imaging for monitoring sonications near metallic hardware. We demonstrate initial feasibility in phantom and ex vivo experiments as well as a patient treatment.

11

Plasma 11



Toward individualized specific absorption rates: Building a surface-based human head model

Mikhail Kozlov¹, Benjamin Kalloch^{1,2}, Pierre-Louis Bazin¹, Mario Hlawitschka², Nikolaus Weiskopf¹, and Harald E Möller¹

¹Max Planck Institute for Human Cognitive and Brain Sciences, Leipzig, Germany, ²Leipzig University of Applied Science, Leipzig, Germany

We built a prototype of a high resolution surface-based human head model that can be simulated in a reasonable time and evaluated the influence of cerebrospinal fluid (CSF) on field propagation estimates of traveling wave excitation at 297.2 and 400 MHz. Combining neighboring triangular faces located in the same plane into a single one is an approach that achieves simulations of high-resolution human models previously not accessible to tetrahedral-mesh-based solvers. If electrical contact between anatomically connected parts of CSF is correctly considered, CSF was found to partially shield brain tissues from the incident RF field.

12

Plasma 12

Patient specific modeling of deep brain stimulation patients for MRI safety studies

Bastien Guerin^{1,2}, Peter Serano^{3,4}, Maria I Iacono³, Todd Herrington^{2,5}, Alik Widge^{2,6}, Darin Dougherty^{2,6}, Giorgio Bonmassar^{1,2}, Leonardo M Angelone³, and Lawrence Wald^{1,2}



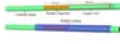
¹Radiology, Massachusetts General Hospital, Charlestown, MA, United States, ²Harvard Medical School, Boston, MA, United States, ³Division of Biomedical Physics, OSEL, CDRH, US Food and Drug Administration, Silver Spring, MD, United States, ⁴Mechanical Engineering, University of Maryland, College Park, MD, United States, ⁵Neurology, Massachusetts General Hospital, MA, United States, ⁶Psychiatry, Massachusetts General Hospital, MA, United States

We propose a semi-automatic processing pipeline for the generation of realistic radiofrequency models of deep brain stimulation (DBS) patients. The whole process takes ~72 hours for model generation and field computation and models the exact DBS path, without intersections, the internal structure of the implant and the patient's anatomical structures (e.g., brain, bones, muscles, lungs). We show that simplification of the DBS implant model results in high (up to 75%) differences in the estimation of energy absorption. The proposed framework allows for fast and precise modeling, which may be needed, pending experimental validation, to evaluate MRI RF-induced heating.

13

Plasma 13

Interventional Magnetic Resonance Imaging Guided Carotid Embolectomy using a Novel MRI-Conditional Resonant Catheter: Demonstration of Preclinical Feasibility



Jeffrey K. Yang¹, Andre Cote¹, Caroline D. Jordan¹, Aaron Losey¹, David McCoy¹, Andrew Chu², Jay F. Yu¹, Teri Moore¹, Carol Stillson¹, Fabio Settecase¹, Matthew D. Alexander¹, Andrew Nicholson¹, Mariam Aboian¹, Daniel L. Cooke¹, Maythem Saeed¹, Dave Barry², Alastair J. Martin¹, Mark W. Wilson¹, and Steven W. Hetts¹

¹Department of Radiology and Biomedical Imaging, UCSF, San Francisco, CA, United States, ²Penumbra Inc, Alameda, CA, United States

MR-guided endovascular interventions can provide real-time imaging biomarkers for procedures such as stroke embolectomy. The purpose of this study is to determine preclinical feasibility and efficacy of imaging wireless resonant circuits embedded in a MR compatible catheter system for *in vivo* MR-guided carotid embolectomy in porcine stroke models. The resonant catheter system performed effectively under real-time MRI with recanalization rates (TICI 2b/3) similar to reported clinical rates in stroke embolectomy. Qualitative physiologic measures of flow under MRI were comparable to those measured under X-ray, demonstrating feasibility of resonant catheter system for *in vivo* carotid occlusion and embolectomy under real-time MRI.

14

Plasma 14

Acousto-optic Based Active MRI Marker for Interventional MRI Devices



Yusuf Samet Yaras¹, Sarp Satir¹, Cagla Ozsoy², Rajiv Ramasawmy³, Adrienne E Campbell-Washburn³, Anthony Faranesh³, Robert Lederman³, Ozgur Kocaturk², and Levent Degertekin¹

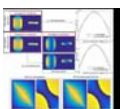
¹G.W. Woodruff School of Mechanical Engineering, Georgia Institute of Technology, Atlanta, GA, United States, ²Institute of Biomedical Engineering, Bogazici University, Istanbul, Turkey, ³Division of Intramural Research, National Heart Lung and Blood Institute, National Institutes of Health, Bethesda, MD, United States

Conspicuous and safe MR markers are essential for tracking interventional MRI devices. The RF induced heating on long conductors used in current active MR markers presents a safety risk. In this work, a novel acousto-optic active MR marker with optical fiber connection is proposed to eliminate RF induced heating. The proposed marker consists of a miniature coil coupled to a piezoelectric transducer which in turn modulates the reflected light in the optical fiber. The linearity of the acousto-optic active marker with flip angle is characterized and initial *in vitro* imaging experiments are performed demonstrating marker visibility under MRI.

15

Plasma 15

MRI based RF safety characterization of implants using the implant response matrix: a simulation study.



Janot P. Tokaya¹, Alexander J.E. Raaijmakers^{2,3}, Peter R. Luijten², and Cornelis A.T. van den Berg¹

¹Radiology, UMC Utrecht, Utrecht, Netherlands, ²Radiology, UMC Utrecht, Utrecht, Netherlands, ³Biomedical Image Analysis, Eindhoven University of Technology, Netherlands

We introduce a general description of the RF response of an implant, defined as the implant response matrix (IRM). An analytical expression for the IRM is derived through basis functions that depend on a limited number of parameters. This analytical model is validated with a simulation study (Pearson correlation coefficients with simulations R: 0.9979-0.9996). This description allows a significant reduction in unknowns enabling IRM assessment by MRI measurements without hardware modifications to scanner or implant. The feasibility of MRI based IRM/TF measurement is shown *in silico*. With the simulated complex B_1^+ fields the IRM is accurately reconstructed (R: 0.974).

Electronic Power Pitch Poster

Poster: 7T Neuroimaging

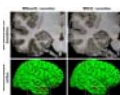
Exhibition Hall

Monday 9:15 - 10:15

16

Plasma 16

The effects of B_1^+ correction of MP2RAGE on estimating cortical thickness and T_1 at 7T



Roy Haast¹, Dimo Ivanov¹, Elia Formisano¹, and Kâmil Uludağ¹

¹Department of Cognitive Neuroscience, Maastricht University, Maastricht, Netherlands

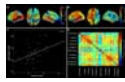
B_1^+ inhomogeneities can significantly affect the quantitative T_1 values derived from MP2RAGE data and also automatic tissue classification, in particular in the inferior temporal and frontal lobes. Here, we investigated the effects of post-hoc correction at 7T on the T_1 and apparent cortical thickness using a B_1^+ map for the residual transmit inhomogeneities in MP2RAGE data. We found that B_1^+ correction reduces these inhomogeneities leading to (1) a lower inter-subject variability, (2) enhanced localization of the GM-CSF border and (3) more accurate cortical thickness measurements.



17

Plasma 17

The relationship between cortical myeloarchitecture and functional connectivity in the human brain

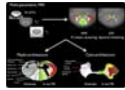
Olivier E. Mougin¹, Benjamin A.E. Hunt¹, Prejaas K. Tewarie¹, Nicolas Geades¹, Peter G. Morris¹, Matthew J. Brookes¹, and Penny A. Gowland¹¹Sir Peter Mansfield Imaging Centre, School of Physics and Astronomy, University of Nottingham, Nottingham, United Kingdom

The human brain relies upon the dynamic formation and dissolution of functional networks to support ongoing cognition. The goal of this study is to establish a relationship between functional and structural networks. Using ultra-high field MRI, structural network defined by grey matter myelination is measured via quantitative Magnetization Transfer. Magnetoencephalography (MEG) was used to elucidate functional networks representing the major electrophysiological pathways of communication in the brain. Our study sheds new light on the way in which cortical microstructure supports functional networks.

18

Plasma 18

Towards in vivo spinal cord cyto- and myelo-architecture deciphering using multi-modal MRI parcellation at 7T

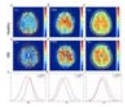
Manuel Taso^{1,2,3}, Aurélien Massire^{1,2,3}, Pierre Besson^{1,2}, Arnaud Le Troter^{1,2}, Maxime Guye^{1,2}, Jean-Philippe Ranjeva^{1,2,3}, and Virginie Callot^{1,2,3}¹CRMBM, Aix-Marseille Univ, CNRS, Marseille, France, ²Pôle d'imagerie médicale, Hôpital de la Timone, CEMEREM, AP-HM, Marseille, France, ³Lab-Spine international associate laboratory, Marseille/Montréal, France

Ultra-high-field MRI offers exciting perspectives for the in vivo structural characterization of central nervous system tissues. Based on high-resolution multi-parametric imaging at 7T, this preliminary work focuses on the generation of new spinal cord (SC) templates, hence proposing a high-resolution T_2^* -w MR average with exquisite anatomical details. Parcellation of the SC substructures into individual WM tracts and motoneurone clusters was also investigated using classification methods and multimodal data ($T_1/T_2^*/DTI$). Preliminary promising results revealed some insights in the underlying SC cyto- and myelo-architecture. Future developments will extend to the whole cervical cord, holding tremendous promises for studying more specific pathophysiological impairments.

19

Plasma 19

7T Quantitative Magnetization Transfer (qMT) of Cortical Gray Matter in Multiple Sclerosis Correlates with Cognitive Disability

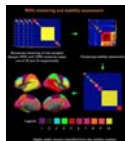
Lydia McKeithan^{1,2}, Bailey D. Lytle^{2,3}, Bailey A. Box^{2,3}, Kristin P. O'Grady^{2,3}, Richard D. Dorch^{1,2,3}, Benjamin N. Conrad², and Seth A. Smith^{1,2,3,4}¹Department of Biomedical Engineering, Vanderbilt University, Nashville, TN, United States, ²Vanderbilt University Institute of Imaging Science, Vanderbilt University Medical Center, Nashville, TN, ³Department of Radiology and Radiological Sciences, Vanderbilt University Medical Center, Nashville, TN, ⁴Department of Ophthalmology, Vanderbilt University Medical Center, Nashville, TN

Cognitive impairment (CI) is a major manifestation of multiple sclerosis (MS) and is responsible for extensively hindering patient quality of life.¹ Cortical gray matter damage is critical to CI, but is poorly characterized by conventional MRI. We employed advanced methods by evaluating SIR-qMT-derived indices for differences between MS patients and healthy volunteers at 7T and derived associations with neuropsychological measures of cognitive impairment. We found significant reduction in k_{mf} in cGM of MS patients, unique association with EDSS score, and strong correlation with cognitive performance indicating that k_{mf} may be a significant biomarker of GM damage in MS.

20

Plasma 20

Changes in structural network connectivity in early-stage multiple sclerosis are associated with cortical demyelination

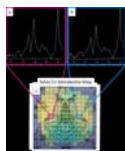
Atef Badji^{1,2}, Gabriel Mangeat^{1,3}, Russell Ouellette^{3,4}, Constantina Andrada Treaba^{3,4}, Tobias Granberg^{3,4,5}, Elena Herranz^{3,4}, Celine Louapre^{3,4}, Nikola Stikov^{1,6}, Jacob Sloane^{4,7}, Pierre Bellec², Caterina Mainero^{3,4}, and Julien Cohen-Adad^{1,2}¹NeuroPoly Lab, Institute of Biomedical Engineering, Polytechnique Montreal, Montreal, QC, Canada, ²Functional Neuroimaging Unit, CRIUGM, Université de Montréal, Montreal, QC, Canada, ³Athinoula A. Martinos Center for Biomedical Imaging, MGH, ⁴Harvard Medical School, ⁵Department of Clinical Science, Intervention and Technology, Karolinska Institutet, ⁶Montreal Health Institute, ⁷Beth Israel Deaconess Medical Center

Cortical disruption and changes in brain connectomics in multiple sclerosis have been recently investigated; however, the relationship between both processes in early disease remains uncertain. We propose an integrative framework that combines diffusion-based graph theory with high-resolution quantitative T1 and T2* at 7 Tesla to investigate the topological alterations of both structural connectomics and cortical demyelination. We found that both cortical myelin loss and increase in brain connectivity were present in early MS, and that the two processes were spatially anti-correlated. This suggests that the increase in brain connectivity in early MS could represent an adaptive role against initial, mild cortical demyelination, though this would be lost with more severe cortical disease.

21

Plasma 21

3D magnetic resonance spectroscopic imaging at 7 Tesla of patients with medically refractory focal epilepsy with non-lesional or inconclusive clinical MRIs: First Results

Rebecca Emily Feldman¹, Madeline Cara Fields², Bradley Neil Delman³, Lara Vanessa Marcuse⁴, and Priti Balchandani¹¹Translational and Molecular Imaging Institute, Icahn School of Medicine at Mount Sinai, New York, NY, United States, ²Department of Neurology, Mount Sinai Hospital, New York, NY, United States, ³Radiology, Icahn School of Medicine at Mount Sinai, New York, NY, United States, ⁴Department of Neurology, Mount Sinai Hospital

SASSI is a B₁-insensitive, low-SAR 7T MRSI technique with reduced chemical shift localization errors. We used 3D SASSI to image the hippocampi of patients with medically refractory focal epilepsy who had non-lesional or inconclusive clinical MRIs. Using SASSI at 7T, we detected decreases in the hippocampal NAA/Cr ratios in suspected temporal lobe epilepsy patients, on the same side as the seizure onset zones and/or 7T structural findings.

22

Plasma 22

The value of 7T in the clinical evaluation of epileptic patients with focal cortical dysplasia

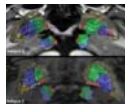
Kaibao Sun^{1,2}, Xueyuan Wang³, Zhongwei Chen^{1,2}, Chang Liu³, Jianfei Cui⁴, Zhentao Zuo¹, Rong Xue^{1,2}, Yan Zhuo¹, Lin Chen^{1,2}, Shuli Liang⁴, Tao Yu³, and Bo Wang¹

¹State Key Laboratory of Brain and Cognitive Science, Beijing MRI Center for Brain Research, Institute of Biophysics, Chinese Academy of Sciences, Beijing, People's Republic of China, ²University of Chinese Academy of Sciences, Beijing, People's Republic of China, ³Xunanwu Hospital Capital Medical University, Beijing, People's Republic of China, ⁴Chinese PLA general hospital, Beijing, People's Republic of China

Focal cortical dysplasia (FCD) is defined as topical malformations of cortical development and often results in intractable epilepsy. However, many epileptic patients with FCD have not been diagnosed because of the lack of high-quality magnetic resonance imaging. 7T MRI, in comparison with 3T, is assessed in this study to allow better characterization of lesion details and detect previously unrevealed FCD abnormalities. The results of comparison were classified for an accurate and appropriate appraisal.

23

Plasma 23



Individualized Tractography-Based Parcellation of the Globus Pallidus Pars Interna using 7T MRI in patients with Parkinson's Disease Prior to DBS Surgery

Rémi Patriat¹, Yuval Duchin¹, Christophe Lenglet¹, Joshua Aman², Scott Cooper², Jerrold Vitek², and Noam Harel¹

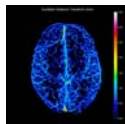
¹CMRR / Radiology, University of Minnesota, Minneapolis, MN, United States, ²Neurology, University of Minnesota, Minneapolis, MN, United States

The success of deep brain stimulation (DBS) surgeries for Parkinson's disease relies on the accurate placement of an electrode within the motor portion of subcortical brain targets. We use 7T MR-tractography to visualize the functional territories of the Globus Pallidus pars Interna. We found that the motor territory is located immediately posteromedially to the associative and limbic territories, akin to the subthalamic nucleus organization. This pattern was reproducible across two DBS patients. These findings shed new light on the functional organization of DBS targets, showing potential for providing valuable information to clinicians for targeting decisions and ultimately enhancing patient's outcomes.

24



Plasma 24



Assessment of cerebral vascular abnormalities in Huntington's Disease at 7Tesla

Richard J Dury¹, Sarah L Mason², Francesca Cicchetti³, Janelle Drouin-Ouellet², Roger A Barker², Penny A Gowland¹, and Susan T Francis¹

¹Sir Peter Mansfield Imaging Centre, University of Nottingham, Nottingham, United Kingdom, ²John van Geest Centre for Brain Repair, University of Cambridge, Cambridge, United Kingdom, ³Département de Psychiatrie & Neurosciences, Université Laval, QC, Canada

Huntington's Disease (HD) is associated with vascular abnormalities and breakdown in the blood-brain barrier (BBB). Here, we use high spatial resolution time-of-flight magnetic resonance angiography (TOF-MRA) and arterial spin labelling (ASL) to assess vascular abnormalities in HD patients. We develop a pipeline to estimate vessel radii and distribution from TOF-MRA data. A significant decrease in the fractional vessel volume and a higher frequency of narrow vessels (0.15-0.45mm radius) was evident in HD patients compared to healthy volunteers across a number of cortical areas. No significant difference was found in cortical perfusion between the HD patients and healthy volunteers.

25

Plasma 25



7T TOF-MRA Shows Different Patterns of Perforating Artery in Patients with Intracranial Atherosclerosis Disease (ICAD) and Cerebral Autosomal-Dominant Arteriopathy with Subcortical Infarcts and Leukoencephalopathy (CADASIL)

Qingle Kong^{1,2}, Qi Yang^{3,4}, Zhaoyang Fan³, Xianchang Zhang^{1,2}, Yun Yuan⁵, Xiaojing Fang⁵, Jing An⁶, Yan Zhuo¹, and Zihao Zhang¹

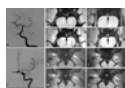
¹State Key Laboratory of Brain and Cognitive Science, Beijing MR Center for Brain Research, Institute of Biophysics, Chinese Academy of Sciences, Beijing, People's Republic of China, ²University of Chinese Academy of Sciences, Beijing, People's Republic of China, ³Biomedical Imaging Research Institute, Cedars-Sinai Medical Center, Los Angeles, CA, United States, ⁴Xuanwu Hospital, Beijing, People's Republic of China, ⁵Department of Neurology, Peking University First Hospital, Beijing, People's Republic of China, ⁶Siemens Shenzhen Magnetic Resonance Ltd., Shenzhen, People's Republic of China

7T high-resolution TOF-MRA has the ability to image perforating arteries of middle cerebral artery (MCA). The distribution patterns of orifices in CADASIL (cerebral autosomal-dominant arteriopathy with subcortical infarcts and leukoencephalopathy) and ICAD (intracranial atherosclerosis disease) patients are still unclear. In this study, for the first time, we investigated the orientation distribution of perforating artery orifices on MCA trunks using 7T TOF-MRA. Specific features are found in the distribution patterns of orifices in patients with CADASIL, ICAD and healthy volunteers. This technique is promising in the pathological studies of intracranial vascular diseases.

26



Plasma 26



Intracranial vessel wall imaging in suspected cerebral vasculitis: evaluation of diagnostic value and treatment effects using 3T and 7T MRI

Nikki Dieleman¹, Anja G. van der Kolk¹, Catharina J.M. Frijns², Anita A. Hartevelde¹, Jaco J.M. Zwanenburg¹, Hugo J. Kuijff³, Arijen Lindenholz¹, L. Jaap Kappelle², Peter R. Luijten¹, and Jeroen Hendrikse¹

¹Radiology, University Medical Center Utrecht, Utrecht, Netherlands, ²Neurology, University Medical Center Utrecht, Utrecht, Netherlands, ³Images Science Institute, University Medical Center Utrecht, Utrecht, Netherlands

Cerebral vasculitis is a rare, but devastating disease that can lead to severe disability or death. Diagnosis is rather challenging, but for treatment purposes, an accurate diagnosis is crucial since different, more aggressive therapy is needed compared with non-inflammatory diseases. In the current study, we investigated the diagnostic value of intracranial vessel wall MRI at 3T and 7T in patients who were suspected of cerebral vasculitis. Our results show that intracranial vessel wall imaging at 3T and 7T MRI should be considered a promising non-invasive diagnostic tool to identify wall enhancement in patients with a suspicion of cerebral vasculitis.

27



Plasma 27



Detection of intracranial vessel wall lesions using 7T MRI: patients with posterior circulation ischemia versus healthy controls

Anita A. Hartevelde¹, Anja G. van der Kolk¹, H. Bart van der Worp², Nikki Dieleman¹, Peter R. Luijten¹, Jaco J.M. Zwanenburg¹, and Jeroen Hendrikse¹

¹Radiology, University Medical Center Utrecht, Utrecht, Netherlands, ²Neurology and Neurosurgery, University Medical Center Utrecht, Utrecht, Netherlands

In this study presence and distribution of vessel wall lesions within the intracranial arteries of patients with recent posterior circulation ischemia and matched asymptomatic volunteers were assessed, using intracranial vessel wall MRI at 7T. Overall, vessel wall lesion presence and distribution were comparable between both groups. On arterial segment level, patients showed significantly higher lesion burden in the posterior cerebral artery, suggesting an association between posterior circulation lesion burden and ischemic events. Furthermore, a large amount of lesions showed contrast-enhancement, while the percentage of enhancing lesions was highest in the posterior circulation of the patient group.

28

Plasma 28

Metabolic differences between asymptomatic C9orf72 carriers and non-carriers assessed by brain 7T MRSI.

Henk-Jan Westeneng¹, Carrie Wismans¹, Abram D. Nitert¹, Renée Walhout¹, Peter R. Luijten², Jannie P. Wijnen², and Leonard H. van den Berg¹

¹Department of Neurology, Brain Center Rudolf Magnus, University Medical Center Utrecht, Utrecht, Netherlands, ²Department of Radiology, University Medical Center Utrecht, Utrecht, Netherlands

Amyotrophic lateral sclerosis (ALS) is an incurable and fatal neurodegenerative disease, which is caused by a C9orf72 repeat expansion in 9% of the cases. This mutation may cause changes of brain metabolism in patients but whether it affects brain metabolism in pre-symptomatic mutation carriers was not studied before. We used 7 Tesla magnetic resonance spectroscopic imaging (MRSI) to study brain metabolism in asymptomatic carriers of the C9orf72 repeat expansion and found lower concentrations of glutamate and N-acetylaspartate+N-acetylaspartylglutamate in the left putamen compared to non-carriers. This might indicate asymptomatic neuronal loss, a developmental defect or possibly a protective mechanism against ALS.

29

Plasma 29

GABA and glutamate in children with Tourette Syndrome: a 7T 1H-MRS study

Nicolaas AJ Puts^{1,2}, Richard AE Edden^{1,2}, Matthew Ryan³, E Mark Mahone^{3,4}, and Harvey S Singer⁵

¹Russell H. Morgan Department of Radiology and Radiological Science, The Johns Hopkins University, Baltimore, MD, United States, ²FM Kirby Research Center for Functional Brain Imaging, Kennedy Krieger Institute, Baltimore, MD, United States, ³Department of Neuropsychology, Kennedy Krieger Institute, Baltimore, MD, United States, ⁴Department of Psychiatry and Behavioral Sciences, The Johns Hopkins University, Baltimore, MD, United States, ⁵Department of Neurology, The Johns Hopkins University, Baltimore, MD, United States

Studies have suggested that altered inhibition and excitation contribute to the pathology of Tourette syndrome, especially in cortical-striatal-thalamo-cortical (CSTC) pathways. GABA and glutamate were measured at 7T in large cohorts of healthy children and children with TS in regions of the CSTC network. GABA and glutamate were increased in the striatum. Glutamate was increased in the premotor region and correlated with reduced motor inhibition. These data support involvement of habitual behavioral pathways in TS. Historically the dopaminergic system has been considered to have a dominant role in TS; however, accumulating evidence strongly suggests involvement of GABA and glutamate neurotransmitter systems.

30

Plasma 30

Multi-Parametric MRI at 7 T Enables Differentiation of MS and Age-Related White Matter Lesions

Zahra Hosseini^{1,2}, David A. Rudko³, Jacob A. Matusinec⁴, Marcelo kremenchutzky⁵, Ravi Menon^{2,6}, and Maria Drangova^{1,6,7}

¹Biomedical Engineering Graduate Program, University of Western Ontario, London, ON, Canada, ²Imaging Research Laboratories, Robarts Research Institute, London, ON, Canada, ³Montreal Neurological Hospital and Institute, McGill University, Montreal, QC, Canada, ⁴Medicine, Schulich School of Medicine & Dentistry, University of Western Ontario, London, ON, Canada, ⁵Department of Clinical Neurological Sciences, Schulich School of Medicine & Dentistry, University of Western Ontario, London, ON, Canada, ⁶Department of Medical Biophysics, University of Western Ontario, London, ON, Canada, ⁷Imaging Research Laboratories, Robarts Research Institute

MRI enables visualization of white matter lesions associated with demyelination in multiple sclerosis (MS). However, subtle white matter hyperintensities are also a sign of normal aging. This study used information collected from multiple 7T MRI contrasts at baseline and four-month follow-up time points to compare signal changes in lesions of five MS patients to those of age-related lesions (ARLs) in five healthy controls.

Electronic Power Pitch Poster

Poster: Body MRI Quantitative

Exhibition Hall

Monday 14:45 - 15:45

112

Plasma 1

Accelerated Segmented Diffusion-Weighted Prostate Imaging for Higher Resolution, Higher Geometric Fidelity, and Multi-b Perfusion Quantification

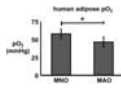
Pelin Aksit Ciris¹, Jr-yuan George Chiou², Daniel Glazer², Shelley Hualei Zhang², Tzu-Cheng Chao³, Bruno Madore², and Stephan Ernst Maier^{2,4}

¹Department of Biomedical Engineering, Akdeniz University, Antalya, Turkey, ²Department of Radiology, Brigham and Women's Hospital, Harvard Medical School, Boston, MA, United States, ³Department of Computer Science, National Cheng Kung University, Tainan City, Taiwan, ⁴University of Gothenburg, Gothenburg, Sweden

An accelerated multi-shot diffusion imaging scheme was developed for prostate imaging. Its robustness to regularization was evaluated. Two-fold improvement in spatial resolution and over three-fold improvement in geometric fidelity were obtained as compared to single-shot EPI, in twenty-five prostate cancer patients. In contrast to the standard protocol, which involves separate scans with high ($b=1400$ and 0 s/mm²) and intermediate ($b=500$ and 0 s/mm²) diffusion weighting, the proposed accelerated protocol extended b-factor coverage to yield an additional 8 b-factors and enabled multi-b perfusion quantification in half the scan time (5 min 43 s vs. 11 min 48 s).

Plasma 2

Towards validation and non-invasive interrogation of the hypoxia-driven insulin resistance hypothesis

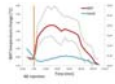


Scott Charles Beeman¹, Gordon Smith², Joel Richard Garbow¹, and Joseph JH Ackerman^{1,3}

¹Mallinckrodt Institute of Radiology, Washington University in St. Louis, St. Louis, MO, United States, ²Department of Medicine, Washington University in St. Louis, St. Louis, MO, United States, ³Department of Chemistry, Washington University in St. Louis

Insulin resistance is a defining feature of type 2 diabetes – a disease associated with severe morbidities and mortality. Recent studies have suggested that adipose tissue hypoxia is a major common pathway to systemic insulin resistance. The goals of this work are to: (i) directly observe evidence of the hypoxia-driven insulin resistance hypothesis in human subjects via gold-standard invasive pO₂ measures and (ii) establish an R₁-based pO₂ metric for future non-invasive studies of adipose pO₂ in metabolic disease. Herein, we report initial progress towards these goals.

Plasma 3



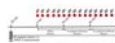
Measuring temperature in brown adipose tissue using the proton chemical shift

Clemens Diwoky¹, Renate Schreiber¹, and Rudolf Zechner¹

¹Institute of Molecular Biosciences, University of Graz, Graz, Austria

Within this work an approach based on the temperature dependence of the proton resonance frequency (PRF) of water and methylene bound protons is followed to monitor in-vivo thermogenesis in the interscapular brown adipose tissue (iBAT) of mice. Measuring the change in chemical shift difference of water and fat rather than water alone, known problems of PRF-based temperature measurements such as magnetic field drift and the temperature dependence of magnetic susceptibility are circumvented. The study determines the temperature coefficient in ex-vivo iBAT tissue extracts and presents the application of the technique in measuring norepinephrine stimulated in-vivo iBAT thermogenesis.

Plasma 4



Development of a Noninvasive Beta Cell Functional Assay Using a Novel Zinc-Sensitive MRI Contrast Agent in Non-Human Primates

Catherine D. G. Hines¹, Veronica Clavijo-Jordan^{2,3}, Liza T Gantert¹, Stacey Conarello⁴, Christian Preihs^{2,5}, Sarah Chirayil², Rachel Ortega⁴, Shu-An Lin¹, Michael Klimas⁶, A. Dean Sherry^{2,3,5,7}, and Jeff Evelhoch⁶

¹Translational Imaging Biomarkers, Merck Research Laboratories, West Point, PA, United States, ²Advanced Imaging Research Center, The University of Texas Southwestern Medical Center, Dallas, TX, United States, ³Radiology, The University of Texas Southwestern Medical Center, Dallas, TX, United States, ⁴Pharmacology, Merck Research Laboratories, West Point, PA, United States, ⁵VitalQuan, LLC, Dallas, TX, United States, ⁶Translational Biomarkers, Merck Research Laboratories, West Point, PA, United States, ⁷Chemistry, The University of Texas at Dallas, Richardson, United States

Pancreatic beta cells secrete insulin to maintain normal blood glucose levels, and the integrity and function of pancreatic beta cells have been found to be compromised in Type-1 and Type-2 diabetes. Therefore, non-invasive beta cell function measurements may provide valuable information for improving diabetes diagnostics and disease management. Currently available diabetes assays lack functional information and spatial identification of properly functioning beta cells. In this work, we introduce a new assay to assess the function and identify functional beta cells in vivo in the non-human primate pancreas non-invasively with MRI using a Gd-based zinc sensor as contrast agent.

Plasma 5



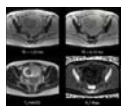
Feasibility of Estimating Placental Oxygen Metabolism in Pregnant Women \$\$\$in\$\$\$ \$\$\$vivo\$\$\$\$: Initial Experience

Ana E Rodríguez-Soto¹, Michael C Langham¹, Nadav Schwartz², and Felix W Wehrli¹

¹Department of Radiology, University of Pennsylvania, Philadelphia, PA, United States, ²Department of Obstetrics and Gynecology, Division of Maternal-Fetal Medicine, University of Pennsylvania, Philadelphia, PA, United States

The development of methods to assess placental oxygen metabolism would allow to clinically evaluate its function. Here, we evaluated the feasibility of estimating oxygen extraction and blood flow in some abdominal and fetal draining veins. Ovarian veins appear to play an important role in draining blood from the uterus in the supine position, where flow increased from the 2nd to 3rd trimester (16.4±8.1 versus 34.3±4.1 mL/min/100g). Additionally, elevation of oxygen saturation (61.6±6.6% versus 68.3±5.0%) at the umbilical vein occurred from the 2nd to 3rd trimester, potentially reflecting increased fetal oxygen demand as pregnancy progresses.

Plasma 6



Free-breathing R2* Characterization of the Placenta During Normal Early Gestation Using a Multiecho 3D Stack-of-Radial Technique

Tess Armstrong^{1,2}, Dapeng Liu¹, Thomas Martin^{1,2}, Alto Stemmer³, Yutaka Natsuaki⁴, Sherin U. Devaskar⁵, Carla Janzen⁶, Teresa Chanlaw⁵, Rinat Masamed¹, Daniel Margolis⁷, Kyunghyun Sung^{1,2}, and Holden H. Wu^{1,2}

¹Radiological Sciences, University of California Los Angeles, Los Angeles, CA, United States, ²Physics and Biology in Medicine, University of California Los Angeles, Los Angeles, CA, United States, ³Siemens Healthcare GmbH, Erlangen, Germany, ⁴Siemens Healthcare, Los Angeles, CA, United States, ⁵Pediatrics, David Geffen School of Medicine at UCLA, Los Angeles, CA, United States, ⁶Obstetrics and Gynecology, David Geffen School of Medicine at UCLA, Los Angeles, CA, United States, ⁷Radiology, Weill Cornell Medical College, New York, NY, United States

Abnormal placental vascular development leads to ischemic-hypoxia thereby causing fetal growth restriction, preterm labor, and spontaneous abortion. Multiecho Cartesian MRI can characterize placental hypoxia by quantifying R2*, but is susceptible to motion artifacts. We have developed a new free-breathing (FB) multiecho R2* quantification technique using 3D stack-of-radial imaging (Radial). In n=16 subjects as part of an IRB-approved study, we observed an R2* range of 5 – 30s⁻¹ at 3 T using the new FB Radial technique in the placenta during early normal gestation. Our new technique and the measured normative range of R2* may improve management of pregnancies with placental ischemic-hypoxia.

Plasma 7



Respiratory \$\$\$alpha\$\$\$-mapping of cystic fibrosis at 1.5T

Orso Pusterla^{1,2}, Grzegorz Bauman^{1,2}, Sylvia Nyilas³, Philipp Madörin¹, Bernd Jung⁴, Michael Ith⁴, Enno Stranzinger⁴, Urs Frey⁵, Philipp Latzin³, and Oliver Bieri^{1,2}



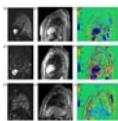
¹Department of Radiology, Division of Radiological Physics, University of Basel Hospital, Basel, Switzerland, ²Department of Biomedical Engineering, University of Basel, Basel, Switzerland, ³Division of Respiratory Medicine, Department of Pediatrics, University Children's Hospital of Bern, Bern, Switzerland, ⁴University Institute for Diagnostic, Interventional and Pediatric Radiology, Bern University Hospital, Bern, Switzerland, ⁵Department of Pediatric Pneumology, University Children's Hospital Basel, Basel, Switzerland

Respiratory α -mapping is based on native 1H multi-volumetric ultra-fast balanced steady-state free precession (ufSSFP) breath-hold imaging of the lung and provides whole lung isotropic pulmonary ventilation-related information. In this work, respiratory α -mapping is evaluated in pediatric patients with cystic fibrosis (CF) and compared to functional lung parameters from nitrogen multiple-breath washout (N_2 -MBW). The percentage of respiratory α -impairments measured with α -mapping is strongly correlated with the lung clearance index (LCI), a parameter for global ventilation inhomogeneity.

119

Plasma 8

5D MRI for late enhancement dynamics in lung fibrosis



Maria Teodora Antuaneta Buzan^{1,2}, Julien Dinkel³, Christopher Rank⁴, Claus Peter Heussel², Marc Kachelrieß⁴, Robert Grimm⁵, and Andreas Wetscherek^{4,6}

¹Department of Radiology, Papworth Hospital NHS Foundation Trust, Cambridge, United Kingdom, ²Department of Diagnostic and Interventional Radiology with Nuclear Medicine, Thoraxklinik at Heidelberg University Hospital, Heidelberg, Germany, ³Institute for Clinical Radiology, Ludwig-Maximilians-University Hospital Munich, Munich, Germany, ⁴Medical Physics in Radiology, German Cancer Research Center, Heidelberg, Germany, ⁵Siemens Healthcare, Erlangen, Germany, ⁶Joint Department of Physics, The Institute of Cancer Research and The Royal Marsden NHS Foundation Trust, London, United Kingdom

We analyzed the contrast agent late dynamics in fibrotic lung lesions of different severity, assessed with perfusion MRI, using a 5D reconstruction (respiratory 4D at different time points) of a 3D radial stack-of-stars spoiled gradient echo sequence with golden-angle spacing acquired in free-breathing. Idiopathic pulmonary fibrosis (IPF) shows late peak enhancement regardless of severity level and possibly no wash-out within the scan interval, while non-IPF lesions have faster time to peak and slower accumulation rate with increasing severity. The method might prove useful for a more thorough characterization of lung fibrosis burden in the context of new anti-fibrotic treatments available.

120

Plasma 9

Quantification of short-T2* Signal Components in the Liver using Radial 3D UTE Chemical Shift-Encoded MRI



Ante Zhu^{1,2}, Diego Hernando^{2,3}, Kevin M. Johnson^{2,3}, and Scott B. Reeder^{1,2,3,4,5}

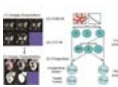
¹Biomedical Engineering, University of Wisconsin-Madison, Madison, WI, United States, ²Radiology, University of Wisconsin-Madison, Madison, WI, United States, ³Medical Physics, University of Wisconsin-Madison, Madison, WI, United States, ⁴Medicine, University of Wisconsin-Madison, Madison, WI, United States, ⁵Emergency Medicine, University of Wisconsin-Madison, Madison, WI, United States

Recent studies have suggested the presence of a short-T2* signal component in the liver. The origin and MR properties of this signal have not been determined but have been shown to confound the liver fat quantification when using short echo times. In this work, we developed a UTE chemical shift-encoded MRI technique and a multi-component reconstruction to characterize short-T2* liver signals. A short-T2* signal fraction of $11.6 \pm 2.4\%$ with an $R2^*$ of $2222 \pm 281 s^{-1}$ was measured in seven healthy volunteers. This study demonstrated the presence of the short-T2* signal component in healthy livers and provided an initial estimate to guide future studies.

121

Plasma 10

REnal Flow and Microstructure Anisotropy (REFMAP) MRI in Normal and Peritumoral Renal Tissue



Andrea Liu¹, Artem Mikheev², Henry Rusinek^{2,3}, William Huang⁴, Hersh Chandarana^{2,3}, and Eric Edward Sigmund^{2,3}

¹NYU School of Medicine, NYU Langone Medical Center, New York, NY, United States, ²Radiology, NYU Langone Medical Center, New York, NY, United States, ³Center for Advanced Imaging and Innovation (CAIIR), New York, NY, United States, ⁴Urology, NYU Langone Medical Center, New York, NY, United States

Using a recently developed joint intravoxel incoherent motion (IVIM)-diffusion tensor imaging (DTI) protocol for kidney evaluation, we present reproducibility analysis of its metrics in normal volunteers, as well as pilot assessments in several patients with renal masses prior to surgery. Reproducibility analysis indicates a subset of robust parameters, including structural and microcirculation markers in both cortex and medulla, for clinical application. Preliminary results in renal mass patients suggest multifactorial differences from controls, supporting the need for advanced diffusion characterization in assessing renal functional reserve.

122

Plasma 11

Addressing Metabolic Heterogeneity in Clear Cell Renal Cell Carcinoma with Quantitative Magnetic Resonance Imaging



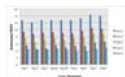
Yue Zhang¹, Durga Udayakumar¹, Ling Cai², Zeping Hu², Payal Kapur³, Eun-Young Kho², Andrea Pavia-Jiménez⁴, Michael Fulkerson¹, Alberto DiazdeLeon¹, Qing Yuan¹, Ivan E Dimitrov⁵, Takeshi Yokoo¹, Jin Ye⁶, Matthew Mitsche⁸, Hyeonwoo Kim⁸, Jeffrey McDonald⁶, Yin Xi¹, Ananth J Madhuranthakam¹, Robert E Lenkinski¹, Jeffrey A Cadeddu⁷, Vitaly Margulis⁷, James Brugarolas⁸, Ralph J Deberardinis², and Ivan Pedrosa¹

¹Radiology, UT Southwestern Medical Center, Dallas, TX, United States, ²Children's Medical Center Research Institute, UT Southwestern Medical Center, Dallas, TX, United States, ³Pathology, UT Southwestern Medical Center, Dallas, TX, United States, ⁴Internal Medicine, UT Southwestern Medical Center, Dallas, TX, United States, ⁵Philips Medical Systems, Cleveland, OH, United States, ⁶Molecular Genetics, UT Southwestern Medical Center, Dallas, TX, United States, ⁷Urology, UT Southwestern Medical Center, Dallas, TX, United States, ⁸Internal Medicine & Kidney Cancer Program, UT Southwestern Medical Center, Dallas, TX, United States

MRI fat fraction (FF, Dixon) and % enhancement (DCE) measurements in vivo in clear cell renal cell carcinoma (ccRCC) were correlated with intracellular fat (Oil Red O), lipidomic profile (mass spectrometry), and cellular metabolomics of tissue samples isolated from anatomically co-registered locations in the same tumor. In vivo FF correlated positively with histologic fat content, spectrometric cholesterol and triglycerides; and negatively with spectrometric free fatty acids and phospholipids. ISUP grade 2 and 3 tumors exhibited marked intra-tumoral heterogeneity in FF whereas grade 4 tumors had reduced lipid accumulation. MRI-derived FF and % enhancement correlated with altered metabolic features of ccRCC.

123

Plasma 12



Liver Fat Reduction Following Bariatric Weight Loss Surgery is Greater in the Right Lobe of the Liver

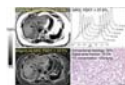
Soudabeh Fazeli Dehkordy¹, Tanya Wolfson², Cheng William Hong¹, Alexandra Schlein¹, Yesenia Covarrubias¹, Jennifer Cui¹, Ethan Z Sy¹, Adrija Mamidipalli¹, Gavin Hamilton¹, Scott B Reeder³, and Claude B Sirlin¹

¹Liver Imaging Group, Department of Radiology, University of California San Diego, San Diego, CA, United States, ²Computational and Applied Statistics Laboratory, University of California San Diego, San Diego, CA, United States, ³Department of Radiology, Medical Physics, Biomedical Engineering, Medicine, and Emergency Medicine, University of Wisconsin Madison, Madison, WI, United States

As liver fat is heterogeneously distributed, longitudinal changes in liver fat may vary between liver segments. We used confounder-corrected chemical-shift-encoded MRI to examine longitudinal changes in proton density fat fraction (PDFF) of individual liver segments in obese adults following a weight-loss program comprising a very low calorie diet (VLCD) followed by bariatric weight loss surgery (WLS). We observed that changes in PDFF in the 5-month postoperative period vary across segments, with right-lobe segments having more rapid reduction in liver fat.

124

Plasma 13



In Vivo Biochemical and Histological Validation of Proton Density Fat Fraction as a Quantitative Biomarker of Hepatic Steatosis

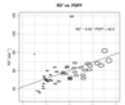
Scott B Reeder^{1,2,3,4,5}, Curtis N Wiens¹, Nathan Artz^{1,6}, Jeffrey B Schwimmer⁷, Rashmi Agni⁸, Rao Watson⁸, Tanya Wolfson⁹, Anthony Gamst¹⁰, Guilherme Campos^{11,12}, Santiago Horgan¹³, Luke Funk¹², Garth Jacobsen¹³, Jacob Greenberg¹², Alexandra Schlein¹⁴, Yesenia Covarrubias¹⁴, Jonathan C Hooker¹⁴, Michael S Middleton¹⁴, Gavin Hamilton¹⁴, Benjamin Ratliff¹³, Alan B McMillan¹, Diego Hernando^{1,2}, and Claude B Sirlin¹⁴

¹Radiology, University of Wisconsin, Madison, WI, United States, ²Medical Physics, University of Wisconsin, Madison, WI, ³Biomedical Engineering, University of Wisconsin, Madison, WI, United States, ⁴Medicine, University of Wisconsin, Madison, WI, United States, ⁵Emergency Medicine, University of Wisconsin, Madison, WI, United States, ⁶Diagnostic Imaging, St. Jude Children's Research Hospital, ⁷Pediatrics, University of California, San Diego, ⁸Pathology, University of Wisconsin, ⁹San Diego Super Computer Center, University of California, San Diego, ¹⁰Mathematics, University of California, San Diego, ¹¹Surgery, Virginia Commonwealth University, Richmond, VA, United States, ¹²Surgery, University of Wisconsin, Madison, WI, ¹³Surgery, University of California, San Diego, San Diego, CA, United States, ¹⁴Radiology, University of California, San Diego

The purpose of this study was to validate complex- and magnitude-based quantitative chemical-shift encoded MRI (CSE-MRI) to quantify PDFF as an accurate biomarker of hepatic steatosis. A biopsy-MRI correlation study was performed in 95 obese subjects undergoing bariatric weight loss surgery. The results of biochemical triglyceride, conventional histological, digital histological, and MR spectroscopy analyses were used as reference standards. Strong correlations were found between MRI-PDFF measured using both complex- and magnitude-based CSE-MRI methods vs. each reference standard. This is the first cross-sectional in-vivo study validating PDFF as a biomarker of hepatic steatosis using biochemical triglyceride concentration as the reference.

125

Plasma 14



Hepatic MRI-PDFF is positively correlated with R2* across a range of fat spectral models

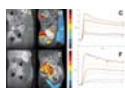
Cheng William Hong¹, Adrija Mamidipalli¹, Jonathan C Hooker¹, Gavin Hamilton¹, Tanya Wolfson², Soudabeh Fazeli Dehkordy¹, Michael S Middleton¹, Scott B Reeder³, Rohit Loomba⁴, and Claude B Sirlin¹

¹Liver Imaging Group, Department of Radiology, University of California, San Diego, San Diego, CA, United States, ²Computational and Applied Statistics Laboratory, University of California, San Diego, San Diego, CA, United States, ³Departments of Radiology, Medical Physics, Biomedical Engineering, Medicine, and Emergency Medicine, University of Wisconsin, Madison, Madison, WI, United States, ⁴NAFLD Research Center, Division of Gastroenterology, Department of Medicine, University of California, San Diego, San Diego, CA, United States

Confounder-corrected estimation of proton-density fat fraction (PDFF) concurrently estimates R2* (1/T2*), a parameter modeled to account for R2* signal decay. Although they are derived from the same mathematical model, PDFF and R2* are generally considered independent parameters. Emerging evidence, however, suggests that PDFF and R2* are positively correlated. This study confirms that PDFF and R2* are positively correlated, and this association is not a spurious result of the applied fat multiplex spectral model.

126

Plasma 15



Anatomical and functional deficits of the placenta identified by MRI in a rat model of preeclampsia

Emily Alexandria Waters¹, Pamela Monahan², Chad R Haney¹, Michael Kevin Fritsch³, Thomas J Meade⁴, and Kelly E Mayo²

¹Center for Advanced Molecular Imaging, Northwestern University, Evanston, IL, United States, ²Molecular Biosciences, Northwestern University, Evanston, IL, United States, ³Pathology, Northwestern University Feinberg School of Medicine, Chicago, IL, United States, ⁴Chemistry, Molecular Biosciences, and Neurobiology, Northwestern University, Evanston, IL, United States

Though a large percentage of poor pregnancy outcomes such as stillbirth and preterm birth are related to placental dysfunction, the gold-standard of diagnosing placental pathology remains examination of the placenta by a pathologist after delivery. We demonstrate that anatomical and functional MRI can detect features of placental pathology correlating with ex vivo measures in a rat model of pre-eclampsia.

Electronic Power Pitch Poster

Poster: Highlights of Multiparametric Acquisition & Reconstruction

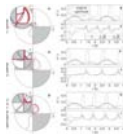
Exhibition Hall

Monday 14:45 - 15:45

Plasma 16

Relaxation in Polar Coordinates: Analysis and Optimization of MR-Fingerprinting

Jakob Assländer^{1,2}, Daniel K Sodickson^{1,2}, Riccardo Lattanzi^{1,2}, and Martijn A Cloos^{1,2}

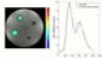


¹Dept. of Radiology - Bernard and Irene Schwartz Center for Biomedical Imaging, New York University School of Medicine, New York, NY, United States, ²Dept. of Radiology - Center for Advanced Imaging Innovation and Research, New York University School of Medicine, New York, NY, United States

This work analyses relaxation in balanced non-steady-state free precession sequences. Transforming the Bloch equation to polar coordinates gives insights in the spin dynamics and provides the basis for robust numerical optimization of the excitation pattern. The employed optimal control algorithm results in spin trajectories that allow for parameter mapping with considerably reduced noise, as shown in in vivo MR-fingerprinting experiments. The simple shapes of the optimized spin trajectories provide a basis for further analysis of the encoding process of relaxation times for parameter mapping.



Plasma 17



Quantification of Flow by Magnetic Resonance Fingerprinting

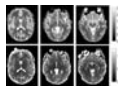
Sebastian Flassbeck¹, Simon Schmidt¹, Mathies Breithaupt^{1,2}, Peter Bachert¹, Mark E. Ladd¹, and Sebastian Schmitter^{1,3}

¹Medical Physics in Radiology, German Cancer Research Center (DKFZ), Heidelberg, Germany, ²Institute for Forensic Medicine and Traffic Medicine, Germany, ³Physikalisch-Technische Bundesanstalt (PTB), Braunschweig and Berlin, Germany

The goal of this work is to investigate and demonstrate 'flow MRF', a technique that quantifies T1 and T2 within static tissue regions around a vessel (e.g. vessel wall) with high spatial resolution while simultaneously quantifying the 3D blood velocity vector within the vessel with high precision and high spatiotemporal resolution. The results show that simultaneous mapping of pulsatile flow and T1/T2 quantification of static tissue is feasible with MRF. The quantification of flow as an additional parameter will further increase the efficiency of MRF and may provide new diagnostic value in cardiovascular diseases.



Plasma 18



Applications of Low Rank Modeling to Fast 3D Magnetic Resonance Fingerprinting (MRF)

Dan Ma¹, Eric Y. Pierre², Debra McGivney¹, Bhairav Mehta¹, Yong Chen¹, Yun Jiang¹, and Mark Griswold¹

¹Radiology, Case Western Reserve University, Cleveland, OH, United States, ²The Florey Institute of Neuroscience and Mental Health, Melbourne, Australia

The goal of this study is to accelerate the acquisition time of 3D magnetic resonance fingerprinting (MRF) using a low-rank model-based method kt-SVD-MRF. With a total factor of 144 acceleration rate, 3D T1, T2 and proton density (M0) maps can be acquired from a whole brain scan with a resolution of 1.17x1.17x3 mm³ in 2.7 minutes.

Plasma 19



Magnetic Resonance Fingerprint Compression with Multiple Channel Transmission

Riccardo Lattanzi^{1,2}, Bei Zhang¹, Florian Knoll¹, Jakob Assländer¹, and Martijn Cloos¹

¹Radiology, Center for Advanced Imaging Innovation and Research (CAI2R) and Bernard and Irene Schwartz Center for Biomedical Imaging, New York University School of Medicine, New York, NY, United States, ²Sackler Institute of Graduate Biomedical Sciences, New York University School of Medicine, New York, NY, United States

Singular value decomposition (SVD) and view-sharing compression can decrease the size of the dictionary without compromising accuracy in magnetic resonance fingerprinting (MRF). While the latter accounts for the B_1+ of multiple transmit channels in the dictionary, the SVD compression scheme was designed for single-channel transmission. In this work we extended SVD-based fingerprint compression to the case of two or more independent RF sources and evaluated its performance in simulation. We showed that accurate parametric maps can be achieved using only six SVD components, both in fully-sampled and highly under-sampled MRF experiments. Future work will include optimization of k-space under-sampling.

Plasma 20



Intra-Voxel Spatial Resolution Using Magnetic Resonance Fingerprinting

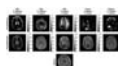
Thomas Amthor¹, Karsten Sommer¹, Peter Koken¹, Jakob Meineke¹, and Mariya Doneva¹

¹Philips Research, Hamburg, Germany

We demonstrate the use of Magnetic Resonance Fingerprinting to retrospectively increase spatial resolution in slice-encoding direction, making use of the non-uniform nature of the excitation slice profile. Assigning individual fingerprints to substances present at different spatial positions within the excited voxel, a multi-compartment analysis recovers the spatial distribution of the components.



Plasma 21



Dictionary approach to partial volume estimation with MR Fingerprinting: Validation and application to brain tumor segmentation

Anagha Deshmane¹, Debra McGivney², Chaitra Badve³, Vikas Gulani^{2,3}, and Mark Griswold²

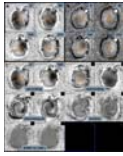
¹Biomedical Engineering, Case Western Reserve University, Cleveland, OH, United States, ²Radiology, Case Western Reserve University, Cleveland, OH, United States, ³Radiology, University Hospitals, Cleveland, OH, United States

MR Fingerprinting signal evolutions can be used to estimate partial volumes of tissues in addition to tissue relaxation times. Two approaches to tissue fraction estimation, a pseudoinverse calculation and dictionary-based or constrained solution, are quantitatively compared in the presence of four potential error sources. The constrained approach is found to more accurately estimate tissue fractions, and also to improve segmentation of pathology.

Plasma 22

Mitigation of Spiral Undersampling Artifacts in Magnetic Resonance Fingerprinting (MRF) by Adapted Interleave Reordering

Josef Pfeuffer¹, Argyrios Kechagias¹, Craig H. Meyer², Gregor Kördörfer¹, and Mathias Nittka¹



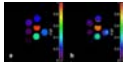
¹Application Development, Siemens Healthcare, Erlangen, Germany, ²Biomedical Engineering, University of Virginia, Charlottesville, VA, United States

In MRF fast spiral scanning is done with variable FA/TR using a highly – up to 48-fold – undersampled trajectory. Spatial undersampling artifacts are mitigated by the MRF dictionary-matching process for the resulting quantitative T1/T2 maps. In this study, we demonstrate how undersampling artifacts can bias MRF results and present strategies to minimize them by spiral-interleave reordering adapted to the specific MRF encoding scheme. An experimental procedure is developed to test for a potential spatial bias in a specific spiral and MRF encoding scheme. The sources of spatial variances are mitigated with appropriate distribution of undersampling artifacts over the temporal MRF encoding.

134

Plasma 23

Fat Signal Fraction Determination Using MR Fingerprinting



Jason Ostenson^{1,2} and E. Brian Welch^{1,3,4}

¹Vanderbilt University Institute of Imaging Science, Vanderbilt University, Nashville, TN, United States, ²Program in Chemical and Physical Biology, Vanderbilt University, Nashville, TN, United States, ³Department of Radiology and Radiological Sciences, Vanderbilt University, ⁴Department of Biomedical Engineering, Vanderbilt University

Magnetic resonance fingerprinting employing multiple echo times is used to quantify fat signal fraction both in phantoms and *in vivo* on a human 3 Tesla scanner. Reasonable agreement is seen in fat signal fraction maps and intra-class correlation between standard and MRF methods.

135

Plasma 24

Accelerated Magnetic Resonance Fingerprinting using Soft-weighted key-Hole (MRF-SOHO)



Gastao Cruz¹, Andreia S. Gaspar¹, Tom Bruijnen², René Botnar¹, and Claudia Prieto¹

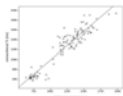
¹Division of Imaging Sciences and Biomedical Engineering, King's College London, London, United Kingdom, ²Center for image sciences, University Medical Center Utrecht, Utrecht, Netherlands

Magnetic Resonance Fingerprinting estimates multi-parametric maps from a series of highly undersampled time-point images. However, MRF scan times are still long due to the large amount of time-point images (~1000) required to produce accurate multi-parametric maps. Here we propose to exploit redundant information in time-point images with similar contrast to accelerate the MRF scan by further undersampling each time-point image and/or significantly reducing the number of required images in the series. The proposed approach achieved an acceleration factor of 5.7× compared to conventional undersampled MRF while maintaining parametric map quality.

136

Plasma 25

Magnetic Resonance Fingerprinting - Evaluation of Brain Gliomas in Comparison to a Conventional Advanced Tumor Protocol - Preliminary Study



Siegfried Trattnig^{1,2}, Wolfgang Bogner¹, Bernhard Strasser¹, Peter Bär¹, Simone Kitzer¹, Pavol Szomolanyi¹, Matthias Nittka³, Wolfgang Marik⁴, Martin Zalaudek¹, Markus Schreiner¹, and Elisabeth Springer¹

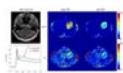
¹Department of Biomedical Imaging and Image-guided Therapy, Medical University of Vienna, High Field MR Center, Vienna, Austria, ²Christian Doppler Laboratory for Clinical Molecular MR Imaging, Vienna, Austria, ³Siemens Healthineers, Erlangen, Germany, ⁴Department of Biomedical Imaging and Image-guided Therapy, Medical University of Vienna, Vienna, Austria

Synopsis: MR Fingerprinting (MRF) was compared to an advanced brain tumor protocol in 10 patients with surgically proven gliomas. The T1 and T2 relaxation times provided by MRF in one scan showed a high correlation with conventionally measured T1 and T2 values. MRF obtained T1 and T2 values allowed a statistically significant differentiation between low and high grade gliomas. MRF with quantitative data and the possibility to generate synthetic MR contrast images may replace conventional MR sequences in the future.

137

Plasma 26

Joint estimation of arterial input function and tracer kinetic parameters from under-sampled DCE-MRI



Yi Guo¹, Sajjan Goud Lingala¹, R Marc Lebel², and Krishna S Nayak¹

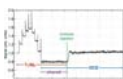
¹Electrical Engineering, University of Southern California, Los Angeles, CA, United States, ²GE Healthcare, Calgary, AB, Canada

Direct reconstruction of tracer kinetic (TK) parameter maps from under-sampled DCE-MRI has recently been demonstrated. However, this method assumes the arterial input function (AIF) is known or pre-determined. Any mismatches between the assumed AIF and the underlying patient-specific AIF can cause large inaccuracies in the final TK parameters. We propose a novel approach to extract patient-specific AIFs from under-sampled data, while jointly estimating the TK parameter maps. Reconstruction is performed by cycling through the problems of AIF extraction, TK parameter estimation and, data consistency. We demonstrate this approach on brain tumor DCE data sets, where high fidelity AIFs are extracted up to an under-sampling rate of 100x.

138

Plasma 27

Highly accelerated DCE imaging with integrated T1 mapping



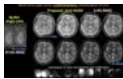
R Marc Lebel^{1,2,3}, Yi Guo⁴, Sajjan Goud Lingala⁴, Richard Frayne^{2,3}, and Krishna S Nayak⁴

¹GE Healthcare, Calgary, AB, Canada, ²Radiology, University of Calgary, Calgary, AB, Canada, ³Seaman Family Centre, Calgary, AB, Canada, ⁴Electrical Engineering, University of Southern California, Los Angeles, CA, United States

Dynamic contrast enhanced (DCE) MRI requires accurate and precise baseline T₁ and M₀ maps for pharmacokinetic modeling. Advances in dynamic acquisitions and reconstructions have enabled high resolution DCE imaging with full anatomical coverage. Rapidly obtaining high SNR T₁/M₀ maps with the same spatial resolution has become a limiting factor for advanced DCE methods. We present a single highly accelerated acquisition that first performs the T₁/M₀ mapping then dynamic imaging. A model-based reconstruction is used to estimate the T₁/M₀ maps. This method makes effective use of scan time and generates maps that are superior to separately acquired ones.

139

Plasma 28



Calibrationless Parallel Imaging in Multi Echo/Contrast Data

Berkin Bilgic¹, Bo Zhao¹, Itthi Chatnuntawech², Lawrence L Wald¹, and Kawin Setsompop¹¹Martinos Center for Biomedical Imaging, Charlestown, MA, United States, ²National Nanotechnology Center, Pathum Thani, Thailand

Parallel imaging relies on fully-sampled calibration data to estimate k-space kernels or sensitivities used to reconstruct subsampled acquisitions. Emerging techniques use low-rank modeling, or joint estimation of sensitivities and image content via nonlinear optimization, to reduce the dependency on calibration data. In a typical study, images at multiple echoes/contrasts are acquired using the same coil sensitivities. Here, we exploit this joint information to dramatically improve conditioning of calibrationless nonlinear inversion and employ joint sparsity to improve reconstruction. To achieve better performance, we also propose complementary k-space undersampling between images to form a composite image with reduced aliasing to initialize the optimization.

140

Plasma 29



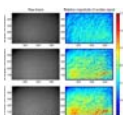
Accelerated Cardiac Diffusion Tensor Imaging Using a Joint Low-Rank and Sparsity Constraint

Sen Ma^{1,2}, Christopher Nguyen¹, Anthony Christodoulou^{1,3}, Daniel Luthringer⁴, Jon Kobashigawa³, and Debiao Li^{1,2}¹Biomedical Imaging Research Institute, Cedars-Sinai Medical Center, Los Angeles, CA, United States, ²Department of Bioengineering, University of California, Los Angeles, Los Angeles, CA, United States, ³Heart Institute, Cedars-Sinai Medical Center, Los Angeles, CA, United States, ⁴Department of Pathology, Cedars-Sinai Medical Center, Los Angeles, CA, United States

We present an image reconstruction technique to accelerate cardiac diffusion tensor imaging by jointly applying a low-rank and spatial sparsity constraint. We evaluated four acquisition schemes at different undersampling levels on 9 ex vivo diseased human heart, evaluating the reconstruction quality based on the resulting helix angle (HA) maps and helix angle transmural (HAT) values. A Wilcoxon signed rank test was performed to statistically evaluate changes in HAT to determine the highest achievable acceleration factor for each acquisition scheme. Our framework shows promise in greatly reducing scan time while preserving the fiber architecture features of heart failure.

141

Plasma 30



An open-source hardware and software system for video-gated MRI

Nicolai Spicher¹, Stephan Orzada², Stefan Maderwald², Markus Kukuk¹, and Mark E Ladd^{2,3}¹University of Applied Sciences and Arts Dortmund, Dortmund, Germany, ²Erwin L. Hahn Institute for Magnetic Resonance Imaging, University Duisburg-Essen, Essen, Germany, ³Division of Medical Physics in Radiology, German Cancer Research Center, Heidelberg, Germany

The limitations of contact-based hardware (e.g. electrocardiography, pulse oximetry) for cardiac activity measurement pose an obstacle in many ultra-high-field MRI examinations. In this work, we present a freely available hardware and software system for acquisition and processing of video signals from human skin that we developed with the aim to make this contact-free method available to other researchers.

Electronic Power Pitch Poster

Poster: Cutting Edge fMRI

Exhibition Hall

Monday 17:15 - 18:15

Moderators: Nicholas Blockley & Eric Wong

237

Plasma 1



Cortical depth-dependent fMRI: heterogeneity across tasks, across participants, across days and along the cortical ribbon

Laurentius Huber¹, Daniel A Handwerker¹, Andrew Hall¹, David C Jangraw², Javier Gonzalez-Castillo¹, Maria Guidi³, Dimo Ivanov⁴, Benedikt A Poser⁴, and Peter A Bandettini¹¹SFIM, NIMH, Bethesda, MD, United States, ²NIMH, United States, ³Max Planck Institute for human cognitive and Brain science, Leipzig, Germany, ⁴MBIC, Maastricht University, Netherlands

Measurements of depth-dependent cortical activity provide insights on directional activity between brain areas. While previous studies demonstrated the feasibility of human depth-dependent fMRI, the stability and reliability of depth-dependent results are less studied. In this work, we investigate sources of inconsistencies in depth-dependent activity profiles. We find that depth-dependent activity profiles are highly reproducible across different scanning sessions. They are, however, quite variable within cortical areas across different cross sections along the cortical ribbon. Only when depth-dependent profiles are considered with respect to their location along the cortical ribbon, task-driven modulations of input-output activity become consistent across participants.

238

Plasma 2



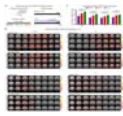
Simultaneous GCaMP6 based fiber photometry and fMRI in rats

Zhifeng Liang^{1,2}, Yuncong Ma², and Nanyin Zhang²¹Institute of Neuroscience, Chinese Academy of Sciences, Shanghai, People's Republic of China, ²Department of Biomedical Engineering, Pennsylvania State University, PA, United States

Measuring neural activities simultaneously with fMRI using electrophysiology approaches has been valuable in elucidating neural basis of BOLD signals, but is also technically challenging due to interferences from MRI scanners. Optical recording of neural activities such as calcium signals has minimal interferences from MRI, and thus has opened new avenues of simultaneous acquisition of neural and BOLD signals. The current study first demonstrated the feasibility of using protein based calcium indicator (GCaMP6) to simultaneously and repeatedly acquire calcium and BOLD signals in the MRI scanner, with significant increases of both signals in response to visual stimulation.

Plasma 3

Optogenetic resting-state fMRI reveals thalamic modulation of long-range sensory networks



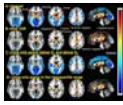
Alex T. L. Leong^{1,2}, Xunda Wang^{1,2}, Russell W. Chan^{1,2}, Leon C. Ho^{1,2}, Yongrong Qiu^{1,2}, Celia M. Dong^{1,2}, and Ed X. Wu^{1,2}

¹Laboratory of Biomedical Imaging and Signal Processing, The University of Hong Kong, Hong Kong, Hong Kong, ²Department of Electrical and Electronic Engineering, The University of Hong Kong, Hong Kong, Hong Kong

One grand challenge in contemporary neuroscience is to achieve an integrated understanding of large-scale brain-wide networks. Resting-state functional MRI (rsfMRI) has helped reveal such brain-wide networks, yet, the neural bases underlying them remain unclear. Utilizing optogenetic excitation and pharmacological inactivation to manipulate the neural activity of somatosensory thalamocortical neurons, the present study demonstrated that rsfMRI connectivity is enhanced and decreased respectively. Furthermore, our findings suggest that optogenetically-evoked propagating low frequency activity (~1Hz) within the thalamo-cortico-thalamic network facilitate the enhancement of rsfMRI connectivity. Our work offers an exciting avenue to dissect the underlying neural bases of brain-wide functional connectivity.

240

Plasma 4



Global signal regression alters the correlation between resting-state BOLD fluctuations and EEG vigilance measures

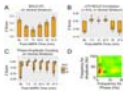
Maryam Falahpour¹, Alican Nalci¹, Chi Wah Wong¹, and Thomas Liu¹

¹Center for functional MRI, University of California San Diego, San Diego, CA, United States

Global signal regression (GSR) is a commonly used preprocessing approach in the analysis of resting state fMRI data. Utilizing simultaneously acquired EEG/fMRI data in humans, we found that GSR alters the correlation between the resting-state BOLD fluctuations and EEG vigilance. We show that GSR reveals BOLD-EEG correlations that are otherwise obscured and use a time segmentation approach to argue that the observed effects are not simply an artifact of GSR.

241

Plasma 5



What is the neurophysiological bases of resting state functional connectivity?

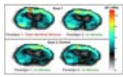
Hanbing Lu¹, Saul Jaime², Elliot A Stein¹, Jose E Cavazos², and Yihong Yang¹

¹National Institute on Drug Abuse, NIH, Baltimore, MD, United States, ²University of Texas Health Science Center at San Antonio, TX, United States

Despite wide application of resting state functional connectivity (rsFC) in systems neuroscience, fundamental aspects of rsFC remain poorly understood. Concurrent multi-channel electrophysiological recording and fMRI were performed in rat striatum along with pharmacological manipulation of VTA dopamine neuronal activity. Results suggest that LFPs of different frequency bands contribute distinctively and differentially to the observed BOLD fluctuations, and that cross-frequency phase-amplitude coupling (PAC) is the organizing mechanism through which low frequency LFPs orchestrate neural activity that underlies the BOLD rsFC. Our data imply that where there is a synchronized low frequency LFP signal, there is also resting state BOLD functional connectivity. rsFC does not necessarily reflect structural connectivity.

242

Plasma 6



Functional Neuroimaging in the Brain using Magnetic Resonance Elastography

Samuel Patz^{1,2}, Navid Nazari³, Paul E. Barbone⁴, Ben Fabry⁵, Dan Fovargue⁶, David Nordsletten⁶, and Ralph Sinkus⁶

¹Radiology, Brigham & Women's Hospital, Boston, MA, United States, ²Harvard Medical School, Boston, MA, United States, ³Biomedical Engineering, Boston University, Boston, MA, United States, ⁴Mechanical Engineering, Boston University, Boston, MA, United States, ⁵Physics, University of Erlangen-Nuremberg, Erlangen, Germany, ⁶Biomedical Engineering, Kings College London, London, United Kingdom

Using electrical stimulation of the hind limb, Magnetic Resonance Elastography (MRE) was used to observe localized changes in the complex shear modulus $G = G' + iG''$ of the mouse brain cortex. "Stimulation" and "no stimulation" paradigms were alternated every 10s to avoid habituation. An average increase of ~14% in G' was observed whereas no significant change was seen for G'' . The effect was observed in six of seven mice studied. The mechanism responsible for this effect is hypothesized to be due to calcium influx into the neuronal cells.

243

Plasma 7



Fully Automated Learning based Method for resting state fMRI Connectomics Analysis

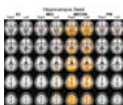
Arathi Sreekumari¹, Radhika Madhavan¹, Rakesh Mullick¹, Teena Shetty², Pratik Mukherjee³, Joseph Masdeu⁴, Luca Marinelli⁵, and Suresh Emmanuel Joel¹

¹GE Global Research, Bangalore, India, ²Hospital for Special Surgery, New York, NY, United States, ³University of California, San Francisco, San Francisco, CA, United States, ⁴Houston Methodist, Houston, TX, Houston, TX, United States, ⁵GE Global Research, Niskayuna, NY, United States

Machine learning approaches are increasingly being used to identify discriminative features derived from functional connectome data that best separate a diseased group from healthy cohorts. Here, we propose a novel framework for longitudinal prediction of disease outcome, using a combination of unsupervised and supervised learning approaches. Using this framework, we achieve 81% accuracy for prediction of mild traumatic brain injury outcome at 3-months by learning features from functional connectomes at the acute stage of injury (<1 week).

244

Plasma 8



A Multiband Multi-Echo Simultaneous ASL/BOLD Acquisition for Resting State Functional Connectivity

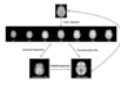
Alexander D. Cohen¹, Andrew S. Nencka¹, and Yang Wang¹

¹Radiology, Medical College of Wisconsin, Milwaukee, WI, United States

A multiband multi-echo simultaneous ASL/BOLD sequence was developed and utilized to evaluate resting state connectivity. ASL sequences have inherently long TRs due to the tagging and delay components. To compensate for this, four echoes were collected allowing multi-echo independent component analysis (ME-ICA) to be employed to denoise the BOLD data. A seed-based analysis was used for the computation of functional connectivity. Temporal signal to noise ratio (tSNR) was significantly higher for the denoised data resulting in an increase in connectivity strength, cluster size, and number of clusters. The sequence also allowed perfusion-weighted connectivity to be computed.

245

Plasma 9



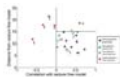
The first two years of whole brain functional development can be separated into three distinct time periods
Weiyun Yin¹ and Weili Lin²

¹Department of Biomedical Engineering and Biomedical Research Imaging Center, University of North Carolina at Chapel Hill, Chapel Hill, NC, United States, ²Department of Radiology and Biomedical Research Imaging Center, University of North Carolina at Chapel Hill, Chapel Hill, NC, United States

Resting functional connectivity has been utilized to characterize early brain functional development. Most of the studies to date have grouped subjects based on biological age, enabling assessment of brain functional maturation. However, this grouping approach assumes that subjects at the same age exhibit similar functional maturation, which may not be valid considering the paces of functional maturation could substantially vary among individuals. In this study, the normalized-Cut method was used to cluster connectivity matrixes of 71 normally developing children, 0 to 2 years of age, into distinct age periods (functional age) reflecting stable brain functional connectivity. We found that brain functional development during the first two years of life consists of three distinct time periods 0 – 2, 3 – 6, and 7 - 26 months, respectively. In addition, 17 core brain regions were identified, which largely drove our clustering results. These regions could be of critical importance for early brain development.

246

Plasma 10



MRI Connectivity Predictors of Post-Surgical Seizure Outcome in Temporal Lobe Epilepsy

Victoria L Morgan¹, Dario J Englot², Adam W Anderson³, Bennett A Landman⁴, Ahmet Cakir⁴, Baxter P Rogers¹, and Bassel Abou-Khalil⁵

¹Institute of Imaging Science, Vanderbilt University, Nashville, TN, United States, ²Neurosurgery, Vanderbilt University, Nashville, TN, United States, ³Biomedical Engineering, Vanderbilt University, Nashville, TN, United States, ⁴Electrical Engineering and Computer Science, Vanderbilt University, Nashville, TN, United States, ⁵Neurology, Vanderbilt University, Nashville, TN, United States

Surgical resection of the mesial temporal lobe is a common treatment of drug-resistant temporal lobe epilepsy (TLE). The ability to more accurately predict post-surgical seizure outcome in these patients is a significant clinical challenge. Towards this end, MRI functional and structural connectivity were used to identify a common pattern across a seizure propagation network in TLE patients with seizure free outcome. Then, in test patients with good and bad outcomes, similarity with the model pattern was significantly associated with seizure outcome. Therefore, this non-invasive method may predict seizure outcomes in TLE, which was not possible from the clinical assessments alone.

247

Plasma 11



CEST fMRI at ultra-high magnetic field

Tangi Roussel¹, Lucio Frydman², Denis Le Bihan¹, and Luisa Ciobanu¹

¹NeuroSpin, Commissariat à l'Energie Atomique et aux Energies Alternatives, Gif-sur-Yvette, France, ²Department of Chemical Physics, Weizmann Institute of Science, Rehovot, Israel

BOLD indirectly measures brain activity based on neurovascular coupling, a reporter which is naturally poor in both its spatial and temporal resolutions. Emerging methods involving spectroscopy (fMRS) and diffusion fMRI suggest that metabolic and structural modifications are taking place in the activated cells. In this paper, we introduce Chemical Exchange Saturation Transfer (CEST)-weighted fMRI as a new method to explore changes in rat brain activation at 17.2T. Monte Carlo simulations were performed to optimize the acquisition and processing methods. Experimentally, CEST-weighted fMRI activation maps showed negative contrast at +1.2ppm most likely originating from changes in the glucose metabolism.

248

Plasma 12



EPI-signal fluctuations at the cardiac frequency: A tissue-specific quantification of inflow, displacement and potential oxygenation effects over the cardiac cycle.

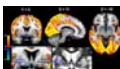
Olivia Viessmann¹ and Peter Jezzard¹

¹FMRIB Centre, Nuffield Department of Clinical Neurosciences, Oxford University, Oxford, United Kingdom

The impact and transmission mechanisms of the cardiac arterial pressure wave into brain tissue are not fully understood. It is hypothesised that age-related arterial stiffening and increased CBF pulsatility leads to propagation of the arterial wave further down the vascular tree causing tissue damage. Here we quantify inflow (\$\$\$\$) and displacement/oxygenation (\$\$\$T_2^\$\$\$) induced fluctuations of the EPI-signal at the cardiac frequency. We relate the EPI-signal phase at the cardiac frequency to the fluctuations of \$\$\$\$_0\$\$\$ and \$\$\$T_2^\$\$\$ over the cardiac cycle in the arteries, veins and tissue.

249

Plasma 13



The global resting-state fMRI signal is associated with opposite changes at subcortical structures regulating arousal.

Xiao Liu^{1,2}, Jacco A de Zwart², David A Leopold³, and Jeff H Duyn²

¹Biomedical Engineering, Pennsylvania State University, University Park, PA, United States, ²National Institute of Neurological Disorders and Stroke, National Institutes of Health, Bethesda, MD, United States, ³National Institute of Mental Health, National Institutes of Health, MD, United States

Spontaneous, large scale fluctuations (LSF) in neocortical fMRI activity may result from arousal variations. To investigate the role of arousal, we examined an fMRI database for local fMRI changes at subcortical arousal-regulating structures associated with widespread fMRI co-activations in the neocortex. We identified three subcortical regions that showed anti-polar signal changes with LSF. These regions, known for promoting wakefulness, included the Nucleus Basalis, the Dorsal Midline Thalamus, and the Substantia Nigra. This finding is further evidence of a putative role of arousal in LSF, and suggest that caution should be exercised when extracting functional connectivity measures from fMRI data.

250

Plasma 14



Functional connectivity is globally altered by schizophrenia-linked genes

Garth J Thompson^{1,2}, Karen Perez De Arce³, Basavaraju G Sanganahalli^{1,2,4}, Stephen M Strittmatter⁵, Thomas Biederer³, and Fahmeed Hyder^{1,2,4,6}

¹Radiology and Biomedical Imaging, Yale University, New Haven, CT, United States, ²Magnetic Resonance Research Center (MRRC), Yale University, New Haven, CT, United States, ³Neuroscience, Tufts University School of Medicine, Boston, MA, United States, ⁴Quantitative Neuroscience with Magnetic Resonance (QNMR) Core Center, Yale University, New Haven, CT, United States, ⁵Cellular Neuroscience, Neurodegeneration, and Repair Program, and Departments of Neurology and Neurobiology, Yale University School of Medicine, New Haven, CT, United States, ⁶Biomedical Engineering, Yale University, New Haven, CT, United States

Resting state fMRI shows increased global synchrony in schizophrenia at rest, but mechanisms remain speculative. We tested mice with knockout of SynCAM1 (related to synaptic organization), LRRTM1 (related to schizophrenia symptoms) and both genes using whisker-stimulation and resting-state fMRI. SynCAM1 was linked to stronger whisker barrel activation and to greater functional connectivity. However, this was lost if global signal regression was performed. Global signal amplitude was significantly higher in SynCAM1 knockout mice, and amplified by the additional knockout of LRRTM1. We hypothesize this is due to disrupted synaptic connections by SynCAM1 knockout, which are partially protected when LRRTM1 is present.

251

Plasma 15



Population Receptive Field Mapping of Human Somatosensory Cortex at 7 T
Michael Asghar¹, Rosa Sanchez-Panchuelo¹, Denis Schluppeck², and Susan Francis¹

¹SPMIC, School of Physics, University of Nottingham, Nottingham, United Kingdom, ²School of Psychology, University of Nottingham, Nottingham, United Kingdom

To advance the investigation of function and structure in human somatosensory areas, detailed topographic maps that are reproducible across time are invaluable. In previous 7 Tesla fMRI studies using travelling wave (TW) and event-related (ER) paradigms, the functional parcellation of digit representations in human S1 has been shown. Here, we present the application of 'population Receptive Field' analysis (pRF) to high-resolution fMRI data from somatosensory cortex. The pRF method can provide information beyond preferred stimulus location, such as measures of receptive field size. We also show how surface coils can be used to improve spatial resolution in somatotopic maps.

Electronic Power Pitch Poster

Poster: Quantitation, Prediction & Machine Learning in the Brain

Exhibition Hall

Monday 17:15 - 18:15

252

Plasma 16



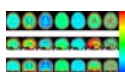
Machine Learning Based Diagnosis of Early Parkinson's Disease using QSM
Seon Lee¹, Joon Yul Choi², Jeehun Kim², Sun Won Park³, and Jongho Lee²

¹Department of Mechanical and Aerospace Engineering, Seoul National University, Seoul, Korea, Republic of, ²Department of Electrical and Computer Engineering, Seoul National University, Seoul, Korea, Republic of, ³Department of Radiology, Seoul National University Boramae Medical Center, Seoul, Korea, Republic of

This study proposed a support vector machine model to classify early PD patients from healthy controls using QSM. The results validated better performance of SVM than conventional logistic regression based on statistical ordering of backward feature selection. This computer aided technique may help to reduce misdiagnosis rate of early-PD patients.

253

Plasma 17



Reproducibility of advanced MR metrics in a multi-site, multi-vendor study of mild traumatic brain injury

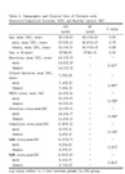
Andrew Scott Nencka¹, Timothy Meier², Yang Wang¹, Yu-Chien Wu³, Brad Swearingen², Robin Karr¹, Melissa Koschnitzke², Andy Saykin³, Michael McCrea², and Kevin M Koch¹

¹Radiology, Medical College of Wisconsin, Milwaukee, WI, United States, ²Neurosurgery, Medical College of Wisconsin, Milwaukee, WI, United States, ³Radiology and Imaging Services, Indiana University, Indianapolis, IN

The Advanced Research Core of the Concussion Assessment Research and Education consortium includes a multi-site, multi-vendor, multi-contrast imaging acquisition protocol with T2 FLAIR, quantitative T2*, task free fMRI, ASL, and DTI. This abstract describes the variance of measurements made in the first year and a half of the study from these imaging methods across a cohort of non-contact sport control athletes. With the variance of these measurements in the collegiate athlete population known, the sensitivities of the individual and combined contrasts to diagnose injury and recovery can be assessed.

254

Plasma 18

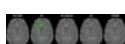


Characteristic Changes of Volume and Shape of Subcortical Structures in Obsessive-Compulsive Disorder
Lianqing Zhang¹, Xinyu Hu¹, Ming Zhou¹, Lu Lu¹, Xiaoxiao Hu¹, and Xiaoqi Huang¹

¹Radiology Department, Huaxi MR Research Center (HMRC), West China Hospital of Sichuan University, Chengdu, People's Republic of China

We analysis subcortical nucleus volume and shape alterations in a relatively large sample of drug-naive adult patients with Obsessive-Compulsive disorder by using an automatically segmentation and vertex-based shape analysis protocol. Our findings indicated that (i)Gender effects were found in OCD, male patients seems are affected in reward system whereas females might have more disrupted stratum-pallidum-thalamus pathway which might be related to chronic stress. (ii)Shape analysis may provide more anatomical change information from a different perspective. Future structural research should consider shape and volume alterations together when explore brain changes.

Plasma 19

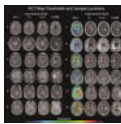


PARTIAL VOLUME ESTIMATION IN MULTIPLE SCLEROSIS LESION SEGMENTATION

Mário João Fartaria^{1,2,3}, Alexandra Şorega⁴, Tobias Kober^{1,2,3}, Gunnar Krueger⁵, Cristina Granziera^{6,7}, Alexis Roche^{1,2,3}, and Meritxell Bach Cuadra^{2,3,8}

¹Advanced Clinical Imaging Technology, Siemens Healthcare AG, Lausanne, Switzerland, ²Department of Radiology, Centre Hospitalier Universitaire Vaudois (CHUV) and University of Lausanne (UNIL), Lausanne, Switzerland, ³Signal Processing Laboratory (LTS 5), Ecole Polytechnique Fédérale de Lausanne (EPFL), Lausanne, Switzerland, ⁴Department of Radiology, Valais Hospital, Sion, Switzerland, ⁵Siemens Medical Solutions USA, Boston, MA, United States, ⁶Martinos Center for Biomedical Imaging, Massachusetts General Hospital and Harvard Medical School, Boston, MA, United States, ⁷Department of Clinical Neurosciences, Centre Hospitalier Universitaire Vaudois (CHUV) and University of Lausanne (UNIL), Lausanne, Switzerland, ⁸Medical Image Analysis Laboratory (MIAL), Centre d'Imagerie BioMédicale (CIBM), Lausanne, Switzerland

Partial volume (PV) is the effect of having a mixture of tissues present within a voxel. This effect occurs in tissue borders and affects small structures such as small multiple sclerosis (MS) lesions. Ignoring PV effects in volumetry may lead to significant estimation errors. Here, we propose a novel automated MS lesion segmentation technique that takes PV effects into account. The proposed method shows higher accuracy in terms of lesion volume estimation compared to a manually segmented ground truth as well as significant improvement in detection of small lesions, also in comparison to two software packages for MS lesion segmentation.



Predictive cytological topography highlights regions of pathologically confirmed non-enhancing hypercellular tumor in glioblastoma patients

Sarah L Hurrell¹, Elizabeth Cochran², Sean D McGarry¹, Amy L Kaczmarowski¹, Jennifer Connelly³, Wade Mueller⁴, Scott D Rand¹, Kathleen M Schmainda¹, and Peter S LaViolette¹

¹Radiology, Medical College of Wisconsin, Milwaukee, WI, United States, ²Pathology, Medical College of Wisconsin, Milwaukee, WI, United States, ³Neurology, Medical College of Wisconsin, Milwaukee, WI, United States, ⁴Neurosurgery, Medical College of Wisconsin, Milwaukee, WI, United States

This study combines clinical brain cancer imaging and pathological microscopy with machine learning to generate predictive maps off pathological features (i.e. new contrasts) based on segmented histological cellularity. Predictive cytological topography (PCT) maps of cellularity were utilized to detect additional pathologically confirmed infiltrative glioblastoma cellularity beyond margins of contrast enhancement.

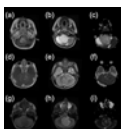


Radiogenomics of 201 WHO grade 2 and 3 gliomas

Manabu Kinoshita^{1,2}, Hideyuki Arita², Masamishi Takahashi³, Yoshitaka Narita³, Yuzo Terakawa², Naohiro Tsuyuguchi², Yoshiko Okita², Masahiro Nonaka², Shusuke Moriuchi², Junya Fukai², Shuichi Izumoto², Kenichi Ishibashi², Yoshinori Kodama², Kanji Mori², Koichi Ichimura³, and Yonehiro Kanemura^{2,4}

¹Neurosurgery, Osaka Medical Center for Cancer and Cardiovascular Diseases, Osaka, Japan, ²Kansai Molecular Diagnosis Network for CNS Tumors, Osaka, Japan, ³National Cancer Center Hospital, Japan, ⁴Osaka National Hospital, Osaka, Japan

Genetic alterations found in WHO grade 2 and 3 gliomas include IDH1/2 and TERT promoter mutations and 1p19q co-deletion. In this research, the authors attempted to test the hypothesis that genetic alterations could contribute to the locations and texture of the tumor by analyzing 201 WHO grade 2 and 3 gliomas using radiogenomic analysis. The authors were able to confirm the hypothesis that genetic alterations do contribute to the locations and textures of the tumor. 15 radiomic features were identified and those features were able to identify 3 genetic subgroups of WHO grade 2 and 3 gliomas.



Classification of Pediatric Brain Tumours using Apparent Diffusion Coefficient – a Multi-Centre Study

Jan Novak^{1,2}, Niloufar Zarinabad^{1,2}, Theodoros N Arvanitis³, Lesley MacPherson⁴, Daniel Rodriguez^{5,6}, Richard Grundy⁶, Dorothee Auer^{7,8}, Tim Jaspan⁶, Shivaram Avula⁹, Laurence Abernethy⁹, Patrick Hales¹⁰, Ramneek Kaur¹⁰, Darren Hargrave¹¹, Dipayan Mitra¹², Simon Bailey¹³, Nigel Davies¹⁴, Christopher Clark¹⁰, and Andrew Peet^{2,15}

¹Institute of Cancer and Genomic Sciences, University of Birmingham, Birmingham, United Kingdom, ²Oncology, Birmingham Children's Hospital, Birmingham, United Kingdom, ³Institute of Digital Healthcare, University of Warwick, Coventry, United Kingdom, ⁴Radiology, Birmingham Children's Hospital, Birmingham, United Kingdom, ⁵Division of Clinical Neuroscience, University of Nottingham, Nottingham, United Kingdom, ⁶The Children's Brain Tumour Research Centre, University of Nottingham, Nottingham, United Kingdom, ⁷Sir Peter Mansfield Imaging Centre, University of Nottingham, Nottingham, United Kingdom, ⁸Department of Neuroradiology, Nottingham University Hospital Trusts, Nottingham, United Kingdom, ⁹Radiology, Alder Hey Children's NHF Foundation Trust, Liverpool, United Kingdom, ¹⁰Developmental Imaging and Biophysics Section, University College London, London, United Kingdom, ¹¹Haematology and Oncology Department, Great Ormond Street Children's Hospital, London, United Kingdom, ¹²The Newcastle upon Tyne Hospitals NHS Foundation Trust, Newcastle, United Kingdom, ¹³Sir James Spence Institute of Child Health, Royal Victoria Infirmary, Newcastle upon Tyne, United Kingdom, ¹⁴Radiation Protection Services, University Hospitals Birmingham NHS Foundation Trust, Birmingham, United Kingdom, ¹⁵Institute of Cancer and Genomic Sciences, University of Birmingham, BIRMINGHAM, United Kingdom

The purpose of the study was to investigate the potential of apparent diffusion coefficient (ADC) to discriminate between paediatric cerebellar tumours on a multicentre basis using histograms. A total of 117 paediatric patients with cerebellar tumours (55 Medulloblastomas, 36 Pilocytic Astrocytomas and 26 Ependymomas) were imaged using diffusion weighted imaging across 12 different hospitals using a total of 18 different scanners. Overall classification accuracies for the ADC histogram metrics were 86 % using Naïve Bayes and 84 % for Random Forest classifier.



Exploiting radiogenomics data for personalised prediction of glioblastoma

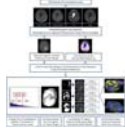
Paul Blakeley^{1,2}, Chia-Feng Lu^{2,3,4}, Fei-Ting Hsu^{2,5}, Li-Chun Hsieh^{2,5}, Yu-Chieh Jill Kao^{2,3}, Huai-Lu Chen^{1,2}, Ping-Huei Tsai^{2,3,5}, Hua-Shan Liu^{2,6}, Gilbert Aaron Lee^{1,2}, and Cheng-Yu Chen^{2,3,5}

¹Department of Medical Research, Taipei Medical University Hospital, Taipei, Taiwan, ²Translational Imaging Research Center, College of Medicine, Taipei Medical University, Taipei, Taiwan, ³Department of Radiology, School of Medicine, College of Medicine, Taipei Medical University, Taipei, Taiwan, ⁴Department of Biomedical Imaging and Radiological Sciences, National Yang-Ming University, Taipei, Taiwan, ⁵Department of Medical Imaging, Taipei Medical University Hospital, Taipei, Taiwan, ⁶School of Biomedical Engineering, College of Biomedical Engineering, Taipei Medical University, Taipei, Taiwan

The present study demonstrates the feasibility of machine learning in radiogenomics to predict patient outcome. The Random Forest Survival model is able to predict patient survival based on apparent diffusion coefficients or gene expression data without any prior knowledge.

260

Plasma 24



Multiparameter MRI Predictors of Extreme Survival in Glioblastoma Multiforme
Natarajan Raghunand¹, Olya Stringfield², John Arrington³, and Robert A Gatenby³

¹Cancer Imaging & Metabolism, Moffitt Cancer Center, Tampa, FL, United States, ²IRAT Shared Service, Moffitt Cancer Center, Tampa, FL, United States, ³Diagnostic Imaging & Interventional Radiology, Moffitt Cancer Center, Tampa, FL, United States

We retrospectively analyzed initial MRI scans in two cohorts diagnosed with Glioblastoma Multiforme (GBM). The Long-Term Survival (LTS) cohort included 13 subjects who survived >36 months post-diagnosis, while the Short-Term Survival (STS) cohort included 12 subjects who survived ≤18 months. Tumor voxels were clustered by the normalized signal intensities on post-contrast T1w and FLAIR sequences into 6 distinct "habitats". The LTS cohort were found to have a significantly higher fraction of Habitat 6 (high signal on T1w and FLAIR sequences) and lower fraction of Habitat 2 (low signal on T1w and high signal on FLAIR) compared with the STS cohort.

261

Plasma 25



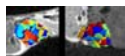
Multi-Site Concordance of DSC-MRI Analysis for Brain Tumors: Results of a NCI Quantitative Imaging Network DSC-MRI Collaborative Project
Kathleen M Schmainda¹, Melissa A Prah¹, Scott D Rand², Mark Muzi³, Swati D Rane³, Xiao Da⁴, Yi-Fen Yen⁵, Jayashree Kalpathy-Cramer⁶, Thomas L Chenevert⁶, Dariya Malyarenko⁶, Benjamin Hoff⁶, Brian Ross⁶, Yue Cao⁷, Madhava P Aryal⁷, Bradley Erickson⁸, Panagiotis Korfiatis⁸, Laura Bell⁹, Leland Hu¹⁰, and Christopher Chad Quarles⁹

¹Radiology, Medical College of Wisconsin, Milwaukee, WI, United States, ²Radiology, Medical College of Wisconsin, WI, United States, ³Radiology, University of Washington, WA, United States, ⁴Radiology, Massachusetts General Hospital, MA, United States, ⁵Radiology, Massachusetts General Hospital, Charlestown, MA, United States, ⁶Radiology, University of Michigan, Ann Arbor, MI, United States, ⁷Radiation Oncology, University of Michigan, Ann Arbor, MI, United States, ⁸Mayo Clinic, MN, United States, ⁹Barrow Neurological Institute, Phoenix, AZ, United States, ¹⁰Radiology, Mayo Clinic, Phoenix, AZ, United States

Though DSC-MRI perfusion is of well-known benefit for the evaluation of brain tumors, clinical translation has been hampered by a lack of confidence in the consistency of the derived RCBV (relative cerebral blood volume) and cerebral blood flow (CBF) values across sites and platforms. This multi-site and multi-platform study, for which the same patient data set was analyzed, demonstrated substantial consistency in RCBV across software sites and platforms and the ability of each to distinguish low-grade from high-grade tumor. In addition, a single RCBV threshold was identified for which all platforms maintained good accuracy.

262

Plasma 26



Perfusion-supervoxels for DCE-MRI based tumor subregion assessment

Benjamin John Irving¹, Jolanta Mirecka¹, Ana L Gomes², Danny Allen², Paul Kinchesh², Veerle Kersemans², Stuart Gilchrist², Sean Smart², Julia A Schnabel³, Sir J Michael Brady², and Michael Chappell¹

¹Institute of Biomedical Engineering, University of Oxford, Oxford, United Kingdom, ²Department of Oncology, University of Oxford, Oxford, United Kingdom, ³Division of Imaging Sciences and Biomedical Engineering, King's College London, London, United Kingdom

Tumors exhibit chaotic and leaky vasculature, which leads to variations in perfusion, and regions of edema, hypoxia and necrosis. We develop a method to extract perfusion-supervoxels, regions of locally similar perfusion, and use these regions with k-means clustering to define tumor subregions that are robust to noise and outliers. This method offers a number of advantages over both mean tumor parameters and voxelwise clustering.

263

Plasma 27



A New Combined Perfusion and Diffusion MRI Biomarker to Distinguish Pediatric High-Grade Glioma from Pilocytic Astrocytoma

Kathleen M Schmainda¹, Melissa A Prah¹, Jose A Palomares¹, Mohit Maheshwari¹, Sean Lew², and Teresa Kelly¹

¹Radiology, Medical College of Wisconsin, Milwaukee, WI, United States, ²Neurosurgery, Medical College of Wisconsin, Milwaukee, WI, United States

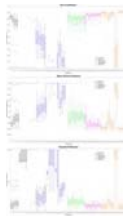
Pediatric high-grade glioma (HGG) and pilocytic-astrocytoma/optic-pathway gliomas (PA+OPG) are each very vascular tumors but vary substantially in their treatment, clinical course and long term prognosis. In this study we demonstrate that measurements that work in adults to distinguish tumor grades (eg RCBV) cannot distinguish between pediatric HGG and PA+OPG, but a new MRI biomarker, the ratio of standardized RCBV (sRCBV) to mean diffusivity (MD) can cleanly making this distinction. This finding has significant implications for treatment management in the pediatric brain tumor population.

264

Plasma 28

A ranking of pipelines for optimal co-registration of anatomical and diffusion weighted images of the cervical spinal cord

Stephanie Alley¹, Francesco Grussu¹, Marios C. Yiannakas¹, Hugh Kearney¹, Olga Ciccarelli¹, Ferran Prados^{1,2}, Sébastien Ourselin², and Claudia AM Gandini Wheeler-Kingshott^{1,3,4}



¹UCL Institute of Neurology, Queen Square MS Centre, University College London, London, United Kingdom, ²Translational Imaging Group, Centre for Medical Image Computing, Department of Medical Physics and Biomedical Engineering, University College London, London, United Kingdom, ³Department of Brain and Behavioural Sciences, University of Pavia, Pavia, Italy, ⁴Brain MRI 3T Mondino Research Center, C. Mondino National Neurological Institute, Pavia, Italy

We conduct the first systematic evaluation of the performance of three widely used registration software toolkits (FLIRT from FSL, NiftyReg and ANTs employing Spinal Cord Toolbox) in an effort to outline a method for reliable co-registration between anatomical and quantitative (EPI-based) spinal cord MRI. We generate a diverse set of registration pipelines and rank them according to quality of co-registration metrics. We find that ANTs and NiftyReg outperform FLIRT, and we report heterogeneity of specifications for optimal co-registration among software toolkits.

265

Plasma 29



Deep-Neural-Network based image diagnosis: comparing various image preprocessing strategies to achieve higher accuracy and understanding of the decision

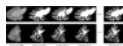
Yasuhiko Tachibana¹, Takayuki Obata¹, Jeff Kershaw¹, Yoko Ikoma¹, Tokuhiko Omatsu¹, Riwa Kishimoto¹, and Tatsuya Higashi²

¹Applied MRI Research, Department of Molecular Imaging and Theranostics, National Institute of Radiological Sciences, Chiba, Japan, ²Department of Molecular Imaging and Theranostics, National Institute of Radiological Sciences, Chiba, Japan

The purpose of this study was to investigate how image preprocessing might help overcome two problems for deep-neural-network (DNN) based image diagnosis: the need for a large training database to achieve high accuracy and the difficulty humans have in understanding the internal decision process. Five DNNs were trained with a brain image series (preprocessed in five different ways), to judge the age-range of a volunteer. The performance of the DNNs was then compared statistically. The results suggested that image preprocessing may facilitate higher accuracy, and also make it easier to understand how and why a judgement was made.

266

Plasma 30



Cerebellum Tissue Segmentation with Ensemble Sparse Learning

Jiawei Chen¹, Li Wang¹, and Dinggang Shen¹

¹Department of Radiology and BRIC, University of North Carolina at Chapel Hill, Chapel Hill, NC, United States

Accurate segmentation of cerebellum is important in studying the structural changes in brain and the alert in different neuro-developmental disorders. However, **cerebellum** has received relatively little attention in the image processing literature, compared with cerebrum segmentation. In fact, cerebellum tissue segmentation is also very challenging due to severe partial volume effect and low contrast. In this study, an ensemble sparse learning is proposed for cerebellum tissue segmentation, where the goal is to segment the tissues in cerebellum into white matter (WM), gray matter (GM) and cerebrospinal fluid (CSF). The experiment results demonstrate that our proposed method show advantages in cerebellum tissue segmentation.

Electronic Power Pitch Poster

Poster: Best of Cardiovascular MR: Hemodynamics & Atherosclerosis

Exhibition Hall

Tuesday 9:15 - 10:15

332

Plasma 1



Utilizing Quantitative Measurements of Carotid Intraplaque Hemorrhage can Improve on Presence Alone in Classifying Patients with and without Acute Cerebral Infarcts

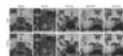
Li Dong¹, Zhaoqi Zhang¹, Wei Yu¹, Sheng Wang², Qiang Shen¹, and Chun Yuan³

¹Department of Radiology, Beijing Anzhen Hospital, Capital Medical University, Beijing, People's Republic of China, ²Department of Vascular disease, Beijing Anzhen Hospital, Capital Medical University, Beijing, People's Republic of China, ³Department of Radiology, University of Washington, Seattle, WA, United States

Histological studies have shown that intraplaque hemorrhage (IPH) size might be important in assessing disease severity. We hypothesizes that the quantitative measurements of IPH by MRI provide additional value towards classify acute cerebral infarcts (ACI) in the carotid territory by brain MRI. We found that the subjects with ACI had larger max % IPH measurements (AUC=84.7%, p=0.015) and IPH closer to the lumen (AUC=85.4%, p=0.012). Further, using the size and distance measurements simultaneously improved the AUC to 96.9%. Beyond the presence of IPH, quantitative measurements of IPH may improve the predictive value of carotid plaque imaging for future stroke.

333

Plasma 2



Whole-Brain Vessel Wall MR Imaging Using Inversion-Recovery Prepared SPACE: Reproducibility and Accuracy of Intracranial Artery Morphology

Na Zhang^{1,2}, Fan Zhang¹, Zixin Deng¹, Qi Yang¹, Xiaoming Bi³, Debiao Li¹, Xin Liu², and Zhaoyang Fan¹

¹Biomedical Imaging Research Institute, Cedars Sinai Medical Center, Los Angeles, CA, United States, ²Shenzhen Institutes of Advanced Technology, Chinese Academy of Sciences, Shenzhen, People's Republic of China, ³Siemens Healthcare

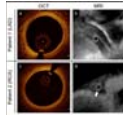
Intracranial atherosclerosis disease is one of the main causes for cerebrovascular events. A T1-weighted whole-brain vessel wall imaging method, inversion-recovery prepared SPACE (IR-SPACE), was developed at 3T demonstrating advantages over conventional SPACE. This study was aimed to determine the reproducibility of scan-rescan, intra-, and inter-observer as well as the accuracy when using the technique for morphology assessment of the intracranial vessel wall. In general, this study demonstrated excellent reproducibility and good agreement between the 3D and 2D techniques. In conclusion, IR-SPACE is a reproducible and accurate MR method for intracranial vessel wall imaging.



Plasma 3

A Preliminary Report on Time-Resolved Coronary Vessel Wall MRI in Heart Transplant Recipients

Giulia Ginami^{1,2}, Jerome Yerly^{1,3}, Jessica AM Bastiaansen¹, Ruud B van Heeswijk¹, Nathalie Lauriers⁴, Juan F Iglesias⁵, Sophie Degrauwe⁵, Andrea Zuffi⁵, Roger Hullin⁵, and Matthias Stuber^{1,3}



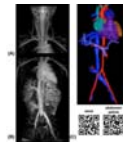
¹Department of Radiology, University Hospital (CHUV) and University of Lausanne (UNIL), Lausanne, Switzerland, ²Division of Imaging Sciences and Biomedical Engineering, King's College London, London, United Kingdom, ³Centre for Biomedical Imaging (CIBM), Lausanne, Switzerland, ⁴Department of Radiology, University Hospital (CHUV) of Lausanne, Lausanne, Switzerland, ⁵Service de Cardiologie, University Hospital (CHUV) of Lausanne, Lausanne, Switzerland

In this study, we applied a recently developed and robust coronary vessel wall MRI method that includes a golden angle trajectory and k-t sparse SENSE to a cohort of heart transplant patients. The coronary vessel wall was visualized with high contrast in all patients and the method holds great promise for quantitative and non-invasive characterization of coronary allograft vasculopathy (CAV) in transplanted patients.

Plasma 4

Non-Gadolinium-Contrast Relaxation-Enhanced MR Angiography in Children with an Inversion Recovery and T2-Prepared 3D mDIXON Gradient-Echo Technique: Preliminary Experience

Amber L. Pokorney¹, Jonathan M. Chia², Dianna ME Bardo¹, Mittun Patel¹, Smita S. Bailey¹, Scott Jorgensen¹, Deepa Biyyam¹, Scott Willard¹, Jeffrey H. Miller¹, Houchun Harry Hu¹, and Masami Yoneyama³



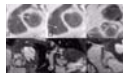
¹Radiology, Phoenix Children's Hospital, Phoenix, AZ, United States, ²Philips HealthTech, Dallas, TX, United States, ³Philips Electronics, Tokyo, Japan

We demonstrate the preliminary clinical feasibility and utility of a 3D non-Gadolinium MR angiography sequence called REACT (Relaxation-Enhanced MR Angiography without Contrast and Triggering) in 21 pediatric patients (age range: 1.7 – 16.1 years). REACT, which collectively utilizes T2-preparation, inversion recovery, and water-fat separation to suppress unwanted signals and exploit the long T1 and T2 times of unenhanced blood, is particularly beneficial in children, a population where Gadolinium administration should be minimized given recent concerns with residual intracranial Gadolinium deposition. We illustrate and compare REACT to Gadolinium-based MRA in the neck, upper and lower extremities, and the chest, abdomen, and pelvis.

Plasma 5

Ultra-High Spatiotemporal Resolution 4D Flow for Valve and Coronary Arterial Delineation

Shreyas S. Vasanawala¹, Furhawn Shah¹, Marcus T. Alley¹, and Joseph Y. Cheng¹



¹Department of Radiology, Stanford University, Stanford, CA, United States

4D flow provides single sequence rapid protocol for assessment of blood flow, ventricular function, and anatomy in congenital heart disease. Though valve function has been well validated for regurgitant flow fraction, assessment of valve leaflet delineation has been limited by relatively low spatiotemporal resolution. Similarly, coronary origin delineation has been limited. Here, we develop an ultra-high spatiotemporal resolution 4D flow acquisition technique and assess its performance for valve and coronary delineation. 4D flow provides superior delineation of coronaries than echo, is highly likely to depict coronary origins, and is highly likely to provide good valve leaflet delineation.



Plasma 6

Noninvasive Functional Evaluation of Coronary Stenosis Using MR Instantaneous wave-Free Ratio (MR-iFR): Pilot patient study using invasive fractional flow reserve as a reference

Zixin Deng^{1,2}, Sang-Eun Lee³, Zhaoyang Fan¹, Christopher Nguyen¹, Yibin Xie¹, Jianing Pang¹, Xiaoming Bi⁴, Qi Yang¹, Byoung-Wook Choi⁵, Jung-Sun Kim³, Daniel Berman¹, Hyuk-Jae Chang³, and Debiao Li¹



¹Biomedical Imaging Research Institute, Cedars-Sinai Medical Center, Los Angeles, CA, United States, ²Bioengineering, University of California, Los Angeles, Los Angeles, CA, United States, ³Cardiology, Severance Cardiovascular Hospital, ⁴Siemens Healthcare R&D, ⁵Radiology, Severance Cardiovascular Hospital

In patients with suspected coronary artery disease undergoing invasive coronary angiography, approximately half has nonsignificant stenosis (stenotic lesions that may not induce ischemia), leading to frequent and unnecessary invasive procedures. Previously, we proposed a noninvasive technique for functional evaluation of coronary stenosis using PC-MRI and Navier-Stokes equations. In this study, we evaluated the feasibility of the technique in patients, using invasive fractional flow reserve as a reference. Good correlation was observed between noninvasive and invasive techniques with high specificity and negative-predictive-value, demonstrating the potential of the proposed technique in identifying patients with functionally nonsignificant stenosis and eliminating unnecessary invasive procedures.

Plasma 7

Analysis of 4D flow hemodynamics parameters in BAV patients using a finite element method

Julio Sotelo^{1,2}, Lydia Dux-Santoy², Andrea Guala³, Jose Rodríguez-Palomares³, Arturo Evangelista³, Daniel Hurtado⁴, and Sergio Uribe⁵

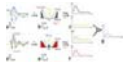


¹Biomedical Imaging Center, Pontificia Universidad Católica de Chile, Santiago, Chile, ²Department of Electrical Engineering, Pontificia Universidad Católica de Chile, Santiago, Chile, ³Department of Cardiology, Hospital Universitari Vall d'Hebron. Vall d'Hebron Institut de Recerca (VHIR). Universitat Autònoma de Barcelona., Barcelona, Spain, ⁴Department of Structural and Geotechnical Engineering, Pontificia Universidad Católica de Chile, Santiago, Chile, ⁵Department of Radiology, School of Medicine, Pontificia Universidad Católica de Chile, Santiago, Chile

Bicuspid aortic valve (BAV) is one of the most common cardiac defects. The progression of the defect can vary with time and may lead to ventricular dysfunction, heart failure and death of the patient. In this work we proposed a method to obtain several hemodynamics parameters including WSS, OSI, vorticity, helicity density, viscous dissipation, energy loss and kinetic energy from 4D-flow data sets of BAV patients and healthy volunteers using a finite-element approach. We found that the viscous dissipation, helicity density, vorticity, WSS and energy loss are the most relevant hemodynamics parameters in the ascending aorta of those patients.

Plasma 8

Phase-Contrast MRI with Hybrid One- and Two-sided Flow-Encoding and Velocity SPectrum SepARation (HOTSPA)



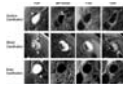
Da Wang^{1,2}, Jiaxin Shao¹, Daniel B. Ennis^{1,2,3}, and Peng Hu^{1,2}

¹Department of Radiological Sciences, David Geffen School of Medicine, University of California, Los Angeles, Los Angeles, CA, United States, ²Biomedical Physics Interdepartmental Graduate Program, University of California, Los Angeles, Los Angeles, CA, United States, ³Department of Bioengineering, University of California, Los Angeles, Los Angeles, CA, United States

In this work, we propose a new and more efficient flow encoding and velocity calculation strategy for PC-MRI using a temporal modulation technique to double the temporal resolution or reduce the scan time by 50%. This is the first study to examine a temporal modulation strategy for an under-sampled M1-space (gradient first moment space including FC, FEx, FEy and FEz encoding steps). Our strategy can be combined with conventional acceleration techniques, i.e. parallel imaging and compressed sensing, to further shorten the scan time of PC-MRI.



Plasma 9



Association between Carotid Atherosclerotic Plaque Calcification and Intraplaque Hemorrhage: A High Resolution Magnetic Resonance Imaging Study

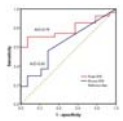
Shuo Chen¹, Ruolan Lin², Gaifen Liu³, Rui Li¹, Yunjing Xue², and Xihai Zhao¹

¹Center for Biomedical Imaging Research, Department of Biomedical Engineering, School of Medicine, Tsinghua University, Beijing, People's Republic of China, ²Department of Radiology, Fujian Union Hospital, People's Republic of China, ³Department of Neurology, Beijing Tiantan Hospital, Capital Medical University, People's Republic of China

Carotid intraplaque hemorrhage (IPH) is associated with cardiovascular events. Calcification, frequently accompanied with IPH, may play a role in occurrence of IPH. In this study we aimed to investigate the associations between calcification characteristics and IPH in carotid plaques. Our results suggest that surface calcification and multiple calcification in carotid atherosclerotic plaques are independently associated with presence IPH. Both quantity and location of calcification may play important roles in occurrence of IPH. These findings may provide novel insights for understanding the mechanism of IPH.



Plasma 10



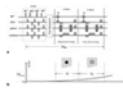
Association between Age of Intraplaque Hemorrhage and Fibrous Cap Rupture in Carotid Artery Atherosclerosis: A High Resolution Magnetic Resonance Imaging Study

Yuanyuan Cui¹, Xihai Zhao², Huiyu Qiao², Dongxiang Xu³, Mingming Lu¹, Xiaoyi Chen^{2,4}, Lu Ma¹, and Jianming Cai¹

¹Department of Radiology, The General Hospital of People's Liberation Army (301 hospital), Beijing, People's Republic of China, ²Center for Biomedical Imaging Research, Department of Biomedical Engineering, Tsinghua University, Beijing, People's Republic of China, ³Department of Radiology, University of Washington, Seattle, United States, ⁴Beijing Institute for Brain Disorders, Capital Medical University, Beijing, People's Republic of China

It has been shown that presence of carotid artery intraplaque hemorrhage (IPH) is associated with fibrous cap rupture (FCR), which is one of the major causes of ischemic cerebrovascular events. However, the role of different age of IPH in occurrence of IPH remains unclear. This study investigated the association between the age of IPH and FCR in carotid arteries using MR imaging. We found that fresh IPH volume was independently associated with FCR (odds ratio: 1.826; 95% CI: 1.130-2.949; P=0.014). Compared with recent IPH, fresh IPH was a stronger predictor for FCR (area under the curve: 0.79 vs. 0.64).

Plasma 11



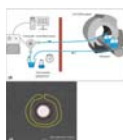
Compressed Sensing based Simultaneous Black- and Gray-blood Carotid Vessel Wall MR Imaging

Bo Li^{1,2}, Hao Li³, Guofu Huang¹, Xia Qian¹, Wei Wang¹, and Li Dong⁴

¹Center Laboratory, The First Hospital of Nanchang City, Nanchang, People's Republic of China, ²Department of Radiology, The Third Affiliated Hospital of Nanchang University, Nanchang, People's Republic of China, ³Department of Radiology, University of Cambridge, Cambridge, United Kingdom, ⁴Department of Radiology, Beijing Anzhen Hospital, Beijing, People's Republic of China

We sought to achieve high-quality simultaneous black- and gray-blood MR imaging using the CS based dual contrast imaging technique proposed on 2015. The performances on the blood suppression efficiency, image quality and morphological measurements for the CS based dual-contrast imaging technique were investigated. Seven healthy volunteers and five patients with carotid artery stenosis were recruited in this study. STR, CTR were calculated. LA and WA were measured. The comparisons for the black- and gray-blood image quality and the presence of plaque calcifications were implemented. This technique provides spatially matched black- and gray- images and excellent visualization for vessel wall imaging.

Plasma 12



Comparison of acceleration algorithms in whole-heart 4D flow MRI for aortic and mitral valve flow assessment

Jos Westenberg¹, Pankaj Garg², Pieter van den Boogaard¹, and Sven Plein²

¹Radiology, Leiden University Medical Center, Leiden, Netherlands, ²University of Leeds, Leeds, United Kingdom

Accelerated acquisition is required to make 4D flow MRI clinically feasible. In this study, three commonly used acceleration approaches are compared. Validation of flow volume and velocity assessment is performed in phantoms and comparison against conventional 2D phase-contrast is done across the aortic and mitral valve in 25 healthy volunteers. 4D flow MRI with echo-planar-imaging shows largest in vitro error in velocity assessment, however, the bias is within clinically acceptable margins. In volunteers, 4D flow MRI with echo-planar-imaging produces most reliable quantitative results in flow volume and velocity and presents the shortest acquisition time with satisfactory image quality.

Plasma 13

Golden Step, Golden Angle, Spiral-Cartesian Imaging for Flexible Gated Three-dimensional Angiography

Grzegorz Tomasz Kowalik¹, Jennifer Anne Steeden¹, David Atkinson², Kristian Mortensen³, and Vivek Muthurangu^{1,3}

¹Institute of Cardiovascular Science, University College London, London, United Kingdom, ²Centre for Medical Imaging, Division of Medicine, University College London, London, United Kingdom, ³Great Ormond Street Hospital for Children, London, United Kingdom



The purpose of this study was to develop and validate a novel 3D hybrid spiral-Cartesian MR angiographic sequence that utilized a golden step, golden angle acquisition strategy to enable flexible reconstruction.

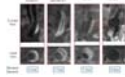
We demonstrate that it is possible to acquire GSA-MRA and reconstruct it in a flexible manner (Real-time and cardiac and/or respiratory gated reconstructions). This may enable better interrogation of anatomy.

The new flexible 3D MRA provide novel ways of assessing cardiac disease.

345



Plasma 14



Distribution of Intraluminal Thrombus Composition in Abdominal Aortic Aneurysms by Diameter: a High Resolution MRI study

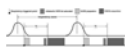
Chengcheng Zhu¹, Bing Tian², Joseph Leach¹, Qi Liu², Jianping Lu², David Saloner¹, and Michael D Hope¹

¹Radiology, University of California, San Francisco, San Francisco, CA, United States, ²Radiology, Changhai Hospital, Shanghai, People's Republic of China

Intraluminal thrombus (ILT) composition as identified by MRI has been suggested to be a marker of likely abdominal aortic aneurysm (AAA) progression. However, little is known about the distribution of ILT composition across different sizes of AAAs. This study investigated the ILT composition by AAA diameter in 62 patients from two centers. We found ILT distributed differentially by size, with an increasing mix of fresh and old ILT in larger AAAs. ILT composition is a potential indicator of AAA progression. Larger, prospective studies are needed to clarify its prognostic value in managing AAA patients.

346

Plasma 15



Evaluation of Portal Vein System in patients after liver transplantation by Unenhanced MR Angiography Using Spatial Labeling with Multiple Inversion Pulses Sequence and by CT portography

hao tang¹, daoyu hu, xiaoyan meng, zi wang, zhen li, and yanchun wang

¹Tongji Hospital, Tongji Medical College, Huazhong University of Science and Technology, Wuhan, People's Republic of China

Unenhanced MR angiography with spatial labeling with multiple inversion pulses (SLEEK) is a reliable method for depicting portal vein system in patients with liver transplantation compared with computed tomographic portography (CTP) results. In a study of 20 patients who underwent liver transplantation, we found that there was excellent correlation between SLEEK and CTP in presenting the diameter of portal vein. Unenhanced MRA using SLEEK is relatively inexpensive and is not associated with renal complications. It can be as a good choice for screening portal vein system in patients with liver transplantation, especially in patients with renal insufficiency.

Electronic Power Pitch Poster

Poster: Brain Physiology: Flow, Oxygen, Metabolism

Exhibition Hall

Tuesday 9:15 - 10:15

347



Plasma 16



Long-term Cerebrovascular Dysfunction Following Repeated Mild Traumatic Brain Injury

Conner Adams^{1,2}, Margaret Koletar¹, Tina L. Beckett¹, Lindsay Cahill³, Lydiane Hirschler^{4,5,6}, Jan M. Warnking^{4,6}, Emmanuel L. Barbier^{4,6}, JoAnne McLaurin^{1,7}, John G. Sled^{2,3}, and Bojana Stefanovic^{1,2}

¹Sunnybrook Research Institute, Toronto, ON, Canada, ²Medical Biophysics, University of Toronto, Toronto, ON, Canada, ³Mouse Imaging Centre, The Hospital For Sick Children, Toronto, ON, Canada, ⁴Grenoble Institut des Neurosciences, Université Grenoble Alpes, Grenoble, France, ⁵Bruker Biospin MRI, Ettlingen, Germany, ⁶Inserm, U1216, Grenoble, France, ⁷Laboratory Medicine and Pathobiology, University of Toronto, Toronto, ON, Canada

Pseudo-Continuous Arterial Spin Labelling (pCASL) was used to assess cerebrovascular dysfunction of mice having traumatic brain injury (TBI) - which had been induced via serial controlled cortical impacts. Resting perfusion was quantified in absolute units via multiple post-label-delay pCASL experiments, and found to be reduced in the lesion. Furthermore, vascular reactivity to hypercapnic challenge, assessed via pCASL, appears to be enhanced in initial results. These results, in conjunction with immunohistochemical analysis and T2-weighted structural images, imply severe damage due to TBI, with vascular adaptation in the form of angiogenesis as the response from the brain.

348

Plasma 17

Parameter	ASL	DCE-MRI
ASL BF	0.12 ± 0.02	0.11 ± 0.02
DCE-MRI K ^{trans}	0.02 ± 0.005	0.02 ± 0.005
ASL BF / DCE-MRI K ^{trans}	6.0 ± 1.0	6.0 ± 1.0

Comparative Study of 3D Arterial Spin Labeling and dynamic contrast-enhanced MRI of Nasopharyngeal Carcinoma perfusion imaging

Bohan Xiao¹, Zhaoxiang Ye¹, Peiguo Wang¹, Ying Liu¹, Yingyu Zhao¹, and Dandan Zheng²

¹Key Laboratory of Cancer Prevention and Therapy, Department of Radiology, Tianjin Medical University Cancer Institute & Hospital, Tianjin, People's Republic of China, ²MR Research China, GE Healthcare, Beijing, People's Republic of China

DCE-MRI is already a standard approach to evaluating tumor perfusion in NPC, but it may induce severe side-effects. ASL is a noninvasive MRI technique that has been mainly used to achieve perfusion imaging in central nerve system. In this study, we attempt to evaluate the application of ASL in NPC. Thirty-eight newly diagnosed NPC patients underwent 3D ASL and DCE-MRI perfusion scans on a 3.0-T MRI system. ASL BF value and DCE-MRI parameters were calculated and compared. Statistically significant correlation was found between them. Therefore, 3D ASL may provide a potential alternative to DCE-MRI in NPC diagnosis and therapy evaluation.

Plasma 18



Non-contrast vascular compliance mapping using time-resolved VASO CBV imaging

Yang Li^{1,2}, Deng Mao^{1,2}, Jay J. Pillai¹, and Hanzhang Lu¹

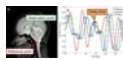


¹Department of Radiology, Johns Hopkins University School of Medicine, Baltimore, MD, United States, ²Graduate School of Biomedical Sciences, UT Southwestern Medical Center, Dallas, TX, United States

Vascular compliance reflects the stiffness of arterial vessel wall and has been related to a number of diseases, such as cardiovascular disease, cerebral arteriosclerosis, and hypertension. However, the vascular compliance at intracranial arteries has been rarely measured due to limited availability of effective methods. In this work, a 3D VASO-CBV-based MR technique was developed to assess the arterial CBV change with respect to pulsation and thus estimate vascular compliance. With this technique, we were able to map vascular compliance along the intracranial arterial tree.



Plasma 19



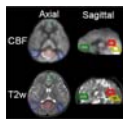
Propagation Patterns of Cardiac-driven and Respiratory-driven Cerebrospinal Fluid Velocity Waves Characterized by Correlation Mapping in Conjunction with Asynchronous 2-Dimensional Phase Contrast Technique

Satoshi Yatsushiro¹, Saeko Sunohara², Mitsunori Matsumae³, and Kagayaki Kuroda^{1,2}

¹Graduate School of Science and Technology, Tokai University, Hiratsuka, Kanagawa, Japan, ²Graduate School of Engineering, Tokai University, Hiratsuka, Kanagawa, Japan, ³Department of Neurosurgery, Tokai University School of Medicine, Isehara, Kanagawa, Japan

Spatial distributions of the propagation patterns of cerebrospinal fluid (CSF) motion driven by cardiac pulsation and respiration were visualized using velocity waveform correlations based on asynchronous 2-dimensional phase contrast (2D-PC) imaging. These two different driving mechanisms were evaluated using spectral analysis of the velocity waveforms for 11 healthy subjects. Delay time maps and maximum correlation maps showed the spatial distribution differences between the cardiac-driven and respiratory-driven CSF motion propagations. Maximum correlation at the prefrontal was 0.83 ± 0.05 for cardiac propagation and 0.74 ± 0.04 for respiratory propagation with a significant difference ($p < 0.01$). Strong propagation may not necessarily cause large CSF displacement.

Plasma 20



Regionally differentiated cerebral blood flow increases during infancy measured with pCASL MRI

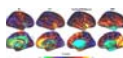
Qinlin Yu^{1,2,3,4}, Huiying Kang^{1,5}, Minhui Ouyang^{1,2}, Yun Peng⁵, Fang Fang^{3,4}, and Hao Huang^{1,2}

¹Department of Radiology, Children's Hospital of Philadelphia, Philadelphia, PA, United States, ²Department of Radiology, Perelman School of Medicine, University of Pennsylvania, Philadelphia, PA, United States, ³School of Psychological and Cognitive Sciences, Peking University, Beijing, People's Republic of China, ⁴Peking-Tsinghua Center for Life Science, Peking University, Beijing, People's Republic of China, ⁵Department of Radiology, Beijing Children's Hospital, Capital Medical University, Beijing, People's Republic of China

During infant brain development, rapid neuronal growth requires increases of cerebral blood flow. In this study, we quantified cerebral blood flow (CBF) at regional level during infant development by using pseudo-continuous arterial spin labeled (pCASL) perfusion MRI. The CBF maps at different infant stages from 0 to 24 months were revealed. The trend lines of CBF at specific regions were charted. It has been found that the CBF increases linearly at different brain regions, with CBF increasing faster in visual, posterior cingulate, medial prefrontal and inferior parietal cortex than whole brain.



Plasma 21



Cerebral blood flow as a marker for cortical parcellation

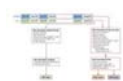
Roy Haast¹, Dimo Ivanov¹, Elia Formisano¹, and Kâmil Uludağ¹

¹Department of Cognitive Neuroscience, Maastricht University, Maastricht, Netherlands

Within-subject differences of T_1 , T_2^* and cortical thickness can be used to automatically parcellate the cortex, e.g. to guide functional analyses or increase statistical power. Here, we evaluate the additional benefit of baseline CBF as a marker for brain metabolism to differentiate regions. We demonstrate that CBF data is not redundant with the other quantitative MRI parameters. Therefore, a data-driven parcellation of brain regions that incorporates perfusion information allows delineation of the cortex into smaller units and enhances subsequent anatomical & functional analysis.



Plasma 22



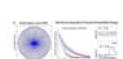
Changes in cerebral blood flow and default mode network connectivity following mTBI observed with pulsed arterial spin labeling

Natalie M. Wiseman¹, Armin Iraj², E. Mark Haacke^{2,3}, and Zhifeng Kou^{2,3}

¹Department of Psychiatry and Behavioral Neurosciences, Wayne State University, Detroit, MI, United States, ²Department of Biomedical Engineering, Wayne State University, Detroit, MI, United States, ³Department of Radiology, Wayne State University, Detroit, MI, United States

Mild traumatic brain injury (mTBI) or concussion disturbs both cerebral blood flow (CBF) and functional connectivity in intrinsic connectivity networks (ICNs). Using pulsed arterial spin labeling (PASL), we derived both CBF and ICNs in mTBI patients and investigated brain CBF responses to network disruptions. We observed that mTBI patients have decreased connectivity within the default mode network (DMN) in two regions as well as increased CBF in a third region which overlaps the DMN. The mismatch of these regions suggests potential repair or compensation for injury.

Plasma 23



A Novel Approach to Measuring Cerebral Oxygen Extraction Fraction and Vascular Reserve Using MRI

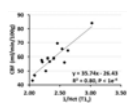
Charles Cantrell¹, Yong Jeong², Kevin Midlash³, Parmede Vakil², Sameer Ansari², and Timothy J Carroll³

¹Northwestern University, Chicago, IL, United States, ²Northwestern University, ³University of Chicago

The length scales associated with parenchymal oxygen extraction fraction (OEF), coupled with the near uniformity of normative OEF across the brain dictate the development of an imaging approach that is sensitive to low-spatial frequency imaging behavior. Previous approaches to measure OEF using MRI have utilized high pass-filters—effectively removing much of the signal. We propose a new method to filter out geometric field inhomogeneity, by imaging temporally through the cardiac cycle. In a study in 11 patients with intracranial atherosclerotic disease, we found elevated OEF on the compromised hemisphere as compared to the healthy contralateral side ($p < 0.0195$).

355

Plasma 24



Measurements of Oxygen Delivery and Consumption Using Hematocrit Derived from Blood T1 Quantification

Feng Xu^{1,2,3}, Wenbo Li^{1,2}, Peiying Liu^{1,2}, Hanzhang Lu^{1,2}, John J. Strouse⁴, James J Pekar^{1,2}, Peter C.M. van Zijl^{1,2}, and Qin Qin^{1,2}

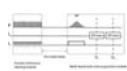
¹F.M. Kirby Center for Functional Brain Imaging, Kennedy Krieger Institute, Baltimore, MD, United States, ²The Russell H. Morgan Department of Radiology and Radiology Science, Johns Hopkins University, Baltimore, MD, United States, ³Developing Brain Research Laboratory, Children's National Medical Center, Washington DC, DC, United States, ⁴Department of Medicine, Duke University, Durham, NC, United States

We verified that venous blood T1 quantified *in vivo* in humans using fast and non-invasive MRI can be used to derive hematocrit (Hct) values reliably. This Hct information can be used for a more individual estimation of oxygen extraction fraction (OEF) from venous blood T2 measurements. Furthermore, inverse correlation between Hct and baseline cerebral blood flow (CBF) was observed across subjects. Measurement of Hct, OEF and CBF allowed determination of oxygen delivery (OD=CBF-Hct) and consumption (cerebral metabolic rate of oxygen, CMRO₂=CBF-Hct-OEF). When compared to CBF, OD and CMRO₂ showed less inter-subject variations among normal volunteers.

356



Plasma 25



Simultaneous cerebral blood flow and bold oxygen level dependent signal assessments using multi-band multi-echo pseudo-continuous arterial spin labeling (M2-PCASL)

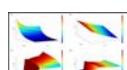
Shiyang Chen¹, Junjie Wu², Kyle Pate², Xiaodong Zhong^{2,3}, Bruce Crosson^{2,4}, and Deqiang Qiu²

¹Georgia Institute of Technology, Atlanta, GA, United States, ²Department of Radiology and Imaging Sciences, Emory University, Atlanta, GA, United States, ³MR R&D Collaborations, Siemens Healthcare, Atlanta, GA, United States, ⁴Department of Neurology, Emory University, Atlanta, GA, United States

We proposed a novel multi-band multi-echo pseudo-continuous arterial spin labeling (M2-PCASL) method to simultaneously measure the cerebral blood flow (CBF) and the blood oxygen level dependent (BOLD) signal. Increased spatial resolution was achieved compared to the conventional method, and experiments were also conducted to show simultaneous measurement of CBF and BOLD signal dynamics in response to hypercapnia. M2-PCASL can be a useful tool for measuring cerebrovascular reactivity and studying neurovascular coupling in various conditions.

357

Plasma 26



Measuring Blood Oxygenation and Hematocrit with a Combined T2 and T1 Approach: Initial Experience in Humans

Thomas Christen¹, Jia Guo¹, Wendy Wei Ni¹, Michael Moseley¹, and Greg Zaharchuk¹

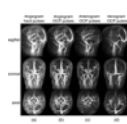
¹Radiology, Stanford University, Palo Alto, CA, United States

In this study, we propose to obtain simultaneous measurements of blood oxygen saturation (SO₂) and hematocrit (Hct) by combining two or more *in vivo* measurements of blood MR relaxation times. We tested our approach in 5 healthy human subjects using T2+T1 values and calibration curves obtained *in vitro*. The results found in the superior sagittal sinus vein (SO₂=62±5% and Hct=46±1%) are in good agreement with literature values and suggest great potential of the approach once it is further validated.

358



Plasma 27



Whole-Brain Arteriography and Venography Using an Improved Velocity-Selective Saturation (VSS) Pulse Trains

Wenbo Li^{1,2}, Feng Xu^{1,2,3}, Jing Liu^{1,4}, Michael Schär¹, Taehoon Shin⁵, Peter van Zijl^{1,2}, Ye Qiao¹, Bruce Wasserman¹, and Qin Qin^{1,2}

¹Department of Radiology, Johns Hopkins University School of Medicine, Baltimore, MD, United States, ²F.M. Kirby Research Center for Functional Brain Imaging, Kennedy Krieger Institute, Baltimore, MD, United States, ³Developing Brain Research Lab, Children's National Medical Center, Washington, DC, United States, ⁴Department of Radiology, People's Hospital, Guangzhou, People's Republic of China, ⁵Department of Diagnostic Radiology and Nuclear Medicine, University of Maryland, Baltimore, MD, United States

Velocity-selective (VS) MRA, a non-subtractive technique and allows large spatial coverage and slow-flow depiction has shown recent promise for cerebral applications at 3T. Here, we improved the velocity-selective saturation (VSS) pulse train by reducing its sensitivity of tissue suppression to B₁ inhomogeneity for both the intracranial and cervical regions. Moreover, we propose that arteriograms or venograms can be obtained by placing spatially selective inversion pulses before the acquisition to selectively null signals from venous or arterial blood. The feasibility of these technical advances for VS MRA is demonstrated on healthy volunteers at 3T.

359



Plasma 28

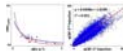


Simultaneous acquisition of oxygen extraction fraction and cerebral blood flow during brain activation

Yayan Yin¹, Yaoyu Zhang¹, Yang Fan², Bing Wu², and Jia-Hong Gao¹

¹Center for MRI Research, Peking University, Beijing, People's Republic of China, ²MR Research China, GE Healthcare, Beijing, People's Republic of China

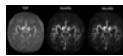
The development of neuroimaging methods to obtain oxygen extraction fraction (OEF) and cerebral metabolic rate of oxygen (CMRO₂) is crucial for understanding mechanisms underlying physiological function and neuronal activity. In the present study, a novel technique termed FAIR-MGESSE combined flow sensitive alternating inversion recovery (FAIR) and multiecho gradient echo sampling of the spin echo (MGESSE) techniques. It is proposed for acquiring OEF and ASL maps in a single repetition time to determine the relative change in CMRO₂ in human subjects. Relative changes in CBF, OEF and CMRO₂ were measured during the visual task and the results agree well with expectations.



Yong Ik Jeong¹, Charles G Cantrell¹, Kevin Midlash², Renee Qian, Parmede Vakil³, Sameer A Ansari³, Gregory Christoforidis², and Timothy J Carroll²

¹Northwestern University, Evanston, IL, United States, ²University of Chicago, ³Northwestern University

In the occurrence of damage to the hemodynamic system of the brain, a response is elicited by changes in the supply of blood and oxygen to the tissue. Depending on these different changes, the severity of the hemodynamic impairment can be defined. In this study, we propose a method of accurately measuring quantitative cerebrovascular reserve. This is achieved by applying water correction factors to multiple contrast-agent injection cerebral blood flow measurements. In multiple studies involving volunteers, animal model, and patients, we confirm the correction factors and compare against microsphere perfusion.



Yuta Akamine¹, Makoto Obara¹, Osamu Togao², Shuhei Shibukawa³, Masami Yoneyama¹, Tomoyuki Okuaki⁴, and Marc Van Cauteren⁴

¹Philips Electronics Japan, Shinagawa, Tokyo, Japan, ²Department of Clinical Radiology, Graduate School of Medical Science, Kyushu University, Fukuoka, Japan, ³Department of Radiology, Tokai University Hospital, Japan, ⁴Asia Pacific, Philips Healthcare, Shinagawa, Tokyo, Japan

Improved acceleration-selective arterial spin labelling (iAccASL) was implemented for Intracranial MR angiography and images were acquired in six healthy volunteers. Additional 180° refocusing pulses in control module will efficiently suppress spin dispersion and flow voids in strongly accelerating middle cerebral artery (MCA) main arteries. The vessel visualizations of MCA main trunk and peripheral vessels were compared with our previously reported AccASL and conventional time-of-flight (TOF) approach. We demonstrated iAccASL could produce better MCA main trunk visualization (without venous signal) compared with conventional AccASL technique with better peripheral visualization than TOF.

Electronic Power Pitch Poster

Poster: Liver

Exhibition Hall

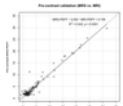
Tuesday 14:45 - 15:45



Tilman Schubert¹, Kevin Johnson², Alejandro Roldan Alzate¹, and Scott Reeder^{1,2}

¹Radiology, UW Wisconsin Madison, Madison, WI, United States, ²Medical Physics, UW Wisconsin Madison, Madison, WI, United States

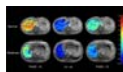
This study used 4D-flow MRI to assess potential correlations between changes in portal-venous blood flow and liver growth after portal vein embolization (PVE). 4 pigs underwent PVE and were examined with 4D flow MRI before and immediately after PVE as well as 1 week and 2 weeks after PVE. The results indicate that a persistent increase in blood flow volume to non-embolized liver segments as opposed to a peak in flow volume that later decrease over time, is likely to influence growth of these segments. Furthermore, 4D-flow MRI is well suited to study changes in portal-venous flow volume after PVE.



Ethan Z Sy¹, Cheng William Hong¹, Soudabeh Fazeli Dehkordy¹, Charlie C Park¹, Alexandra Schlein¹, Jonathan C Hooker¹, Jennifer Cui¹, Gavin Hamilton¹, and Claude B Sirin¹

¹University of California, San Diego, San Diego, CA, United States

Proton density fat fraction (PDFF) is a widely-used magnetic resonance imaging (MRI)-based biomarker for noninvasive quantification of hepatic steatosis. PDFF derived from low-flip-angle magnitude-based multi-gradient-echo MRI (MRI-M) without intravenous contrast has been shown to have high accuracy for estimating fat fraction. However, this MRI-M technique has a relatively low signal-to-noise ratio (SNR), which makes it difficult to visualize anatomical features. In this analysis of ninety-two patients, high-flip-angle contrast-enhanced (with either gadoxetate disodium or gadobutrol) MRI-M imaging had no significant difference in fat-grading accuracy from the standard low-flip-angle pre-contrast PDFF, using MR spectroscopy (MRS)-PDFF as the reference standard.



Tomoyuki Okuaki¹, Kosuke Morita², Tomohiro Namimoto², Morikatsu Yoshida³, Shinya Shiraiishi³, Yasuyuki Yamashita³, and Marc Van Cauteren¹

¹MR Clinical Science, Philips Healthtech, Tokyo, Japan, ²Department of Central Radiology, Kumamoto University Hospital, Kumamoto, Japan, ³Department of Diagnostic Radiology, Faculty of Life Sciences, Kumamoto University, Kumamoto, Japan

We calculated the uptake fraction (k_{Hep}) based on a pharmacokinetics model of gadolinium ethoxybenzyl-diethylenetriamine pentaacetic acid (Gd-EOB-DTPA) uptake using R1 changes in the hepatocyte. The k_{Hep} and $\Delta T1$ values were compared to indexes determined by ^{99m}Tc-GSA scintigraphy for three different scan time points. The correlation coefficients of the blood clearance indexes (HH15) and receptor indexes (LHL15) were 0.307 and 0.497 for the $\Delta T1$ and 0.537 and 0.570 for k_{Hep} values, respectively. The results indicate that the proposed quantification value of k_{Hep} is a more robust index for liver function compared with the $\Delta T1$ value.

Detection of Advanced Liver Fibrosis and Cirrhosis using MR elastography compared to liver surface nodularity measurement, EOB-DTPA uptake and blood tests



Cecilia Besa¹, Mathilde Wagner^{1,2}, Grace Lo¹, Sonja Gordic¹, Manjil Chatterji¹, Ashley Stueck³, James Babb⁴, Andrew Smith⁵, and Bachir Taouli¹

¹Translational and Molecular Imaging Institute, Icahn School of Medicine at Mount Sinai, New York, NY, United States, ²Radiology, Groupe Hospitalier Pitié Salpêtrière, Paris, France, ³Pathology, Icahn School of Medicine at Mount Sinai, New York, NY, United States, ⁴Radiology, New York University Langone Medical Center, New York, United States, ⁵Radiology, University of Mississippi Medical Center, Jackson, MS, United States

This study compares the diagnostic performance of multiparametric MRI including qualitative and quantitative assessment of MR-elastography (MRE), liver surface nodularity (LSN) software measurement, hepatic enhancement ratios on Gd-EOB-DTPA (EOB-ER), and serum markers (APRI and FIB4) for the detection of liver fibrosis and cirrhosis. When comparing different MRI methods and serum markers with histologic findings, liver stiffness measured with MRE showed better performance than other methods for detection of advanced liver fibrosis and cirrhosis, especially when combined with blood tests (FIB4).

Diagnostic performance of LI-RADS major features, ancillary features, and categories on MRI for diagnosis of hepatocellular carcinoma

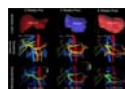


Milena Cerny¹, Catherine Bergeron¹, Jean-Sébastien Billiard¹, Jessica Murphy-Lavallée¹, Damien Olivé¹, Joshua Bérubé¹, Boyan Fan¹, Héléne Castel², Simon Turcotte³, Pierre Perrault¹, and An Tang^{1,4}

¹Department of Radiology, Centre hospitalier de l'Université de Montréal (CHUM), MONTREAL, QC, Canada, ²Department of Gastroenterology and Hepatology, Centre hospitalier de l'Université de Montréal (CHUM), MONTREAL, QC, Canada, ³Department of Surgery, Centre hospitalier de l'Université de Montréal (CHUM), MONTREAL, QC, Canada, ⁴Centre de recherche du Centre hospitalier de l'Université de Montréal (CRCHUM), MONTREAL, QC, Canada

Diagnosis of hepatocellular carcinoma (HCC) is largely based on imaging. MRI is ideally suited for the non-invasive diagnosis of HCC because it has numerous tissue contrast mechanisms and is the only modality that can assess all major and ancillary imaging features. We evaluated the diagnostic performance of MRI-determined LI-RADS major features, ancillary features, and categories for the diagnosis of HCC. Our results suggest that interpretation that includes ancillary features increases the sensitivity, while preserving a high specificity for definite HCC and a slightly lower specificity for probable HCC. Further, ancillary features in favor of benign entities have high specificity for benignity.

Longitudinal Characterization of Liver Regeneration and Portal Hemodynamics in Living Donor Liver Transplant



Alejandro Roldán-Alzate^{1,2,3}, David R Rutkowski², Luis A Fernandez⁴, and Scott B Reeder^{1,3,5,6}

¹Radiology, University of Wisconsin, Madison, WI, United States, ²Mechanical Engineering, University of Wisconsin, Madison, WI, United States, ³Biomedical Engineering, University of Wisconsin, Madison, WI, United States, ⁴Surgery, University of Wisconsin, Madison, WI, United States, ⁵Medical Physics, University of Wisconsin, Madison, United States, ⁶Medicine, University of Wisconsin, Madison, United States

The purpose of this study was to evaluate longitudinal liver regeneration and hemodynamic changes of living donor liver transplant (LDLT) donors in response to surgical liver resection. Five living related liver donors were studied. Subjects were imaged using 4D Flow MRI before and at several times following partial hepatectomy. The ability to longitudinally evaluate liver regeneration and portal hemodynamic changes non-invasively demonstrates that 4D flow MRI is a suitable tool for both surgical planning of LDLT, and for improved understanding of the liver regeneration and hemodynamic changes that occur in the remnant liver of the donor.

4D flow MRI of Liver Hemodynamics: Influence of Velocity Encoding, Different Field Strength and Contrast Application on Visualization and Quantification of blood flow



Zoran Stankovic¹, Bernd Jung¹, Alan Arthur Peters¹, Jelena Surla², Edouard Semaan², Michael Ith¹, Johannes Heverhagen¹, Michael Markl², and Jeremy D. Collins²

¹DIPR, Inselspital, University Hospital Bern, University of Bern, Bern, Switzerland, ²Radiology, Northwestern University, Chicago, IL, United States

4D flow MRI offers the possibility for complete volumetric and functional assessment of liver blood flow in patients with liver cirrhosis. This study reveals a significant difference when using a lower venc for visualization of the portal vein branches. Similar results are obtained for contrast application and different field strengths. For qualitative assessment of the intrahepatic branches by 4D flow MRI a lower venc is recommended.

Quantitative Free-Breathing Dynamic Contrast-enhanced MRI in Hepatocellular Carcinoma Using Gd-EOB-DTPA : Correlations With Ki67 Proliferation Status and Histological Grades

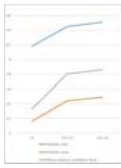


Jie Chen¹, Chenyang Chen¹, Chunchao Xia², and Bin Song²

¹West China Medical School of Sichuan University, Chengdu, People's Republic of China, ²Departmento of Radiology, West China Hospital of Sichuan University, Chengdu, People's Republic of China

This study aims to validate a free-breathing DCE-MRI in HCC patients using gadoteric acid, and to determine the relationship between DCE-MRI parameters and histological results. Perfusion parameters (K^{trans} , K_{ep} , V_e and $iAUC$) from 34 patients were compared with CT results and correlated with Ki67 indices and the histological grades of HCC. Significant relationship was found between DCE-MRI and CT results, indicating the validity of this protocol in evaluating the vascular change of HCC. The DCE-MRI derived K^{trans} and $iAUC$ were significantly correlated with the histological grades of HCC, suggesting the potential of those parameters in predicting the malignancy of tumors.

The value of high resolution gadoxetic acid-enhanced MR cholangiography for evaluating biliary anatomy of living liver donor: comparison with T2 weighted (T2W) MR cholangiography and conventional gadoxetic acid enhanced MR cholangiography



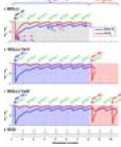
Hyo-Jin Kang¹, Jeong Min Lee¹, Jeong Hee Yoon¹, Won Chang¹, Ijin Joo¹, and Joon Koo Han¹

¹Radiology, Seoul National University Hospital, Seoul, Korea, Republic of

The addition of gadoxetic acid-enhanced sFOV T1W-MRC to T2W-MRC is able to provide more precise depiction of biliary anatomy, which is crucial for the prevention of post-operative biliary complications of living liver donors.

435

Plasma 10



Water-Only Look-Locker Inversion recovery (WOLLI) T₁ mapping

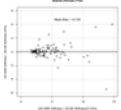
Liam D. Garrison¹, Christina Levick^{1,2}, Michael Pavlides^{1,2}, Tom Marjot³, Ferenc Mozes¹, Leanne Hodson³, Stefan Neubauer¹, Matthew Robson¹, and Christopher T. Rodgers¹

¹OCMR, RDM Cardiovascular Medicine, University of Oxford, Oxford, United Kingdom, ²Translational Gastroenterology Unit, Nuffield Department of Medicine, University of Oxford, Oxford, United Kingdom, ³Oxford Centre for Diabetes, Endocrinology and Metabolism (OCDEM), Radcliffe Department of Medicine, University of Oxford, United Kingdom

We propose a new "Water-Only Look-Locker Inversion recovery" (WOLLI) sequence, based on MOLLI, that enables water-selective T₁-mapping in an 8hb breath-hold at 3T. WOLLI uses a hypergeometric (HG) inversion pulse to selectively invert water with negligible effect on fat. To separate the steady-state fat and water signals, WOLLI adds one or more fat-inversions starting from the plateau of the water T₁* recovery. WOLLI uses an extended Deichmann-Haase formula to correct for readout-induced saturation. We validated this approach by simulations, scans in a phantom containing 19 fat/water mixtures, and liver scans in 12 subjects (volunteers and liver disease patients).

436

Plasma 11



Region-of-interest size of hepatic 2D MR elastography decreases with increasing R₂* for gradient-echo but not spin-echo techniques

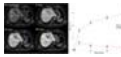
Cheng William Hong¹, Adrija Mamidipalli¹, Ethan Z Sy¹, Jonathan C Hooker¹, Calvin Andrew Tran¹, Tanya Wolfson², Soudabeh Fazeli Dehkordy¹, Scott B Reeder³, Rohit Loomba⁴, and Claude B Sirlin¹

¹Liver Imaging Group, Department of Radiology, University of California, San Diego, San Diego, CA, United States, ²Computational and Applied Statistics Laboratory, University of California, San Diego, San Diego, CA, United States, ³Departments of Radiology, Medical Physics, Biomedical Engineering, Medicine, and Emergency Medicine, University of Wisconsin, Madison, Madison, WI, United States, ⁴NAFLD Research Center, Division of Gastroenterology, Department of Medicine, University of California, San Diego, San Diego, CA, United States

MR elastography (MRE) is an emerging technique for the non-invasive assessment of hepatic stiffness and fibrosis, and can be based on gradient-echo (GRE) or spin-echo (SE) acquisition. This study demonstrates that 2D-SE provides significantly larger reliable-wave-quality regions-of-interest (ROIs) than 2D-GRE at 3T. Additionally, 2D-GRE ROI sizes are negatively correlated with hepatic R₂*, while 2D-SE ROI sizes are not associated with R₂*. This suggests that 2D-SE may be the preferred MRE sequence at 3T and in patients with known iron overload.

437

Plasma 12



Estimating Liver Function in Chronic Liver Disease Patients Using DCE-MRI and Whole-Body Pharmacokinetic Modeling

Markus Karlsson^{1,2}, Mikael F Forsgren^{1,2}, Olof Dahlqvist-Leinhard^{1,2}, Nils Dahlström^{1,2}, Bengt Norén², Mattias Ekstedt¹, Stergios Kechagias¹, Gunnar Cedersund³, and Peter Lundberg^{1,2}

¹Department of Health and Medicine, Linköping University, Linköping, Sweden, ²Center for Medical Image Science and Visualisation, Linköping University, Linköping, Sweden, ³Department of Biomedical Engineering, Linköping University, Linköping, Sweden

Dynamic contrast enhanced MRI with Gd-EOB-DTPA is a promising method for investigating liver function. However, many of the proposed procedures relies on such a high temporal resolution, and low spatial resolution, that the images are rendered unsuitable for radiographic reading. Here we have tested and validated a recently developed procedure using a whole-body pharmacokinetic model in a cohort of patients with chronic liver disease. Moreover we also show that the approach can separate advanced from mild fibrosis.

438

Plasma 13



Prognostic Role of Liver Stiffness Measurement Using Magnetic Resonance Elastography in Patients with Compensated Chronic Liver Disease

Dong Ho Lee¹ and Jeong Min Lee²

¹Radiology, Seoul National University Hospital, Seoul, Korea, Republic of, ²Korea, Republic of

Liver stiffness measurement (LSM) using magnetic resonance elastography (MRE) can estimate the degree of liver fibrosis. We retrospectively evaluate the prognostic role of LSM using MRE in compensated chronic liver disease patients. A total of 217 patients with compensated chronic liver disease who underwent MRE were included. After a mean and median follow-up of 44.5±17.8 months and 46.0 months, LSM value obtained from MRE was turned out to be significant predictive factor for overall survival, development of hepatic decompensation and occurrence of hepatocellular carcinoma.

439

Plasma 14



Epidemiology and spatial heterogeneity of hepatic fat and iron deposition: an MRI-based analysis

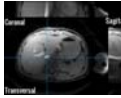
Daniel R Ludwig¹, Tyler J Fraum¹, Scott Kilian², and Kathryn J Fowler¹

¹Mallinckrodt Institute of Radiology, Washington University School of Medicine, St Louis, MO, United States, ²Southern Illinois University School of Medicine

MRI has emerged as a reliable, noninvasive means of liver fat and iron quantification. We retrospectively studied 1006 patients that underwent standard-of-care liver MRI at a single tertiary care center. Multivariate analysis was used to identify factors predictive of the severity and spatial heterogeneity of hepatic fat deposition (HFD) and hepatic iron deposition (HID). Greater spatial heterogeneity of HFD and HID generally occurred as the severity of HFD and HID increased, suggesting higher risk for misclassification by biopsy with more advanced disease. Overall, by globally evaluating the liver, MRI constitutes a robust tool for assessing hepatic fat and iron deposition.

440

Plasma 15

Free breathing T2* mapping of the Liver using a compressed sensing reconstruction

Paul de Heer¹, Oliver J Gurney-Champion¹, Jurgen H. Runge^{1,2}, Remy Klaassen³, Jasper Schoormans¹, Bram F. Coolen⁴, Hanneke W.M. van Laarhoven³, Gustav J. Strijkers⁴, Jaap Stoker¹, and Aart J. Nederveen¹

¹Radiology, AMC, Amsterdam, Netherlands, ²Division of Imaging Sciences and Biomedical Engineering, King's College London, London, United Kingdom, ³Medical Oncology, AMC, Amsterdam, Netherlands, ⁴Biomedical Engineering & Physics, AMC, Amsterdam, Netherlands

Hemochromatosis (iron overload) occurs in a range of liver diseases. (1,2) Iron content can be measured invasively with liver biopsy but is commonly replaced by non-invasive MR measurements, including T2* mapping. This is commonly done in a breath-hold to reduce the effects of respiratory motion. In this work we show that a stack of stars radial golden angle T2* mapping multi echo sequence during free breathing in combination with CS reconstruction facilitates high resolution imaging in the liver. This approach bears promise beyond liver imaging for visualizing smaller organs and pathologies, e.g. the pancreas and lymph nodes.

Electronic Power Pitch Poster**Poster: Reconstruction Highlights**

Exhibition Hall

Tuesday 14:45 - 15:45

441

Plasma 16

Joint Reconstruction of Phase-Cycled Balanced SSFP with Constrained Parallel Imaging

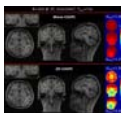
Berkin Bilgic¹, Thomas Witzel¹, Himanshu Bhat², Lawrence L Wald¹, and Kavin Setsompop¹

¹Martinos Center for Biomedical Imaging, Charlestown, MA, United States, ²Siemens Medical Solutions, Charlestown, MA, United States

Balanced SSFP is an SNR-efficient sequence with unique T_2/T_1 contrast, but suffers from banding artifacts due to B_0 sensitivity. These artifacts can be mitigated through RF phase-cycling at a cost of significant increase in scan time. Here, we propose Joint L1-SPIRiT to jointly reconstruct highly accelerated/undersampled phase-cycled images and convert the different banding artifacts of these images into additional spatial encoding. This enables highly accelerated 2D and Simultaneous Multi-Slice imaging, thus mitigating scan time burden of phase-cycled bSSFP while producing banding-free images. In particular, Joint L1-SPIRiT provides around 2-fold decrease in both the average g-factor and RMSE relative to GRAPPA.

442

Plasma 17

Wave-CAIPI for Highly Accelerated MP-RAGE Imaging

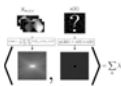
Daniel Polak^{1,2}, Kavin Setsompop^{1,3,4}, Stephen F. Cauley^{1,3}, Borjan A. Gagoski^{3,5}, Himanshu Batt⁶, Florian Maier², Lawrence L. Wald^{1,3,4}, and Berkin Bilgic^{1,3}

¹Massachusetts General Hospital, Boston, MA, United States, ²German Cancer Research Center, Heidelberg, Germany, ³Harvard Medical School, Boston, MA, United States, ⁴Harvard-MIT Health Sciences and Technology, Boston, MA, United States, ⁵Boston Children's Hospital, Boston, MA, United States, ⁶Siemens Medical Solutions Inc, Malvern, PA, United States

We introduce a highly accelerated T1-weighted MP-RAGE acquisition that utilizes a novel reordering scheme and Wave-CAIPI encoding to retain high image quality. R=9-fold accelerated in vivo MP-RAGE scans were performed in 71 sec, with maximum and average g-factor of $g_{max}=1.27$ and $g_{avg}=1.06$. Compared to the state-of-the-art 2D-CAIPIRINHA method, this is a factor of 4.6/1.4 improvement in g_{max}/g_{avg} . In addition, we demonstrate a 57 sec acquisition at 7T with R=12-fold acceleration. This acquisition had a g-factor performance of $g_{max}=1.15$ and $g_{avg}=1.04$. Wave encoding overcomes the g-factor noise amplification penalty and allows for an order of magnitude acceleration of MP-RAGE acquisitions.

443

Plasma 18

Differential Domain Analysis for 3D Cartesian Sampling

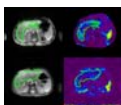
Evan Levine^{1,2} and Brian Hargreaves²

¹Electrical Engineering, Stanford University, Stanford, CA, United States, ²Radiology, Stanford University, Stanford, CA, United States

Selection of arbitrary 3D Cartesian sampling patterns for support-constrained MRI, parallel MRI, and dynamic MRI can be heuristical, and g-factor calculations require a computationally expensive simulation. To provide theoretical guidance and a method to optimize 3D Cartesian sampling, a novel concept of a differential distribution is introduced to represent a distribution of pairwise differences between sample locations, and is related to point-spread-functions. Its relationship to noise amplification in a generalized sensitivity encoding model and linear reconstruction is then used to efficiently optimize multidimensional k-space sampling. Examples in support-constrained MRI, parallel MRI, and dynamic MRI demonstrate reduced noise amplification

444

Plasma 19

Comparison of 2D and 3D MR Liver Elastography in 600 Patients

Bogdan Dzyubak¹, Kevin J. Glaser¹, Sudhakar K. Venkatesh¹, and Richard L. Ehman¹

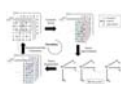
¹Radiology, Mayo Clinic, Rochester, MN, United States

2D Magnetic Resonance Elastography (MRE) is a validated method for staging liver fibrosis via liver stiffness measurements produced by introducing and imaging acoustic waves. Newer 3D MRE additionally images waves propagating out-of-plane. This retrospective study compared 2D and 3D liver MRE stiffness measurements across 600 patient exams. The two methods had excellent agreement, with 3D MRE yielding 6% lower stiffness and having lower failure rate. 3D MRE, which has the same acquisition time, is a good alternative for liver imaging as it does not suffer from out-of-plane propagation bias and has the added potential to characterize smaller abdominal organs.

445



Plasma 20



Calibrationless Parallel Imaging Reconstruction Using Hankel Tensor Completion (HTC)

Yilong Liu^{1,2}, Jun Cao^{1,2}, Mengye Lyu^{1,2}, and Ed X. Wu^{1,2}

¹Laboratory of Biomedical Imaging and Signal Processing, The University of Hong Kong, Hong Kong, People's Republic of China, ²Department of Electrical and Electronic Engineering, The University of Hong Kong, Hong Kong, People's Republic of China

Autocalibrating parallel imaging requires sufficient autocalibration signals (ACS) for reliable estimation of coil sensitivity. However, this is not feasible in some applications, for example, spectroscopic imaging where matrix size is relatively small. Recent publications (SAKE, P-LORAKS, and ALOHA, etc.) proposed to construct k-space data into block-wise Hankel matrix, and perform parallel imaging reconstruction with low rank matrix completion. In this study, we proposed to construct a block-wise Hankel tensor, and use tensor completion techniques to synthesize the unacquired samples. This method can also be extended to reconstruct multiple slices simultaneously and provide more accurate reconstruction.

446

Plasma 21



Highly Accelerated Magnetic Resonance Elastography via Bayesian Modeling

Christopher Ebersole^{1,2}, Rizwan Ahmad¹, Adam Rich¹, Lee C. Potter¹, and Arunark Kolipaka²

¹Electrical and Computer Engineering, The Ohio State University, Columbus, OH, United States, ²Radiology, The Ohio State University Wexner Medical Center, Columbus, OH, United States

While magnetic resonance elastography (MRE) provides a non-invasive method of estimating tissue stiffness, which is indicative of a variety of diseases, MRE scans typically require lengthy breath-holds which are prohibitive for many patients. We have extended a recently proposed Bayesian imaging method, called ReVEAL, for MRE. This method is capable of reconstructing images from highly undersampled data by leveraging both sparsity and the near equal magnitude across multiple offsets, inherent to MRE acquisition, as reconstruction constraints. This reconstruction method is validated against SENSE using a retrospectively downsampled phantom dataset and three retrospectively downsampled in vivo liver datasets.

447



Plasma 22



RACE-GRASP: Respiratory-weighted and Aortic Contrast Enhancement-guided GRASP MRI

Li Feng¹, Krishna Shanbhogue¹, Daniel K Sodickson¹, Hersh Chandarana¹, and Ricardo Otazo¹

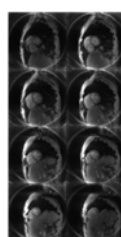
¹Center for Advanced Imaging Innovation and Research (CAI2R), New York University School of Medicine, New York, NY, United States

This work proposes a technique named RACE-GRASP (**R**espiratory-weighted and **A**ortic **C**ontrast **E**nhancement guided **G**olden-angle **R**Adial **S**parse **P**arallel imaging) for robust free-breathing DCE-MRI of the liver. First, the aortic contrast enhancement curve is automatically detected from continuously acquired data and is used to guide k-space sorting to ensure precise capture of desired contrast-enhancement phases. Second, k-space data of each contrast phase are binned into different respiratory motion states, and each motion bin is weighted differently during image reconstruction to reduce motion blurring. The performance of RACE-GRASP was demonstrated in 5 healthy volunteers and was compared with conventional GRASP.

448



Plasma 23



Real-time 3D cardiac MRI using through-time radial GRAPPA and GPU-enabled reconstruction pipelines in the Gadgetron framework

Dominique Franson¹, James Ahad², Jesse Hamilton¹, Wei-Ching Lo¹, Yun Jiang¹, Yong Chen³, and Nicole Seiberlich^{1,3}

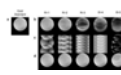
¹Biomedical Engineering, Case Western Reserve University, Cleveland, OH, United States, ²School of Medicine, Case Western Reserve University, Cleveland, OH, ³Radiology, University Hospitals, Cleveland, OH

An accelerated 3D cardiac dataset (8 partitions; in-plane spatial resolution: 2.34 x 2.34 mm²; partition thickness = 8 mm) can be reconstructed using through-time radial GRAPPA and GPU-enabled pipelines in the Gadgetron framework in approximately 515.5 ms. This work may enable real-time, 3D imaging in the heart with on-line reconstruction.

449



Plasma 24



Navigator-free EPI ghost correction using low-rank matrix modeling: Theoretical insights and practical improvements

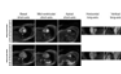
Rodrigo A. Lobos¹, Tae Hyung Kim¹, W. Scott Hoge^{2,3}, and Justin P. Haldar¹

¹Electrical Engineering, University of Southern California, Los Angeles, CA, United States, ²Radiology, Brigham and Women's Hospital, Boston, MA, United States, ³Radiology, Harvard Medical School, Boston, MA, United States

While the formation of ghost-free images from EPI data can be a difficult problem, recent low-rank matrix modeling methods have demonstrated promising results. In this abstract, we provide new theoretical insight into these approaches, and show that the low-rank ghost correction optimization problem has infinitely many solutions without using additional constraints. However, we also show that SENSE-like or GRAPPA-like constraints can be successfully used to make the problem well-posed, even for single-channel data. Additionally, we show that substantial performance gains can be achieved over previous low-rank ghost correction implementations by using nonconvex low-rank regularization instead of previous convex approaches.

450

Plasma 25



Non-ECG First-Pass Myocardial Perfusion T1 Mapping with Low-Rank Tensor Cardiovascular MR Multitasking

Anthony G. Christodoulou^{1,2}, Jaime L. Shaw^{1,3}, Xiaoming Bi⁴, Behzad Sharif^{1,5}, and Debiao Li^{1,3}

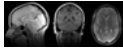
¹Biomedical Imaging Research Institute, Cedars-Sinai Medical Center, Los Angeles, CA, United States, ²Cedars-Sinai Heart Institute, Cedars-Sinai Medical Center, Los Angeles, CA, United States, ³Department of Bioengineering, University of California, Los Angeles, Los Angeles, CA, United States, ⁴Siemens Healthcare, Los Angeles, CA, United States, ⁵Department of Biomedical Sciences, Cedars-Sinai Medical Center, Los Angeles, CA, United States

Quantitative first-pass myocardial perfusion imaging is a potentially powerful tool for diagnosing coronary artery disease. However, quantification is complicated by ECG misfires and the nonlinear response of signal intensity to contrast agent concentration. Here we propose a method overcoming the curse of dimensionality to simultaneously image cardiac motion, contrast dynamics, and T1 relaxation in 2D and 3D, using a low-rank tensor imaging framework for cardiovascular MR multitasking. This non-ECG, first-pass myocardial perfusion T1 mapping method accounts for the signal intensity nonlinearity, allowing direct quantification of contrast agent concentration at any cardiac phase in any cardiac cycle.

451



Plasma 26



T1-T2 Shuffling: Multi-Contrast 3D Fast Spin-Echo with T1 and T2 Sensitivity

Jonathan I Tamir¹, Valentina Taviani², Shreyas S Vasanawala³, and Michael Lustig¹

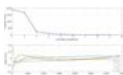
¹Electrical Engineering and Computer Sciences, University of California, Berkeley, Berkeley, CA, United States, ²MR Applications and Workflow, GE Healthcare, Menlo Park, CA, United States, ³Radiology, Stanford University, CA, United States

Volumetric fast spin-echo (3DFSE) imaging is clinically desirable because of its robustness to off-resonance and its utility for obtaining many types of image contrasts at isotropic resolution. However, its routine clinical use is inhibited by blurring due to long echo trains needed to maintain scan efficiency. Here we present T1-T2 Shuffling, a 3DFSE-based acquisition and reconstruction scheme that mitigates image blur and retrospectively synthesizes T1-weighted and T2-weighted image contrasts. The acquisition, an extension of T2 Shuffling, employs a randomizing echo train view ordering with variable repetition times (TRs). The use of short TRs increases scan efficiency while providing T1 sensitivity.

452



Plasma 27



Simultaneous T1/T2 measurements in combination with PCA-SENSE reconstruction (T1* shuffling) and multicomponent analysis

Julian Pfister¹, Martin Blaimer¹, Peter M. Jakob², and Felix A. Breuer¹

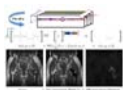
¹Magnetic Resonance and X-ray Imaging, Fraunhofer Development Center X-ray Technology (EZRT), Würzburg, Germany, ²Experimental Physics 5, University of Würzburg, Würzburg, Germany

An inversion recovery TrueFISP sequence with a golden angle based radial readout in combination with a view sharing KWIC filter reconstruction is able to produce quantitative M0, T1 and T2 maps within a single shot. However the KWIC filter leads to temporal blurring especially at high spatial frequencies. Here, we propose an alternative reconstruction method based on the principle component analysis (PCA) for providing an improved temporal fidelity. Furthermore this approach is extended for a multicomponent analysis by an inverse Laplace transform. Results from brain measurements demonstrate that this technique can identify different tissue types within a single voxel.

453



Plasma 28



Accelerated 3D Multispectral MRI with Robust Principal Component Analysis for Separation of On and Off-resonance Signals

Evan Levine^{1,2}, Kathryn Stevens², and Brian Hargreaves²

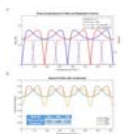
¹Electrical Engineering, Stanford University, Stanford, CA, United States, ²Radiology, Stanford University, Stanford, CA, United States

3D multispectral imaging (MSI) corrects most distortion in MRI near metallic implants at the cost of prolonged scan time by phase encoding to resolve slice distortions. However, existing methods to accelerate 3D MSI do not exploit the redundancy of slice-phase encoding for the dominant on-resonance signal. A novel compact representation of 3D-MSI images based on a decomposition of on- and off-resonance via robust principal component analysis (RPCA) is introduced to exploit this redundancy in a calibration and model-free reconstruction and push the current limits of accelerated 3D MSI. A complementary randomized sampling strategy is used to vary undersampling in different spectral bins to enable the separation. Experiments with retrospective and prospective undersampling show comparable image quality between standard MSI images and 2.6-3.4-fold accelerated RPCA and improvement over bin-by-bin compressed sensing reconstruction.

454



Plasma 29



Field Map Combination Method for Multiple-Acquisition bSSFP

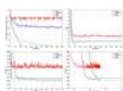
Anjali Datta¹ and Dwight G Nishimura¹

¹Electrical Engineering, Stanford University, Stanford, CA, United States

FIESTA-C/CISS enables the reconstruction of banding-free bSSFP images, but residual ripple remains in the combined images. Also, in the heart, flow near a stop-band may cause a component image to include significant contributions from out-of-slice spins; this hyper-intense signal persists in images combined using conventional methods. Here, we use a B₀ map to combine FIESTA-C/CISS cardiac cine images. Knowledge of B₀ enables us to only include pass-band signal in the final image and exclude stop- and bright-bands. In phantom and in vivo studies, the proposed method had less ripple and greatly reduced flow artifacts compared to maximum-intensity projection and root-sum-of-squares.

455

Plasma 30



Stochastic Primal-Dual Optimization for Locally Low-Rank MRI Reconstruction: A Stable Alternative to Cycle Spinning

Joshua D. Trzasko¹

¹Radiology, Mayo Clinic, Rochester, MN, United States

Locally low rank (LLR) reconstruction is an effective strategy that has found application across a range of MRI applications. In lieu of processing all overlapping image blocks each iteration, most LLR implementations employ "cycle spinning", where only a random subset of blocks is processed. Cycle spinning improves efficiency, but may compromise reconstruction convergence and introduce artifacts. We propose a primal-dual algorithm for LLR reconstruction and show that stochastically updating the dual variable provides similar computational advantage as cycle spinning but avoids its primary disadvantages. Reconstruction performance benefits are demonstrated on both a numerical phantom and in vivo.

Poster: Best of Cardiovascular MR: Myocardial Tissue Characterization

Exhibition Hall

Tuesday 17:15 - 18:15

540

Plasma 1



Three-dimensional holographic visualization of high-resolution myocardial scar on HoloLens

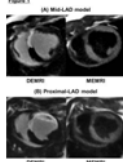
Jihye Jang^{1,2}, Gifty Addae¹, Warren Manning^{1,3}, and Reza Nezafat¹

¹Department of Medicine, Beth Israel Deaconess Medical Center and Harvard Medical School, Boston, MA, United States, ²Department of Computer Science, Technical University of Munich, Munich, Germany, ³Department of Radiology, Beth Israel Deaconess Medical Center and Harvard Medical School, Boston, MA, United States

We present a framework for 3D holographic visualization of high-resolution 3D late gadolinium enhancement (LGE) of myocardial scar on augmented-reality glass HoloLens via two approaches; 1) voxel-wise 3D scar rendering and 2) surface projection of the scar. Holographic visualization of high-resolution 3D LGE data will provide a true 3D perception of the complex scar architecture with an immersive experience to explore the clinical standard LGE images in a more interactive and interpretable way, which may facilitate MR-guided scar-related ventricular tachycardia ablation.

541

Plasma 2



Inducibility of ventricular arrhythmia correlates with the indices of myocardial viability using manganese enhanced MRI (MEMRI) in a porcine ischemia reperfusion model

Atsushi Tachibana^{1,2,3}, Junaid Zaman¹, Yuko Tada¹, Michelle R. Santoso¹, and Phillip C. Yang¹

¹Cardiovascular Medicine, Stanford University, Stanford, CA, United States, ²Radiology, AIC Yaesu Clinic, Tokyo, Japan, ³Graduate School of Human Health Sciences, Tokyo Metropolitan University, Tokyo, Japan

Peri-infarct region (PIR), containing the viable but injured myocardium, has been related to the occurrence of ventricular arrhythmia. Reliable *in vivo* detection of arrhythmogenic region presents significant challenge. While delayed enhanced MRI (DEMRI) with gadolinium (Gd) detects the myocardial infarction, the non-specific property does not detect the viable but injured cardiomyocytes in the PIR. Manganese (Mn) enters the live cells via L-type calcium channel, and enables dual enhancement technique to identify the overlapping viable region in PIR. We measured the correlation between the volume of the PIR and inducibility of ventricular arrhythmia using porcine ischemia reperfusion model.

542

Plasma 3



In Vivo Hyperpolarized MRS Study Showing Improved Cardiac Metabolism in Type 1 Diabetes with Daily L-Carnitine Treatment.

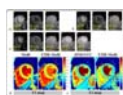
Dragana Savic¹, Kerstin N. Timm, Vicky Ball, Lisa Heather, and Damian J. Tyler

¹University of Oxford, Oxford, United Kingdom

Carnitine acts as a buffer of acetyl-CoA units in the mitochondria, as well as facilitating transport of fatty acids, and carnitine levels are decreased in the diabetic heart. The purpose of this study was to investigate the effect of L-Carnitine supplementation on cardiac function and metabolism in the diabetic rat heart. We show that daily injections of L-Carnitine can alter cardiac metabolism in the *in vivo* diabetic rat heart, and can increase flux through pyruvate dehydrogenase. Such studies will allow a better understanding of the interactions between metabolism and function in the diabetic heart and may provide new insight into novel therapeutics.

543

Plasma 4



Integrated T2 preparation and Inversion Recovery pulse (T2IR) for combined myocardium T1 and T2 mapping

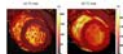
Rui Guo¹, Zhensen Chen¹, Jianwen Luo¹, and Haiyan Ding¹

¹Center for Biomedical Imaging Research, Department of Biomedical Engineering, School of Medicine, Tsinghua University, Beijing, People's Republic of China

In this study we designed a novel hybrid T1 and T2 magnetization preparation pulse (T2IR) and implement a combined T1 and T2 mapping sequence based on MOLLI scheme. Phantom experiments showed that the proposed sequence has high consistency with reference methods for both T1 ($R^2=0.99$) and T2 ($R^2=0.97$) measurements. *In vivo* results showed that high quality T1 and T2 maps of myocardium could be obtained by the proposed sequence.

544

Plasma 5



Non-contrast assessment of vasodilator response using native myocardial T1 and T2 mapping and Arterial Spin Labeled CMR

Nilesh R Ghugre^{1,2,3}, Hung P Do⁴, Kenneth Chu³, Venkat Ramanan¹, Krishna S Nayak⁵, and Graham A Wright^{1,2,3}

¹Physical Sciences Platform, Sunnybrook Research Institute, Toronto, ON, Canada, ²Schulich Heart Program, Sunnybrook Research Institute, Toronto, ON, Canada, ³Department of Medical Biophysics, University of Toronto, Toronto, ON, Canada, ⁴Department of Physics and Astronomy, University of Southern California, Los Angeles, CA, United States, ⁵Ming Hsieh Department of Electrical Engineering, University of Southern California, Los Angeles, CA, United States

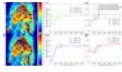
Myocardial vasodilator response is an important indicator of microvascular function and integrity in ischemic injury. The objective of our study was to systematically compare myocardial stress response with native contrast mechanisms involving quantitative T2, T1 and Arterial spin labeled (ASL) imaging. Our findings suggest that oxygenation (T2 BOLD effect), blood volume (T1 effect) and perfusion (ASL) taken together could offer a complementary contrast-free framework to identify vasodilator dysfunction in heart disease. These could potentially offer insights into the myocardial remodeling process particularly in the remote territory, which develops hypertrophy and fibrosis in the high-risk patients in the chronic stage.

545

Plasma 6

Dictionary-based Reconstruction for Free-Breathing Myocardial T₁ Mapping

Jinkyu Kang^{1,2}, Jihye Jang¹, Vahid Tarokh², and Reza Nezafat¹

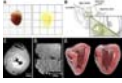


¹Department of Medicine, Beth Israel Deaconess Medical Center and Harvard Medical School, Boston, MA, United States, ²School of Engineering and Applied Science, Harvard University, Cambridge, MA, United States

In this study, we propose a novel reconstruction framework for myocardial T_1 mapping based on a dictionary-based reconstruction algorithm that simultaneously reduces scan time while compensating for respiratory and cardiac-induced motions between different T_1 -weighted images of T_1 mapping sequence.

546

Plasma 7



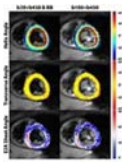
Validation of Cardiac Diffusion Tensor MRI using Transparent Tissue Preparation (CLARITY) with 3D Optical Microscopy
Christopher Nguyen¹, Sang-Eun Lee², Jongjin Yoon³, Hyuk-Jae Chang², Sekeun Kim², Chul Hoon Kim³, and Debiao Li^{1,4}

¹Biomedical Imaging Research Institute, Cedars-Sinai Medical Center, Los Angeles, CA, United States, ²Division of Cardiology, Yonsei University College of Medicine, Seoul, Korea, Republic of, ³Departement of Pharmacology, Yonsei University College of Medicine, Seoul, Korea, Republic of, ⁴Bioengineering, University of California Los Angeles, Los Angeles, CA, United States

The myocardium consists of a complex 3-dimensional (3D) microstructure has been shown to be perturbed in the presence of myocardial ischemia. Recently, diffusion tensor magnetic resonance imaging (DT-CMR) was introduced which can characterize the 3D tissue microstructure in intact myocardium. However, past histologic validation of DTI has been limited since traditional pathology allows only 2D optical microscopy after potentially destructive tissue sectioning. We present a novel approach to validate the derivation of the myocardial fiber orientation (MFO) using DT-CMR with 3D histology using a non-destructive, transparent-tissue preparation technique (CLARITY). Results indicate MFO derived from 3D histology and DT-CMR are strongly concordant.

547

Plasma 8



Free-breathing Black-blood Prepared Cardiac Diffusion Tensor Imaging

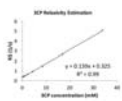
Constantin von Deuster¹, Georg Spinner¹, Robbert van Gorkum¹, Christian T. Stoeck¹, and Sebastian Kozerke¹

¹Institute for Biomedical Engineering, ETH and University Zurich, Zurich, Switzerland

In vivo cardiac Diffusion Tensor Imaging (DTI) can be influenced by myocardial perfusion. To address this limitation, reference images with moderate diffusion weighting can be employed, which, however, reduce diffusion contrast and require the acquisition of three orthogonal diffusion encoding directions. In this work, blood suppression was implemented using black blood preparation to reduce contribution of perfusion to the diffusion weighted signal. This allows for the use of a marginally weighted reference image resulting in a reduction in scan time by about 17% with improved or comparable accuracy of diffusion metrics relative to previous methods.

548

Plasma 9



First-Pass Nitroxide-Enhanced MRI for Imaging Myocardial Perfusion without Gadolinium

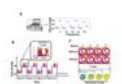
Sophia Xinyuan Cui¹ and Frederick H. Epstein^{1,2}

¹Biomedical Engineering, University of Virginia, Charlottesville, VA, United States, ²Radiology, University of Virginia, Charlottesville, VA, United States

First-pass MRI using gadolinium-based contrast agents is widely used to image myocardial perfusion. However, gadolinium is contraindicated for patients with severely impaired renal function (a substantial portion of heart disease patients), and methods that do not employ gadolinium are needed. Nitroxide stable free radicals are non-metallic compounds with an unpaired electron and, correspondingly, are paramagnetic and T1-shortening. We investigated first-pass nitroxide-enhanced perfusion MRI of the heart as an alternative to first-pass gadolinium-enhanced MRI. Five C57Bl/6 mice underwent first-pass imaging with the nitroxide agent 3CP and the results showed that nitroxide-enhanced MRI can quantify regional myocardial blood flow, as the average myocardial perfusion was 7.0 ± 1.3 ml/g/min, a value in the normal range for mice.

549

Plasma 10



Cardiac fMRI - A Novel Approach for Reliably Detecting Myocardial Oxygenation Changes with Precise Modulation of Arterial CO₂

Hsin-Jung yang¹, Ilkay Oksuz², Michael Klein³, Olivia Sobczyk³, Damini Dey¹, Jane Sykes⁴, John Butler⁴, Xiaoming Bi⁵, Behzad Sharif¹, Ivan Cokic¹, Debiao Li¹, Piotr Slomka¹, Frank S Prato⁴, Joseph Fisher³, Sotirios Tsaftaris², and Rohan Dharmakumar¹

¹Cedars Sinai Medical Center, Los Angeles, CA, United States, ²IMT School for Advanced Studies Lucca, ³University of Toronto, ⁴Lawson Health Research Institute, ⁵Siemens Healthcare

Although cardiac BOLD MRI can detect ischemic heart disease without ionizing radiation and contrast agents, its reliability remains poor due to the low sensitivity and specificity. We propose a novel strategy to overcome these barriers through: (i) an improved MRI strategy with free gas-exchange capability; (ii) repeat stimulation of heart using a validated prospective arterial CO₂ targeting technique; and (iii) a statistical framework to increase the confidence measure of BOLD signal changes. Our results show that the proposed approach can be used to significantly increase the confidence in detecting myocardial BOLD response in conditions of health and disease.

550

Plasma 11



High-fat diet feeding in mice may partially protect the heart from pressure overload induced heart failure - a longitudinal study of cardiac metabolism and function

Emmy Manders¹, Desiree Abdurrahim¹, Miranda Nabben², Klaas Nicolay¹, and Jeanine J Prompers^{1,3}

¹Department of Biomedical Engineering, Biomedical NMR, Eindhoven University of Technology, Eindhoven, Netherlands, ²Department of Genetics and Cell Biology, CARIM school for cardiovascular diseases, Maastricht University, Netherlands, ³Department of Radiology, University Medical Center, Utrecht, Netherlands

Obesity increases the risk of heart failure, but obese heart failure patients have a better prognosis and survival. Altered cardiac energy metabolism is proposed to be an important contributor to this discrepancy. With an in vivo longitudinal approach measuring cardiac function (MRI), energetics (³¹P-MRS) and lipid content (¹H-MRS) during the development of heart failure we have shown that cardiac function was less impaired in obese mice compared with lean mice after induction of pressure overload. This suggests that metabolic adaptations in obese mice are not detrimental and may even be beneficial in heart failure development.

551



Plasma 12



Cardiac Magnetic Resonance Elastography for Quantitative Assessment of Elevated Myocardial Stiffness in Cardiac Amyloidosis

Arvin Arani¹, Shivaram P. Arunachalam¹, Ian CY Chang², Francis Baffour¹, Kevin J Glaser¹, Joshua D Trzasko¹, Kiaran McGee¹, Armando Manduca¹, Martha Grogan², Angela Dispenzieri^{3,4}, Richard L Ehman¹, and Philip A Araoz¹

¹Radiology, Mayo Clinic, Rochester, MN, United States, ²Cardiovascular Diseases, Mayo Clinic, Rochester, MN, United States, ³Medicine: Division of Hematology, Mayo Clinic, Rochester, MN, United States, ⁴Laboratory Medicine and Pathology, Mayo Clinic

Myocardial stiffness plays an important role in cardiac function. The objective of this study is to evaluate if 3D high frequency cardiac MR elastography (MRE) can measure increased myocardial stiffness in cardiac amyloidosis patients compared to healthy volunteers. Twenty-two patients with cardiac amyloidosis and 16 healthy volunteers were enrolled. The myocardial stiffness of cardiac amyloid patients (median: 11.4 kPa, min: 9.2, max: 15.7) was found to be significantly stiffer ($p < 0.01$) than healthy controls (median: 8.2 kPa, min: 7.2, max: 11.8). These results motivate future investigation of 3D high frequency cardiac MRE in different patient cohorts.

552

Plasma 13



Ungated myocardial perfusion imaging with complete left ventricular coverage using radial simultaneous multi-slice imaging

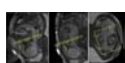
Ganesh Adluru¹, Jason Mendes¹, Ye Tian¹, Brent Wilson², and Edward DiBella¹

¹Radiology and Imaging Sciences, University of Utah, Salt lake city, UT, United States, ²Cardiology, University of Utah, Salt lake city, UT, United States

Myocardial perfusion imaging is a promising tool to determine the downstream effects of blocked coronary arteries. Ungated perfusion imaging is a promising alternative to conventional ECG-gated acquisitions. Existing ungated methods can acquire only 4-5 short-axis slices often with large slice gaps. Continuous and complete coverage is desired in order to avoid missed regions of perfusion deficit. Here we use an undersampled radial simultaneous multi-slice (SMS) acquisition to obtain complete coverage of the left ventricle. We use a block matching constrained reconstruction that is robust to inter-time frame cardiac and respiratory motion. We obtain 12 short axis slices in ~250 msec.

553

Plasma 14



As Easy as Echo: Interactive Fetal Cardiac MR Imaging

Davide Piccini^{1,2,3}, Jérôme Yerly^{2,4}, Jérôme Chaptin², Milan Prsa⁵, Yvan Mivelaz⁵, Leonor Alamo², Yvan Vial⁶, Gregoire Berchier², Chantal Rohner², Peter Speier⁷, Tobias Kober^{1,2,3}, and Matthias Stuber^{2,4}

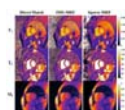
¹Advanced Clinical Imaging Technology, Siemens Healthcare AG, Lausanne, Switzerland, ²Department of Radiology, University Hospital (CHUV) and University of Lausanne (UNIL), Lausanne, Switzerland, ³LTS5, École Polytechnique Fédérale de Lausanne (EPFL), Lausanne, Switzerland, ⁴Center for Biomedical Imaging (CIBM), Lausanne, Switzerland, ⁵Department of Pediatrics, University Hospital (CHUV) and University of Lausanne (UNIL), Lausanne, Switzerland, ⁶Department of Gynecology-Obstetrics, University Hospital (CHUV) and University of Lausanne (UNIL), Lausanne, Switzerland, ⁷Magnetic Resonance, Siemens Healthcare GmbH, Erlangen, Germany

Although fetal echocardiography remains the gold standard for prenatal detection of congenital heart disease, mainly due to its ease-of-use, availability, and high diagnostic performance, MRI is occasionally used as a complementary and safe modality. However, MRI workflow is problematic as bulk fetal motion can occur anytime during acquisition, but can only be identified retrospectively, after image reconstruction. We describe an acquisition scheme that changes this workflow and allows interactive real-time planning of the fetal cardiac scan. The operator can easily find the desired scan plane even in a moving imaging target. This technique is applied and tested in two pregnant patients.

554



Plasma 15



Low Rank Compressed Sensing Reconstruction for More Precise Cardiac MRF Measurements

Jesse Ian Hamilton¹, Yun Jiang¹, Dan Ma², Yong Chen², Shivani Pawha², Wei-Ching Lo¹, Joshua Batesole², Mark Griswold^{1,2}, and Nicole Seiberlich¹

¹Biomedical Engineering, Case Western Reserve University, Cleveland, OH, United States, ²Radiology, University Hospitals, Cleveland, OH, United States

A low rank compressed sensing and parallel imaging reconstruction termed Sparse MRF is introduced to improve the precision of mapping myocardial T_1 and T_2 with MR Fingerprinting. Sparse MRF enforces data consistency while also constraining the temporal signal evolutions using a low dimensional subspace derived from the SVD of the dictionary along time. Different reconstruction parameters are investigated in simulations with a cardiac phantom. Results from phantom and in vivo cardiac scans indicate that Sparse MRF yields approximately the same mean T_1 and T_2 measurements as other MRF matching techniques but with smaller standard deviations.

Electronic Power Pitch Poster

Poster: New Molecular & Metabolic Imaging Approaches

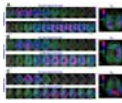
Exhibition Hall

Tuesday 17:15 - 18:15

555

Plasma 16

Dynamic Hyperpolarized ¹³C Metabolic Imaging of Patients with Brain Tumors



Ilwoo Park¹, Peder EZ Larson¹, Jeremy Gordon¹, Lucas Carvajal¹, Hsin-Yu Chen¹, Mark VanCriekinge¹, Robert Bok¹, Jason C Crane¹, Adam Elkhaled¹, Joanna Phillips², James B Slater¹, Marcus Ferrone³, John Kurhanewicz¹, Dan Vigneron¹, Susan Chang², and Sarah J Nelson¹

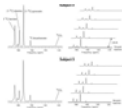
¹Radiology and Biomedical Imaging, University of California San Francisco, San Francisco, CA, United States, ²Neurological Surgery, University of California San Francisco, San Francisco, CA, United States, ³Department of Clinical Pharmacy, University of California San Francisco, San Francisco, CA, United States

Dynamic ¹³C data were acquired following injection of hyperpolarized [1-¹³C]pyruvate from 3 patients previously diagnosed with glioblastoma. Pyruvate, lactate and bicarbonate signal with high SNR were detected in human brain. Lactate/Pyruvate appeared to be relatively high in the contra-lateral, normal appearing brain. In contrast, tumor regions produced higher Lactate/Bicarbonate than contra-lateral brain. The contrast-enhancing lesion of one patient, who underwent surgical resection shortly after ¹³C imaging due to suspected recurrence, produced a relatively low level of Lactate/Pyruvate compared to contra-lateral brain and Lactate/Bicarbonate similar to the value in contra-lateral brain. Subsequent biopsy of the contrast-enhancing lesion indicated treatment effect.

556

Plasma 17

Hyperpolarized ¹³C MRS of the Human Heart



Albert P. Chen¹, Justin Y.C. Lau^{2,3}, Benjamin J. Geraghty^{2,3}, William J. Perks⁴, Idan Roifman⁵, Graham A. Wright^{2,3,5}, Kim A. Connelly⁶, and Charles H. Cunningham^{2,3}

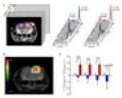
¹GE Healthcare, Toronto, ON, Canada, ²Physical Sciences, Sunnybrook Research Institute, Toronto, ON, Canada, ³Medical Biophysics, University of Toronto, Toronto, ON, Canada, ⁴Pharmacy, Sunnybrook Health Sciences Centre, Toronto, ON, Canada, ⁵Schulich Heart Program, Sunnybrook Health Sciences Centre, Toronto, ON, Canada, ⁶Cardiology, St. Michael's Hospital, Toronto, ON, Canada

The feasibility of acquiring hyperpolarized ¹³C images from human hearts following injections of HP [1-¹³C]pyruvate solution has been recently demonstrated. Following the rapid multi-slice ¹³C imaging acquisition, ¹³C spectroscopic data were acquired from the whole heart to detect any residual hyperpolarized magnetization. ¹³C pyruvate, lactate, alanine and bicarbonate were observed in all 5 subjects. ¹³CO₂ was also detected in two of the datasets. Good inter-subject consistency in the observed metabolite ratios from these spectra demonstrated the potential for changes in cardiac metabolism due to disease to be interrogated with simple whole-heart spectroscopy.

557

Plasma 18

In vivo metabolic imaging of neuroinflammation following traumatic brain injury using hyperpolarized [1-¹³C] pyruvate



Caroline Guglielmetti^{1,2}, Austin Chou^{1,2}, Karen Krukowski^{1,2}, Maria Serena Paladini^{1,2}, Lara-Kirstie Riparip^{1,2}, Susanna Rosi^{1,2,3}, and Myriam Chaumeil^{2,4}

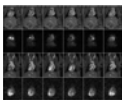
¹Brain and Spinal Injury Center, University of California San Francisco, San Francisco, CA, United States, ²Department of Physical Therapy and Rehabilitation Science, University of California San Francisco, San Francisco, CA, United States, ³Department of Neurological Surgery, University of California San Francisco, San Francisco, CA, United States, ⁴Surbeck Laboratory of Advanced Imaging, Department of Radiology and Biomedical Imaging, University of California San Francisco, San Francisco, CA, United States

This study demonstrates that metabolic imaging of hyperpolarized [1-¹³C] pyruvate can detect increased hyperpolarized lactate production *in vivo* in a preclinical model of Traumatic Brain Injury. Correlative assays further demonstrate that this increased lactate is linked to the presence of pro-inflammatory macrophages that upregulate pyruvate dehydrogenase kinase 1, subsequently leading to regional pyruvate dehydrogenase inhibition. Metabolic imaging of hyperpolarized [1-¹³C] pyruvate thus has great potential to provide a novel tool for *in vivo* detection of neuroinflammation.

558

Plasma 19

Toward Dynamic 3D Cardiac Perfusion Imaging Using bSSFP and Hyperpolarized tert-Butanol



Timothy Pagliaro¹, Gopal Varma¹, Li Zhao¹, David C Alsop¹, and Aaron K Grant¹

¹Radiology, Beth Israel Deaconess Medical Center and Harvard Medical School, Boston, MA, United States

Perfusion imaging is a promising application for hyperpolarized tracers, as they provide high signal with no endogenous background. Hyperpolarized ¹³C labeled tert-butanol is a perfusion agent with long T1 and T2 relaxation times *in vivo*. Moreover, because it diffuses freely through tissue, bolus injections of tert-butanol are largely extracted from the vasculature on a first pass, and the residence time in tissue is on the order of tens of seconds. This provides a long time frame for dynamic imaging. Here we demonstrate the feasibility of time-resolved 3D cardiac perfusion imaging in rats.

559

Plasma 20

Detection of Bacteria-specific metabolism using hyperpolarized ¹³C pyruvate



Renuka Sriram¹, Jinny Sun¹, Javier Villanueva-Meyer¹, Justin DesLos Santos¹, Christopher Mutch¹, Oren Rosenberg², Mark Van Criekinge¹, John Kurhanewicz¹, David Wilson¹, and Michael Ohliger¹

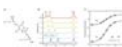
¹Radiology and Biomedical Imaging, University of California San Francisco, San Francisco, CA, United States, ²Department of Infectious Diseases, University of California San Francisco, San Francisco, CA, United States

Bacterial infection is a major health problem, with high morbidity and mortality. Current imaging techniques have limited ability to differentiate infection from either tumor or sterile inflammation, and invasive tissue sampling is frequently required. There is currently no clinically-available non-invasive method to directly detect living bacteria *in vivo*. We describe a method for detecting bacteria specific metabolism using hyperpolarized ¹³C pyruvic acid.

560

Plasma 21

In vivo pH imaging using hyperpolarized ¹³C-labelled zymonic acid



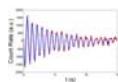
Stephan Duiwel^{1,2,3}, Christian Hundshammer^{1,2}, Malte Gersch⁴, Benedikt Feuerecker¹, Axel Haase³, Steffen J Glaser², Markus Schwaiger¹, and Franz Schilling¹

¹Department of Nuclear Medicine, Technical University of Munich, Munich, Germany, ²Department of Chemistry, Technical University of Munich, Garching, Germany, ³Institute of Medical Engineering, Technical University of Munich, Garching, Germany, ⁴Medical Research Council Laboratory of Molecular Biology, Cambridge, United Kingdom

Pathologies which overrule natural pH regulatory mechanisms such as ischemia, inflammation or tumors can trigger local pH changes in the human body. Currently, clinical routine measurement of extracellular pH is limited to measuring systemic blood pH. We synthesized, characterized, calibrated and applied [1,5-¹³C₂]zymonic acid (ZA) as a novel hyperpolarized ¹³C pH biosensor. With its demonstrated features both *in vitro* and *in vivo* (bladder, healthy kidney, Mat B III adenocarcinoma), we believe that ZA could help localize and quantify regions with aberrant acid-base balance, allowing for improved understanding, diagnostics and therapy of common diseases.

561

Plasma 22



A new method for measuring T_{1ρ} of hyperpolarized radioactive isotopes using gamma rays

Yuan Zheng^{1,2}, Gordon D. Cates¹, William A. Tobias¹, and G. Wilson Miller³

¹Department of Physics, University of Virginia, Charlottesville, VA, United States, ²UIH America, Houston, TX, United States, ³Radiology and Medical Imaging, University of Virginia, Charlottesville, VA, United States

We have developed a novel technique that combines MR and gamma detection for measuring T_{1ρ} of radioactive isotopes. Gamma-ray emission is anisotropic with respect to the polarization direction of hyperpolarized radioactive nuclei (spin > 1/2). When the spins are flipped into the transverse plane and subjected to a spin-locking field, the emission anisotropy also precesses and gamma detectors in the transverse plane will observe an oscillating count rate. Decay of the oscillation amplitude during SL can be used to fit T_{1ρ}. This technique also vastly reduces the number of spins needed for a meaningful measurement since gamma-ray detection is highly efficient.

562



Plasma 23



Occupational Manganese Exposure: Reversibility of Increased GABA Levels and Brain Mn Accumulation

David A. Edmondson¹, Ruoyun Ma¹, Chien-Lin Yeh¹, S. Elizabeth Zauber², Sandy Snyder¹, Eric Ward¹, and Ulrike Dydak¹

¹School of Health Sciences, Purdue University, West Lafayette, IN, United States, ²Department of Neurology, Indiana University School of Medicine, Indianapolis, IN, United States

While manganese (Mn) is known in the pre-clinical community as a T1 contrast agent, it is also notorious as a neurotoxin that can cause irreversible parkinsonian symptoms at high enough exposure levels. In an occupational setting, workers are exposed to Mn through processes such as welding, smelting, and other metalwork. As the workload changes over time, so does the level of exposure. Using MRI and MRS, effects of exposure such as elevated thalamic GABA levels and brain Mn deposition can be detected and show evidence of reversibility. This may help identifying meaningful no-observed-adverse-effect levels (NOAEL) as used in occupational settings.

563

Plasma 24



CM101: an optimized MR probe targeting type I collagen for detection of liver fibrosis

Christian T. Farrar¹, Richard Kennan², Eric Gale¹, Ian Ramsay^{1,3}, Ricard Masia⁴, Gunisha Arora⁵, Kailyn Looby⁵, Lan Wei⁵, Michelle Bunzel², Chunlian Zhang², Yonghua Zhu², Taro Akiyama², Michael Klimas², Shirly Pinto², Himashinie Diyabalana³, Valerie Humblet³, Bryan C. Fuchs⁵, and Peter Caravan¹

¹Athinoula A. Martinos Center for Biomedical Imaging, Department of Radiology, Massachusetts General Hospital and Harvard Medical School, Charlestown, MA, United States, ²Merck Research Laboratories, Kenilworth, NJ, United States, ³Collagen Medical, Belmont, MA, United States, ⁴Pathology, Massachusetts General Hospital, Boston, MA, ⁵Surgical Oncology, Massachusetts General Hospital, Boston, MA, United States

Recent molecular MR approaches targeting collagen demonstrated the promise of noninvasive detection and staging of liver fibrosis and monitoring treatment response, but the molecular probe used was not suitable for clinical translation due to the low stability of the Gd chelator chosen. CM-101 is a new peptide based probe using the highly stable Gd-DOTA chelate that is rapidly eliminated from plasma intact into the urine and shows no sign of Gd accumulation. CM-101 robustly detected liver fibrosis in a bile duct ligation model in rats and in a CCl₄ mouse model.

564

Plasma 25



A High Throughput, MEMRI-Based Imaging Pipeline to Study Mouse Models of Sporadic Human Cancer

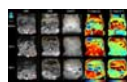
Harikrishna Rallapalli^{1,2}, I-Li Tan³, Alexandre Wojcinski³, Alexandra L Joyner³, and Daniel H Turnbull^{1,2}

¹Kimmel Center for Biology and Medicine at the Skirball Institute of Biomolecular Medicine, New York University School of Medicine, New York, NY, United States, ²Biomedical Imaging Graduate Program and Department of Radiology, New York University School of Medicine, New York, NY, United States, ³Developmental Biology, Sloan Kettering Institute, New York, NY, United States

A high-throughput imaging pipeline is presented to quantify the heterogeneity in longitudinal disease progression in mouse models of human brain cancer and to test the efficacy of novel anti-cancer therapeutics in accurate mouse models of sporadic human cancer.

565

Plasma 26



In vivo quantification of IONP-labeled PAR T-cells using positive contrast MRI

Jinjin Zhang¹, Sidath C Kumarapperuma², Qi Shao³, Lakmal Kotelawala², John C Bischof³, Carston R Wagner², and Michael Garwood¹

¹Center for Magnetic Resonance Research, Department of Radiology, University of Minnesota, Minneapolis, MN, United States, ²Department of Medicinal Chemistry, University of Minnesota, Minneapolis, MN, United States, ³Department of Mechanical Engineering, University of Minnesota, Minneapolis, MN, United States

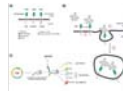
Immunotherapies have received increasing attention as novel therapeutics for the treatment of cancer and autoimmune disease. In this study, IONP labeled PAR T-cells were tracked and quantified in vivo using the SWIFT sequence for positive contrast imaging and T1 mapping. The longitudinal relaxation rate constant (R1) showed a linear dependence on the cell density in vitro and thus was used to quantify T cell density in vivo in liver. These preliminary results demonstrate how positive contrast from an ultra-short T2 sensitive sequence can provide a tool to quantify the bio-distribution of T cells.

566

Plasma 27

A Unique 'Cargo Internalization Receptor (CIR)' System for In Vivo Tracking of Individual Cell Populations by 19F MRI

Pascal Bouvain¹, Paul Baran², Tuba Güden-Silber¹, Sebastian Temme¹, Jens Moll², Doreen Floss², Christoph Grapentin³, Jürgen Scheller², and Ulrich Flögel¹



¹Molecular Cardiology, Heinrich-Heine University, Düsseldorf, Germany, ²Biochemistry and Molecular Biology II, Heinrich-Heine University, Germany, ³Pharmaceutical Technology and Biopharmacy, Albert-Ludwigs-University

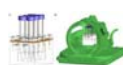
Synopsis: We demonstrate the capability of unique 'cargo internalization receptors' (CIR) for specific cell tracking. A nanobody for green fluorescent protein (GFP) was used to engineer surface receptors which undergo rapid internalization after GFP binding. For ¹⁹F MR visibility, the GFP carrier was equipped with perfluorocarbon (PFC) contrast cargo. PFC cargo uptake after CIR transfection was verified by flow cytometry, confocal microscopy, and ¹H/¹⁹F MRI. The results show that this approach can be successfully used for targeted contrast agent internalization, which can be extended to a cell-specific CIR expression in transgenic mice for in vivo cell tracking by ¹⁹F MRI.

567

Plasma 28

Characterization of Gd-DOTA-APC, a novel cancer-targeting MRI contrast agent

Christina Brunnquell¹, Ray Zhang², Benjamin Cox^{1,3}, Anatoly Pinchuk², Alan McMillan², and Jamey Weichert²



¹Medical Physics, University of Wisconsin-Madison, Madison, WI, United States, ²Radiology, University of Wisconsin-Madison, Madison, WI, United States, ³Medical Engineering Group, Morgridge Institute for Research, Madison, WI, United States

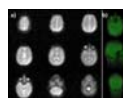
In this work we characterize the relaxivity, chemical stability, and tumor-specific uptake of a cancer-targeting T₁-shortening contrast agent, Gd-DOTA-APC. We observe striking longitudinal relaxivity of up to 16.5 s⁻¹/mM and 10.6 s⁻¹/mM at 1.5T and 3.0T, respectively. High chemical stability was measured, with less than 0.1% free Gd³⁺ detected after dissolution of the agent in buffer. Finally, we observe tumor-specific T₁-weighted signal enhancement following Gd-DOTA-APC delivery, sustained out to seven days after administration. These observations indicate that Gd-DOTA-APC holds potential as a safe and effective agent for targeted cancer imaging.

568

Plasma 29

CMRO₂ Quantification in Human Brain with Direct ¹⁷O-MRI: Profile Likelihood Analysis for Optimization of Temporal Resolution

Dmitry Kurzhunov¹, Robert Borowiak^{1,2,3}, Ali Caglar Özen¹, and Michael Bock¹



¹Dept. of Radiology, Medical Physics, Medical Center – University of Freiburg, Freiburg, Germany, ²German Cancer Consortium (DKTK), Heidelberg, Germany, ³German Cancer Research Center (DKFZ), Heidelberg, Germany

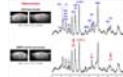
In this study the temporal resolution of ¹⁷O-MRI protocols for quantification of the cerebral metabolic rate of oxygen consumption (CMRO₂) in human brain were optimized using the profile likelihood (PL) method. For this, retrospective analysis of the influence of temporal resolution on the CMRO₂ values and their PL-based confidence intervals (CI) was performed. Dynamic ¹⁷O-MRI was implemented with a 3D golden-angle radial acquisition during and after inhalation of ¹⁷O gas. The results showed that ¹⁷O-MRI data acquired at a temporal resolution 120 ≤ Δt ≤ 165 seconds gave identifiable CMRO₂ values of 0.82–1.18/0.92–1.42 μmol/g_{issue}/min in WM/GM brain regions.

569

Plasma 30

Region-Specific Effects of AMP-Activated Protein Kinase on the Neurochemical Profiles of the Hippocampus and Midbrain in Mice

Ivan Tkac¹, Biplab Dasgupta², and Raghavendra Rao³



¹Center for Magnetic Resonance Research, University of Minnesota, Minneapolis, MN, United States, ²Division of Oncology, Cincinnati Children's Hospital Medical Center, Cincinnati, OH, United States, ³Department of Pediatrics, Division of Neonatology, University of Minnesota, Minneapolis, MN, United States

Adenosine monophosphate-activated protein kinase (AMPK) is an evolutionarily conserved signaling molecule essential for cellular energy balance. AMPK senses metabolic stress and integrates diverse physiological signals to restore energy balance. Its role in the normal brain development is not well understood. The purpose of this study was to assess whether neurochemical profiles of developing mouse brain are affected by knocking out of AMPK enzyme in a region-specific manner. Observed changes in metabolite levels (Lac, Glu) indicate reduced energy metabolism in AMPK knockout mice relative to WT controls. In addition, changes in *myo*-Ins suggest osmotic stress.

Electronic Power Pitch Poster

Poster: Marching on Musculoskeletal

Exhibition Hall

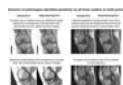
Wednesday 9:15 - 10:15

645

Plasma 1

Accelerated knee imaging using a deep learning based reconstruction

Florian Knoll^{1,2}, Kerstin Hammernik³, Elisabeth Garwood^{1,2}, Anna Hirschmann⁴, Leon Rybak^{1,2}, Mary Bruno^{1,2}, Tobias Block^{1,2}, James Babb^{1,2}, Thomas Pock^{3,5}, Daniel K Sodickson^{1,2}, and Michael P Recht^{1,2}

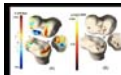


¹Radiology, NYU, New York, NY, United States, ²CAI2R, NYU, New York, NY, United States, ³Institute of Computer Graphics and Vision, Graz University of Technology, Graz, Austria, ⁴Radiology, University Hospital Basel, Basel, Switzerland, ⁵Austria Safety & Security Department, AIT Austrian Institute of Technology GmbH, Vienna, Austria

The goal of this study is to determine the diagnostic accuracy and image quality of a recently proposed deep learning based image reconstruction for accelerated MR examination of the knee. 25 prospectively accelerated cases were evaluated by three readers and show excellent concordance to the current clinical gold standard in identification of internal derangement.

646

Plasma 2



Anterior Tibial Translation Following ACL Reconstruction is Associated with Postsurgical Cartilage Matrix Changes.

Alan K Li¹, Valentina Pedaia², Keiko Amano², Jonathan Ochoa², Qi Li², Benjamin Ma², and Xiaojuan Li²

¹University of California, Berkeley, Berkeley, CA, United States, ²University of California, San Francisco, San Francisco, CA, United States

Biomechanical abnormalities and accelerated cartilage matrix changes are commonly seen following ACL injury; however, the association between the two remains unclear. The purpose of this study was to analyze the relationship between altered joint kinematics and long term cartilage health. Utilizing voxel based relaxometry with T_{1ρ} and T₂ mapping sequences, in conjunction with MRI kinematics of the tibia and femur bone, allowed for the assessment of local cartilage matrix changes 2 years following ACL reconstruction. Notably, anterior translation of the tibia in the injured knee was associated with greater cartilage degeneration in the medial femoral and tibial cartilage.

647



Plasma 3



Longitudinal characterization of deformation-induced skeletal muscle damage by T2-mapping, DWI and MRE

Jules L. Nelissen^{1,2}, Willeke A. Traa³, Larry de Graaf¹, Cees W. J. Oomens³, Jurgen H. Runge^{4,5}, Ralph Sinkus⁴, Klaas Nicolay¹, Aart J. Nederveen⁵, Martijn Froeling⁶, and Gustav J. Strijkers²

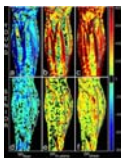
¹Biomedical NMR, Eindhoven University of Technology, Eindhoven, Netherlands, ²Preclinical and Translational MRI, Academic Medical Center, Amsterdam, Netherlands, ³Biomechanics of Soft Tissues, Eindhoven University of Technology, Eindhoven, Netherlands, ⁴Division of Imaging Sciences & Biomedical Engineering, King's College London, London, United Kingdom, ⁵Radiology, Academic Medical Center, Amsterdam, Netherlands, ⁶Department of Radiology, University Medical Center Utrecht, Utrecht, Netherlands

Skeletal muscle injury is often accompanied by fibrosis, fatty infiltration, and edema. There is great need for imaging readouts to detect and quantify such compositional changes, which would aid understanding and greatly assist in the development of emerging therapies. The goal of this work was to use a multi-modality approach, combining magnetic resonance elastography (MRE; muscle stiffness, fibrosis) with diffusion-weighted imaging (DWI; myocyte integrity) and T₂-mapping (edema, inflammation) to provide a comprehensive assessment of muscle injury development and regeneration. The multi-modality assessment provided differential readouts of the deformation-induced muscle injury development and regeneration process.

648



Plasma 4



Age Related Differences in Shear Strain in Medial Gastrocnemius: Implications for Lateral Transmission of Force

Vadim Malis¹, Usha Sinha², Robert Csapo³, and Shantanu Sinha³

¹Physics, UC San Diego, San Diego, CA, United States, ²Physics, San Diego State University, San Diego, CA, United States, ³Radiology, UC San Diego, San Diego, CA, United States

The disproportionate loss of muscle force in comparison to loss of muscle mass with age remains unexplained. Recent studies indicate that the remodeling of the extracellular matrix (ECM) may disrupt lateral force transmission pathways mediated by the ECM. Shear strain is the mechanism that supports lateral transmission of force. We quantified shear strain in muscle from the strain rate tensor derived from velocity encoded phase contrast dynamic images of the in-vivo human calf muscle under isometric contractions. The maximal shear strain was significantly lower in the older cohort compared to the younger cohort which potentially identifies that lateral force transmission decreases with age.

649 Plasma 5

Parameter	High-BW TSE	CS-SEM TSE	CS-SEM TSE
Reliability	0.85	0.92	0.95
Repeatability	0.88	0.93	0.96
Precision	0.82	0.91	0.94
Symptom Correlation	0.75	0.85	0.88
Malrotation	0.78	0.88	0.91
CS-SEM TSE	0.80	0.90	0.93
High-BW TSE	0.85	0.92	0.95

Metal Artifact Reduction MRI for the Assessment of the Rotational Alignment Knee Arthroplasty Implants: Compressed Sensing SEMAC TSE versus High-Bandwidth

Filippo Del Grande^{1,2}, Benjamin Fritz³, Satre Stuelke⁴, Steven E Stern⁵, Susanne Bensler³, and Jan Fritz¹

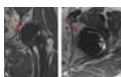
¹Radiology, The Johns Hopkins University School of Medicine, Baltimore, MD, United States, ²Radiology, Ospedale Regionale di Lugano, Lugano, Switzerland, ³University Hospital Balgrist, Zurich, Switzerland, ⁴Radiology, The Johns Hopkins University School of Medicine, Baltimore, MD, ⁵Queensland University of Techn

Malrotation of

knee arthroplasty implants is a source of pain following total knee arthroplasty and maybe measured on metal artifact reduction MR images; however, it is unclear Therefore, we compared the reliability, repeatability, and precision of rotational alignment measurements that were obtained on optimized high-bandwidth and CS SEMAC TSE MR images and their relationships with symptoms. CS-SEM TSE MRI afforded the highest reliability, repeatability and precision of rotational alignment which correlate best with symptoms. CS-SEM TSE MRI may be preferred over high-BW TSE for rotational alignment measurements of knee arthroplasty implants.

650

Plasma 6



Ability of MAVRIC MRI to Predict Component Loosening in Total Hip Arthroplasty

Allissa Jo Burge¹, Gabrielle P Konin¹, Jennifer Berkowitz¹, Matthew Koff¹, Douglas Padgett², and Hollis Potter³

¹Radiology and Imaging, Hospital for Special Surgery, New York, NY, United States, ²Adult Reconstruction and Joint Replacement, Hospital for Special Surgery, New York, NY, United States, ³Hospital for Special Surgery, New York, NY, United States

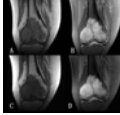
Improved metal reduction techniques for conventional MRI pulse sequences and the addition of MAVRIC (multiacquisition variable resonance image combination) have been established as useful in assessing component osteolysis and synovial reactions. The purpose of this retrospective study was to determine the utility of MRI in assessing loosening of total hip arthroplasty in a cohort of patients using surgical confirmation of loosening as the gold standard. Our results show that loosening can be predicted with high sensitivity and specificity; however, intraoperative variability in assessing loosening and the overall low frequency of implant loosening are limiting factors.

651

Plasma 7

Simultaneous multi-slice TSE for clinical MR Imaging of lesions in the knee

Xiaona Li¹, Zhigang Peng¹, Yi Sun², Panli Zuo², Dingxin Wang³, and Jianling Cui¹



¹Radiology, the Third Hospital of Henbei Medical University, Shijiazhuang, People's Republic of China, ²MR Collaboration NE Asia, Siemens Healthcare, Shang Hai, People's Republic of China, ³Siemens Medical Solutions USA, Inc., Minneapolis, MN, United States

To introduce simultaneous multiple slices (SMS) turbo spin echo (TSE) and to evaluate its image quality and diagnostic accuracy for lesions in the knee. Participants were examined by SMS and routine TSE sequences. Both sequences were evaluated by three radiologists with subjective and objective scores in T1- and PD-weighted images. The diagnostic value in lesions was evaluated. SMS requires less scan time and offers similar imaging quality and diagnostic rate compared to routine TSE sequence. SMS is a valuable technique for MR examination of the knee.

652

Plasma 8

Simultaneous T2 Relaxometry and Morphometry of Cartilage and Meniscus with Double-Echo in Steady-State in Five Minutes

Akshay S Chaudhari¹, Marianne S Black¹, Bragi Sveinsson¹, Garry E Gold¹, and Brian A Hargreaves¹



¹Radiology, Stanford University, Stanford, CA, United States

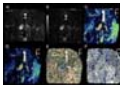
Quantitative MRI parameters such as T₂ relaxation times and morphometry are potential biomarkers for tracking spatial and temporal changes in musculoskeletal diseases and injuries. While cartilage has been widely studied, the short-T₂ of meniscus makes it challenging to quantify in short scan times. In this study, we optimized the double-echo steady-state (DESS) pulse sequence to produce high-resolution and high signal-to-noise ratio images in five minutes. We compared the relaxometry and morphometry measures against established methods and found no significant differences. This suggests that a five-minute DESS scan could be used for simultaneous relaxometry and morphometry of the cartilage and meniscus.

653

Plasma 9

Soft Tissue Tumors: Use of Intravoxel Incoherent Motion MR Imaging for Assessment of Diffusion and Perfusion for the Differentiation of Benign from Malignant Tumors

Haijun Wu¹ and Changhong Liang¹



¹Department of Radiology, Guangdong General Hospital, Guangdong Academy of Medical Sciences, Guangzhou, People's Republic of China

The apparent diffusion coefficient (ADC) had better diagnostic performance than other Intravoxel incoherent motion (IVIM)-derived parameters did for differentiating malignancies from benign soft-tissue tumors. The f values of intermediate soft-tissue tumors are significantly lower than those of benign and malignant soft-tissue tumors. The combination of ADC and f values is significantly better than other IVIM parameters at differentiating soft-tissue tumors.

654

Plasma 10

1-year Follow-Up of T_{1ρ} for Assessing Radiocarpal Cartilage Matrix Changes after Anti-TNF treatment for Rheumatoid Arthritis: Preliminary Results

Eric Ku¹, Valentina Pedita¹, Matthew Tanaka¹, Hyo Jin Choi¹, Ursula Heilmeier¹, Andrew Burghardt¹, Jonathan Graf², John Imboden², Thomas Link¹, and Xiaojuan Li¹



¹Department of Radiology and Biomedical Imaging, UCSF, San Francisco, CA, United States, ²Department of Medicine, UCSF, San Francisco, CA, United States

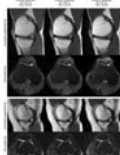
MR T_{1ρ} is used to investigate biochemical changes in cartilage composition, but few studies have looked at its application in radiocarpal wrist cartilage. In this study, we assess 1-year changes in T_{1ρ} following rheumatoid arthritis treatment and its relationship with changes in clinical disease activity scores and patient-reported outcomes. Changes between 1-year and baseline T_{1ρ} values correlated significantly with disease activity score changes and approached significance with patient-reported outcome changes during the same period. Changes in T_{1ρ} values at 3-months also correlated significantly with 1-year changes in metacarpophalangeal and wrist bone erosion volume measured with high-resolution peripheral quantitative CT (HR-pQCT).

655

Plasma 11

Simultaneous Multi-Slice Accelerated High Resolution MRI of the Knee: Comparison with In-plane Parallel Imaging Acceleration

Jan Fritz¹, Benjamin Fritz², Jialu Zhang^{3,4}, Dharmdev H Joshi¹, Gaurav K Thawait¹, Li Pan⁵, and Dingxin Wang^{3,5}



¹The Johns Hopkins University School of Medicine, Baltimore, MD, United States, ²Orthopaedic University Hospital Balgrist, ³University of Minnesota, ⁴Zhejiang University, ⁵Siemens Healthcare USA

Simultaneous multi-slice acceleration techniques excite, acquire, and reconstruct multiple slices simultaneously and provide the potential to create substantially accelerated clinical TSE protocols with similar spatial and contrast resolution to current TSE protocols. We quantified the signal-to-noise and contrast-to-noise ratios of various combinations of parallel and simultaneous multi-slice acceleration and compared two 4-fold accelerated TSE protocols against a clinical 2-fold accelerated TSE standard. Our results demonstrate that 4-fold TSE acceleration enables 43-60% shorter acquisition times with similar image quality, structural visibility and observer satisfaction than standard parallel imaging acceleration.

656

Plasma 12

New insights into the predilection sites of Juvenile Osteochondritis Dissecans using Quantitative Susceptibility Mapping



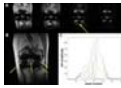
Jutta Ellermann¹, Casey P Johnson², Luning Wang³, Ferenc Toth⁴, Kevin Shea⁵, Cathy Carlson⁶, and Mikko J Nissi^{7,8}

¹Radiology, University of Minnesota, Minneapolis, MN, United States, ²Radiology, CMRR, University of Minnesota, ³University of Minnesota, ⁴College of Veterinary Medicine, University of Minnesota, ⁵St. Lukes Orthopaedics, Boise, ID, ⁶College of Veterinary Medicine, University of Minnesota, St. Paul, MN, ⁷Department of Applied Physics, University of Eastern Finland, ⁸Diagnostic Imaging Center, Kuopio University Hospital, Kuopio, Finland

The unique utilization of tissue-inherent MRI contrast using QSM for depicting the intraepiphyseal vascular supply provides high resolution and accuracy without using exogenous contrast making it a noninvasive tool for future in vivo studies. A better understanding of the development of the epiphyseal cartilage vascularity during skeletal maturation may shed light on the etiology of many developmental diseases, such as Juvenile Osteochondritis Dissecans that are precursors to osteoarthritis.

657

Plasma 13



Pile up correction for 3D-Multi Spectral Imaging using Gaussian Spectral Modeling and Bin Expansion

S Sivaram Kaushik¹ and Kevin Koch²

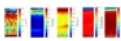
¹MR Applications and Workflow, GE Healthcare, Waukesha, WI, United States, ²Radiology, Medical College of Wisconsin, Milwaukee, WI, United States

The difficulty of imaging around metal implants has been overcome using pulse sequences such as MAVRIC SL and SEMAC. While the images are largely artifact-free, subtle intensity fluctuations, or 'pile up' artifacts still remain. The post-processing approach presented here uses information extracted from a spectral-domain model to identify and correct local fluctuations in image intensity. In these regions, the spectral bins are expanded using a moving average filter. When the expanded bins are combined, the pile up is significantly reduced. This pile up correction can improve the aesthetic quality of the images, and significantly improve their diagnostic ability.

658



Plasma 14



Correlation Time Mapping of Articular Cartilage: correlation with tissue composition and structure

Hassaan Elsayed^{1,2}, Stefan Zbyn², Mikko J Nissi^{3,4}, Jari Rautiainen^{1,2,3,5}, Matti Hanni^{1,2,5}, and Miika T Nieminen^{1,2,5}

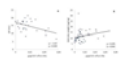
¹Medical Research Center, University of Oulu and Oulu University Hospital, Oulu, Finland, ²Research Unit of Medical Imaging, Physics and Technology, University of Oulu, Oulu, Finland, ³Department of Applied Physics, University of Eastern Finland, Kuopio, Finland, ⁴Diagnostic Imaging Center, Kuopio University Hospital, Kuopio, Finland, ⁵Department of Diagnostic Radiology, Oulu University Hospital, Oulu, Finland

Correlation time (τ_c) is a physical property of the tissue that describes the dynamics of water molecules in their microenvironment. In this study, τ_c and T2 maps were obtained from enzymatically digested bovine samples. To evaluate the relationship between τ_c and macromolecular components of cartilage, depth-wise τ_c profiles were correlated with quantitative histological measurements. The same comparison was performed for T2 data. Our results suggest that τ_c is sensitive to the laminar architecture of cartilage and to the proteoglycan content in the radial zone. τ_c provides complementary information to conventional T2 mapping.

659



Plasma 15



Correlation of 7T gagCEST MRI with Electromechanical and Biochemical Properties of Femoral Articular Cartilage

Sander Brinkhof¹, Razmara Nizak², Sotcheadt Sim³, Vitaliy Khlebnikov¹, Dennis Klomp¹, and Daniel Saris^{2,4}

¹Radiology, University Medical Center Utrecht, Utrecht, Netherlands, ²Orthopaedics, University Medical Center Utrecht, Utrecht, ³Biomomentum Inc., Laval, QC, Canada, ⁴MIRA Institute for Biomedical Technology and Technical Medicine, University of Twente, Enschede, Netherlands

The purpose of this study was to validate the 7T 3D gagCEST measurements obtained in patients in vivo, using correlation of MRI GAG values with electromechanical mapping of the articular cartilage and biochemical analyses. Five patients were scanned before their total knee replacement, after which the extracted cartilage samples were used for electromechanical mapping and biochemical analyses. GAG content as determined by gagCEST MRI shows to be significantly correlated with biochemically measured GAG dry weight and with electromechanical mapping. This work shows that the electromechanical properties of cartilage are correlated with gagCEST MRI values.

Electronic Power Pitch Poster

Poster: Cancer Imaging in the Body

Exhibition Hall

Wednesday 9:15 - 10:15

660

Plasma 16



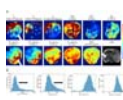
Interobserver Agreement and Diagnostic Performance of LI-RADS v2014 on contrast-enhanced MRI for non-HCC malignancies.

Nataly de Souza Maciel Rocha Horvat¹, Ines Nikolovski¹, Niamh Long¹, Scott Gerst¹, Jian Zheng¹, Linda Ma Pak¹, Junting Zheng¹, Lorenzo Mannelli¹, and Richard Kinh Gian Do¹

¹Memorial Sloan Kettering Cancer Center, NY, NY, United States

Patients at risk for hepatocellular carcinoma (HCC) are often also at risk for intrahepatic cholangiocarcinoma (ICC) and combined hepatocellular cholangiocarcinoma (cHCC-ICC). The purpose of this study was to evaluate the sensitivity and specificity of MRI in 4 radiologists using LI-RADS v2014 and their inter-reader agreement for diagnosing non-HCC malignancies (ICC and cHCC-ICC). Applying LI-RADS v2014, we found sensitivities between 74% to 88% for the diagnosis of non-HCC malignancies with moderate to substantial interreader agreement for LI-RADS category as LR-M or non LR-M. However, lower sensitivity was seen for smaller tumors, which are known to overlap with HCC in imaging appearance.

Plasma 17



Quantification of hepatocellular carcinoma tumor heterogeneity with multiparametric MRI

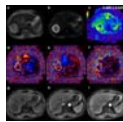
Stefanie Hectors¹, Mathilde Wagner¹, Octavia Bane¹, Cecilia Besa¹, Sara Lewis², Romain Remark³, Nelson Chen¹, M. Isabel Fiel⁴, Hongfa Zhu⁴, Sacha Gnjatich⁵, Miriam Merad³, Yujin Hoshida⁶, and Bachir Taouli¹

¹Translational and Molecular Imaging Institute, Icahn School of Medicine at Mount Sinai, New York, NY, United States, ²Department of Radiology, Icahn School of Medicine at Mount Sinai, New York, NY, United States, ³Immunology Institute, Icahn School of Medicine at Mount Sinai, New York, NY, United States, ⁴Department of Pathology, Icahn School of Medicine at Mount Sinai, New York, NY, United States, ⁵Oncological Science, Icahn School of Medicine at Mount Sinai, New York, NY, United States, ⁶Department of Medicine/Division of Liver Diseases, Icahn School of Medicine at Mount Sinai, New York, NY, United States

We assessed tumor heterogeneity in hepatocellular carcinoma using multiparametric MRI (mpMRI) combining DWI, BOLD-MRI, TOLD-MRI and DCE-MRI measurements. Histogram characteristics (central tendency parameters mean and median and heterogeneity parameters standard deviation, kurtosis and skewness) of mpMRI data were quantified in the lesions and correlated between MRI methods and with histopathology and gene expression levels in a subset of patients. We observed that central tendency and heterogeneity parameters were largely complementary in terms of the assessed correlations. The proposed histogram analysis is therefore promising for noninvasive HCC characterization on the functional, immunohistochemical and genomics level.

662

Plasma 18



3D MR Elastography in Prediction of Tumor Capsule Formation of Hepatocellular Carcinoma (HCC) in Patients with Hepatitis B Virus Infection

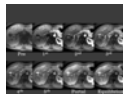
Jin Wang¹, Hao Yang¹, Yong Liu², Jingbiao Chen¹, Tianhui Zhang¹, Kevin J. Glaser³, Xin Li⁴, Jun Chen³, Yao Zhang¹, Qungang Shan¹, Bingjun He¹, Zhuang Kang¹, Yin Meng³, Dzyubak Bogdan³, Venkatesh SK³, Ronghua Yan¹, Xi Long¹, and Richard L. Ehman³

¹Department of Radiology, the Third Affiliated Hospital, Sun Yat-sen University (SYSU), Guangzhou, People's Republic of China, ²Department of Pathology, the Third Affiliated Hospital, Sun Yat-sen University (SYSU), Guangzhou, People's Republic of China, ³Department of Radiology, Mayo Clinic, Rochester, United States, ⁴GE Healthcare MR Research China, Guangzhou, People's Republic of China

Hepatocellular carcinoma (HCC) is one of the leading causes of cancer-related deaths around the world. Tumor capsule formation is a significant and independent predictor of survival and recurrence. We explored the potential value of HCC stiffness using 3D MR elastography for the prediction of tumor capsule formation. Results in 50 examinations showed that HCC stiffness has promise for the preoperative prediction of tumor capsule formation, thus providing motivation for further evaluation of HCC characteristics with MRE.

663

Plasma 19



Dynamic Contrast Enhanced MR Imaging of Hepatopancreatobiliary lesions in Combined use of Parallel Imaging and Compressed Sensing

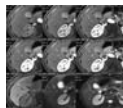
Takayuki Masui¹, Motoyuki Katayama¹, Yuji Iwadate², Naoyuki Takei², Kang Wang³, Kevin King⁴, Kei Tsukamoto¹, Mitsuteru Tsuchiya¹, Yuki Hayashi¹, Masako Sasaki¹, Takahiro Yamada¹, Kenichi Mizuki¹, Harumi Sakahara⁵, Koji Yoneyama¹, and Yuki Takayanagi¹

¹Radiology, Seirei Hamamatsu General Hospital, Hamamatsu, Japan, ²Global MR Applications and Workflow, GE Healthcare Japan, Hino, Japan, ³Global MR Applications and Workflow, GE Healthcare, Madison, WI, United States, ⁴Global MR Applications and Workflow, GE Healthcare, Waukesha, WI, United States, ⁵Radiology, Hamamatsu University School of Medicine, Hamamatsu, Japan

The feasibility of dynamic Gd-contrast study using turbo LAVA with ARC and CS for evaluation of pancreatobiliary lesions was evaluated. Acceptable image quality and good temporal resolutions with selective recognition of vasculatures, and lesion detections in the liver and pancreas could be made. With this technique, dynamic contrast imaging with high temporal and spatial resolutions can cover the wide area. It takes acceptable time for imaging reconstruction with ARC and CS at clinical 3T MR unit.

664

Plasma 20



Detection and measurement of neuroendocrine tumors liver metastases using Gd-EOB-DTPA enhanced MRI: comparison between multiple arterial phases, hepatobiliary phase, and DWI

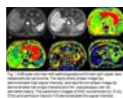
Jia Xu¹, Xuan Wang¹, Hua dan Xue¹, Shi tian Wang¹, Hui Liu², and Zheng yu Jin¹

¹Department of Radiology, Peking Union Medical College Hospital, Beijing, People's Republic of China, ²Siemens Ltd, Shanghai, People's Republic of China

The detection and evaluation of liver metastasis (LM) is important in initial staging and follow-up examinations of neuroendocrine tumors patients. Our aim is to compare different sequences including multiple arterial phases (MA), hepatobiliary phase (HA), diffusing-weighted imaging (DWI), and T2WI in Gd-EOB-DTPA-enhanced MRI, to find which sequence is better for detecting LM and which is better for size measurement. MA using CDT-VIBE were superior for the detection of small lesions. HBP imaging shows better repeatability in size measuring and may be a better choice for lesion size measurement during follow-up.

665

Plasma 21



Integrated slice-specific shimming (iShim) intravoxel incoherent motion diffusion-weighted MR imaging in the liver: the value of differential diagnosis between benign and malignant hepatic tumors

Hongxia Wang¹, Qingbo Li², Bin Wang³, Qinglei Shi⁴, Yan Feng¹, Xingyue Jiang¹, and Peigong Zhang³

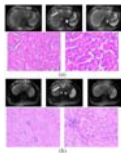
¹Radiology Department, Binzhou Medical University Hospital, Binzhou, People's Republic of China, ²Emergency Department, Binzhou People's Hospital, Binzhou, People's Republic of China, ³Binzhou Medical University, Yantai, People's Republic of China, ⁴MR Scientific NE Asia, Siemens Healthcare, Beijing, People's Republic of China

This study investigated the value of ADC value, D, Dstar, ADC₅₀₀₋₈₀₀ acquired with prototype iShim sequence at 3T. All those parameters demonstrated high diagnostic capacity in distinguishing benign and malignant hepatic lesions and in distinguishing different types of malignant hepatic lesions, among which ADC₅₀₀₋₈₀₀ demonstrated the best diagnostic performance, which may have great value in clinical practice in future.

666

Plasma 22

Quantitative texture feature to predict Microscopic portal vein invasion of Hepatocellular carcinoma with contrast-enhanced MR images



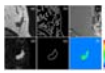
Wu Zhou¹, Qiyao Wang¹, Su Yao², Guangyi Wang³, Zaiyi Liu³, Changhong Liang³, and Lijuan Zhang¹

¹Shenzhen Institutes of Advanced Technology, Chinese Academy of Sciences, Shenzhen, People's Republic of China, ²Department of Pathology, Guangdong General Hospital, Guangdong Academy of Medical Sciences, ³Department of Radiology, Guangdong General Hospital, Guangdong Academy of Medical Sciences

Portal vein invasion of Hepatocellular carcinoma (HCC) is a well-known prognostic factor for patients after hepatic resection or liver transplant. Typical risk factors of microscopic venous infiltration (MVI) include large tumor size, multifocality, poor histological grade and non-smooth tumor margins. In this work, we adopt a new technique for quantitative texture feature Gray-level-run-length nonuniformity (GLRLN) to predict MVI of HCC based on the contrast-enhanced magnetic resonance images (CE-MRI). The present study showed that the proposed texture feature GLRLN in the portal vein phase of CE-MRI yielded best performance as compared with typical markers for the prediction of MVI.

667

Plasma 23



Conductivity of different malignancy grades of invasive ductal carcinomas and fibroadenomas

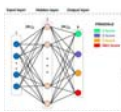
Ulrich Katscher¹, Mussa Gagiyev¹, Naoko Mori², Keiko Tsuchiya³, Jochen Keupp¹, and Hiroyuki Abe⁴

¹Philips Research Europe, Hamburg, Germany, ²Tohoku University, Sendai, Japan, ³Shiga University, Hikone, Japan, ⁴University of Chicago, IL, United States

In ex vivo studies, breast tumors exhibit a significantly altered electric conductivity, measurable in vivo using "Electric Properties Tomography". A significant conductivity difference was reported between benign and malignant breast tumors and between invasive and in situ carcinomas. This study tested a correlation between conductivity and WHO grade of invasive ductal carcinomas (IDCs) and benign fibroadenomas. A clear conductivity difference was found between IDC grade 1 and grade 2, as well as between IDC grade 1 and grade 3. No clear difference was found between fibroadenoma and IDC grade 1, as well as between IDC grade 2 and grade 3.

668

Plasma 24



A computer aided diagnosis (CAD) scoring tool: prostate cancer risk evaluation with PI-RADS v2 Guidelines

Lian Ding¹, Ge Gao², Yajing Zhang³, Chengyan Wang¹, Jue Zhang^{1,4}, Xiaoying Wang^{1,2}, and Jing Fang^{1,4}

¹Academy for Advanced Interdisciplinary Studies, Peking University, Beijing, People's Republic of China, ²Department of Radiology, Peking University Frist Hospital, Beijing, People's Republic of China, ³Philips Healthcare, Suzhou, China, Beijing, People's Republic of China, ⁴College of Engineering, Peking University, Beijing, People's Republic of China

The second version of the Prostate Imaging Reporting and Data System (PI-RADSV2) indicates the likelihood of a clinically significant cancer with a simplified 5-point scale. To assist radiologists in making diagnostic decisions consistent with the PI-RADSV2, we proposed a machine learning-based computer aided diagnosis (CAD) scoring tool of prostate cancer risk evaluation by combining apparent diffusion coefficient (ADC) and T2-weighted MRI-based features. The tool could provide a malignancy prediction color map of 5 scores. The statistical results of the total score test for 130 patients between radiologist graded and the CAD tool showed high accuracy and AUC.

669

Plasma 25



Deep learning to improve prostate cancer diagnosis

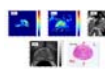
Nikolaos Dikaos¹, Edward W Johnston², Harbir S Sidhu², Mrishta B Appaya², Alex Freeman³, Hashim U Ahmed⁴, and Shonit Punwani²

¹Electrical Engineering, University of Surrey, Guildford, United Kingdom, ²Centre for Medical Imaging, University College London, ³Histopathology, University College London, ⁴Surgery and Interventional Science, University College London

Multiparametric MRI (mp-MRI) can localize tumour within the prostate, guide biopsy, and assess disease burden. Nevertheless, mp-MRI itself remains imperfect. Almost 40% of mp-MRI studies are reported as indeterminate for significant cancer. An indeterminate mp-MRI confers no patient benefit, such patients require either repeat interval mp-MRI and/or subsequent biopsy. There remains a clear unmet need to improve diagnostic imaging over and above standard mp-MRI protocols. Previous work has developed zone specific logistic regression (LR) models for the determination of significant cancer (any cancer-core-length (CCL) with Gleason>3+3 or any grade with CCL≥4 mm) in the peripheral (PZ) and the transition zone (TZ) based on quantitative mp-MRI parameters following MR imaging. This work proposes a state-of-art deep learning method to detect prostate cancer both in the PZ and the TZ. The proposed model is trained on a cohort of patients imaged at a 3T scanner, and validated on independent cohort of patients imaged at a 1.5T scanner. The performance of the model was compared with LR, Support Vector Machines and traditional Neural Networks.

670

Plasma 26



Comparing the Diagnostic Accuracy of Luminal Water Imaging with Diffusion-Weighted and Dynamic Contrast-Enhanced MRI for Evaluation of Prostate Cancer.

Shirin Sabouri¹, Silvia D Chang^{2,3,4}, Richard Savdie², Edward C Jones⁵, S. Larry Goldenberg^{2,3}, Peter C Black^{2,3}, and Piotr Kozlowski^{2,3,4,6}

¹Department of Physics and Astronomy, University of British Columbia, Vancouver, BC, Canada, ²Department of Urologic Sciences, University of British Columbia, Vancouver, BC, Canada, ³Vancouver Prostate Centre, Vancouver, BC, Canada, ⁴Department of Radiology, University of British Columbia, Vancouver, BC, Canada, ⁵Department of Pathology and Laboratory Medicine, University of British Columbia, Vancouver, BC, Canada, ⁶UBC MRI Research Center, Vancouver, BC, Canada

Luminal water imaging (LWI) is a newly developed MRI technique that has shown promising results for diagnosing and grading of prostate cancer. Incorporating LWI in clinical settings requires a profound investigation on its diagnostic accuracy by comparing it to existing clinical protocols. In this pilot study we have acquired and analyzed LWI, DWI, and DCE-MRI data from 15 patients to compare the diagnostic accuracy of LWI with the other two techniques. Our results show that LWI provides equal or higher accuracy in detection of tumors and better correlation with tumor grade compared to DWI and DCE-MRI.

671

Plasma 27

Novel Informatics Modeling of Magnetic Resonance Imaging Metrics for Characterizing Prostate Lesions with Pathology Correlation.

Katarzyna J. Macura^{1,2}, Vishwa Parekh³, Seyed Saied⁴, and Michael A. Jacobs^{1,2}

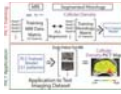


¹The Russell H. Morgan Dept of Radiology and Radiological Science, The Johns Hopkins University School of Medicine, Baltimore, MD, United States, ²Sidney Kimmel Comprehensive Cancer Center, The Johns Hopkins University School of Medicine, Baltimore, MD, United States, ³Computer Science, The Johns Hopkins University, Baltimore, MD, United States, ⁴Dept of Radiology, University of Minnesota, Minneapolis, United States

Precision medicine is increasingly being used in radiological applications. Advanced machine learning coupled with informatics modeling of clinical and radiological variables can provide the foundation to relate to precision medicine in patients with prostate cancer. We test our modeling using multiparametric prostate MR imaging (mpMRI) and MR-guided prostate biopsy with magnetic resonance-transrectal ultrasound (MR-TRUS) fusion to correlate the imaging features with histopathological results.

672

Plasma 28



Predictive Cytological Topography (PiCT): a Radiopathomics Approach to Mapping Prostate Cancer Cellularity

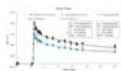
Amy Kaczmarowski¹, Kenneth A Iczkowski², Sarah L Hurrell¹, Sean D McGarry¹, Kenneth Jacobsohn³, William A Hall⁴, Mark Hohenwarter¹, William See³, and Peter S LaViolette¹

¹Radiology, Medical College of Wisconsin, Milwaukee, WI, United States, ²Pathology, Medical College of Wisconsin, Milwaukee, WI, United States, ³Urology, Medical College of Wisconsin, Milwaukee, WI, United States, ⁴Radiation Oncology, Medical College of Wisconsin, Milwaukee, WI, United States

This study combines radiographic images and pathological microscopy with machine learning to generate predictive maps of pathological features (i.e. new contrasts) based on segmented histological features. Predictive cytological topography (PiCT) maps of cellularity were utilized to detect additional pathologically confirmed high-grade prostate cancer tumors missed by radiologists.

673

Plasma 29



Estimating breast tumor blood flow and blood volume using MRI: DCE vs IVIM

Leonidas Georgiou¹, Nisha Sharma², Daniel Wilson³, and David L Buckley¹

¹Division of Biomedical Imaging, University of Leeds, Leeds, United Kingdom, ²Department of Radiology, Leeds Teaching Hospital NHS Trust, ³Department of Medical Physics and Engineering, Leeds Teaching Hospital NHS Trust

There is an increasing interest on whether IVIM parameters can be used as surrogates of perfusion and thus complement information on tumor microstructure. DCE-MRI techniques on the other hand have been widely used to characterise perfusion and hence offer the opportunity to test this hypothesis. In this study, we use high temporal resolution DCE-MRI and IVIM-DWI techniques to monitor patients with advanced breast cancer at various stages of their neoadjuvant chemotherapy, and assess the physiological relationship between perfusion and IVIM parameters.

674

Plasma 30



Discrimination of Malignant versus Benign Mediastinal Lymph Nodes Using Diffusion MRI with An IVIM Analysis

Li-Ping Qi^{1,2}, Wan-Pu Yan³, Ke-Neng Chen³, Zheng Zhong^{2,4}, Kejia Cai^{2,5}, Xiao-Ting Li¹, Ying-Shi Sun¹, and Xiaohong Joe Zhou^{2,6}

¹Radiology, Peking University Cancer Hospital and Institute, Beijing, People's Republic of China, ²Center for MR Research, University of Illinois at Chicago, Chicago, IL, United States, ³Thoracic Surgery, Peking University Cancer Hospital and Institute, Beijing, People's Republic of China, ⁴Bioengineering, University of Illinois at Chicago, Chicago, IL, United States, ⁵Radiology and Bioengineering, University of Illinois at Chicago, Chicago, IL, United States, ⁶Radiology, Neurosurgery, and Bioengineering, University of Illinois at Chicago, Chicago, IL, United States

Noninvasive discrimination of mediastinal lymph nodes (MLN) is crucial for management of cancer patients such as those with non-small cell lung carcinoma. This study aims at investigating the value of IVIM diffusion parameters (D , D^* , and f) as well as ADC for discrimination of malignant and benign MLN. A total of 91 MLN from 35 patients with histopathologic proven lesions were studied. D and f of malignant mediastinal lymph nodes were significantly different from those in the benign ones. The combination of f and D produced the highest diagnostic performance as evaluated by a receiver operating characteristic (ROC) analysis.

Electronic Power Pitch Poster

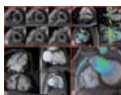
Poster: RF Arrays & Systems

Exhibition Hall

Wednesday 14:45 - 15:45

755

Plasma 1



Development and Clinical Implementation of Very Light Weight and Highly Flexible AIR Technology Arrays

Shreyas S Vasanawala¹, Robert Stormont², Scott Lindsay², Thomas Grafendorfer², Joseph Y Cheng¹, John M Pauly³, Michael Lustig⁴, Greig Scott³, Jorge X Guzman², Victor Taracila², Daniel Chirayath², and Fraser Robb²

¹Radiology, Stanford University, Stanford, CA, United States, ²GE Healthcare, ³Electrical Engineering, Stanford University, ⁴Electrical Engineering and Computer Science, UC Berkeley

Pediatric body MRI faces challenges of widely varying patient sizes, heterogenous imaging indications, and limited patient cooperation. These difficulties are compounded by receiver array coils that are often mismatched to patients' size. In this work, we develop a novel light-weight flexible coil array that can be placed on a patient, and combined with a high-density posterior array and determine feasibility of clinical use in a pediatric setting. The resulting coil is well received in the clinic and yields good image quality.

756

Plasma 2

The Optimality Principle for MR signal excitation and reception: new physical insights into ideal RF coil design

Daniel K. Sodickson^{1,2}, Riccardo Lattanzi^{1,2}, Manushka Vaidya^{1,2}, Gang Chen^{1,2}, Dmitry S. Novikov^{1,2}, Christopher M. Collins^{1,2}, and Graham C. Wiggins^{1,2}



¹Center for Advanced Imaging Innovation and Research (CAI2R) and Bernard and Irene Schwartz Center for Biomedical Imaging (CBI), Department of Radiology, New York University School of Medicine, New York, NY, United States, ²Sackler Institute of Graduate Biomedical Sciences, New York University School of Medicine, New York, NY, United States

Despite decades of collective experience, RF coil optimization has remained a largely empirical process, with clear insight into what might constitute truly task-optimal, as opposed to merely “good,” coil performance being difficult to come by. We introduce a new principle, the Optimality Principle, which allows one to predict the form of signal-optimizing current patterns on any arbitrary surface, using a simple conceptual framework. After a brief derivation of the principle, we illustrate its use in generating ideal current patterns for various experimental conditions, and in understanding the emergence of electric dipoles as strong performers at high frequency.

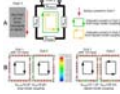
757



Plasma 3

Self-Decoupled RF Coils

Xinqiang Yan^{1,2}, John C. Gore^{1,2,3}, and William A. Grissom^{1,2,3}



¹Institute of Imaging Science, Vanderbilt University, Nashville, TN, United States, ²Department of Radiology and Radiological Sciences, Vanderbilt University, Nashville, TN, United States, ³Department of Biomedical Engineering, Vanderbilt University, Nashville, TN, United States

RF arrays with large numbers of independent elements are desirable for parallel imaging and transmission. However, electromagnetic (EM) coupling between elements becomes significant as the number of coils increases and can severely impact coil performance. Several methods such as overlapping elements, L/C networks and auxiliary resonators have been proposed to reduce coupling, and are effective in decoupling adjacent elements, but are usually less effective for non-adjacent elements, and are not directly applicable to recently-proposed mixed arrays such as combinations of dipoles/monopoles and loop arrays. To address these problems, we propose a simple, geometry-independent self-decoupled RF coil design in which the two induced current modes in a loop coil can be adjusted to cancel each other. The method is validated in EM simulations, bench tests and MR experiments.

758



Plasma 4

Optically Controlled Four-Channel Transceiver for 7T imaging with RF Monitoring Feedback

Natalia Gudino¹, Jacco A de Zwart¹, Peter van Gelderen¹, and Jeff H Duyn¹



¹Advanced MRI Section, LFMI/NINDS, National Institutes of Health, Bethesda, MD, United States

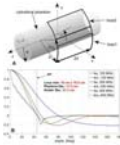
In multi-channel RF transmission, monitoring and accurate control of amplitude and phase of the transmit signal is necessary to ensure safety. To this end, we present a four-channel transceiver array for 7T imaging built from optically-controlled on-coil amplifiers with optical real-time RF signal monitoring. Based on this monitoring signal an amplitude and phase control can be implemented for flexible, accurate and rapid control of B1 and SAR.

759

Plasma 5

Double-Row 16-element Tight-Fit Transceiver Phased Array with High Transmit Performance for Whole Human Brain Imaging at 9.4T.

Nikolai I. Avdievich¹, Ioannis A. Giapitzakis¹, and Anke Henning^{1,2}



¹Max Planck Institute for Biological Cybernetics, Tübingen, Germany, ²Institute of Physics, Ernst-Moritz-Arndt University, Greifswald, Germany

At ultra-high fields (UHF, $\geq 7T$) a simple increase of the length of a single-row human head transmit (Tx) phased array cannot provide an adequate longitudinal coverage for the whole brain imaging. Multi-row (≥ 2) arrays together with RF shimming have to be used instead. In this work, we constructed a 9.4T (400 MHz) 16-loop double-row transceiver array based on the analytical modeling. We demonstrated that simply by overlapping a very good decoupling can be obtained without additional decoupling strategies. This provides a recipe of a simple, robust, and very Tx-efficient design for parallel transmission and whole brain imaging at UHFs.

760

Plasma 6

Compact iPRES coil assembly for Magnetic Resonance Fingerprinting

Michael Twieg¹, Bhairav B Mehta², Simone Coppo², Haoqin Zhu³, Labros Petropoulos³, Hiroyuki Fujita³, and Mark A Griswold⁴



¹Dept of Radiology, Case Western Reserve University, Cleveland Heights, OH, United States, ²Dept of Radiology, Case Western Reserve University, Cleveland, OH, United States, ³Quality Electrodynamics, Mayfield Village, OH, United States, ⁴Dept of Radiology, Case Western Reserve University, OH, United States

Magnetic Resonance Fingerprinting (MRF) makes use of spatially and temporally incoherent encoding schemes to produce orthogonal signals from different tissues. Here we present a coil optimized for MRF that integrates parallel receive, excitation, and shimming (iPRES) to provide an ideal method of modulating all three available magnetic fields (B_{1^-} , B_{1^+} , and ΔB_0). In order to be useful in quantitative imaging, an iPRES array must convey these fields accurately, and cost effectively. Here we demonstrate an iPRES coil element with all three field amplifiers located on-coil, providing improved sensitivity and efficiency relative to remote amplifiers.

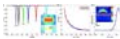
761



Plasma 7

Wireless coil based on meta-technologies for MRI implementations

Alena Shchelokova¹, Alexey Slobozhanyuk^{1,2}, Irina Melchakova¹, Andrew Webb³, Yuri Kivshar^{1,2}, and Pavel Belov¹



¹Department of Nanophotonics and Metamaterials, ITMO University, St.Petersburg, Russian Federation, ²Nonlinear Physics Center, Research School of Physics and Engineering, Australian National University, Canberra, Australia, ³Department of Radiology, Leiden University Medical Center, Leiden, Netherlands

We demonstrate experimentally how to improve the performance of MRI by employing wireless coil based on a hybrid tunable metasurface. We fabricate metasurface formed by an array of nonmagnetic metallic wires with high permittivity dielectric loads and investigate it in 1.5 T MRI machine. The metasurface enhances the SNR value in more than 7 times in the region of interest in comparison with the birdcage coil and 2 times versus the dedicated flat local coil.

762



Plasma 8



Development and performance evaluation of the second prototype of a RF-coil integrated PET insert for existing 3T MRI systems

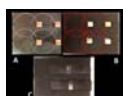
Md Shahadat Hossain Akram¹, Fumihiko Nishikido¹, Takayuki Obata¹, Mikio Suga², Eiji Yoshida¹, Hedeaki Tashima¹, Keiji Shimizu³, Masanori Fujiwara², Akram Mohammadi¹, and Taiga Yamaya¹

¹National Institute of Radiological Sciences, Chiba, Japan, ²Chiba University, Chiba, Japan, ³Hamamatsu Photonics K.K., Hamamatsu, Japan

We developed an RF-coil integrated DOI-PET insert for the 3T MRI system for human brain imaging. In this study we have given details of the second prototype system developed recently and evaluated performance for MRI-only, PET-only and simultaneous PET/MRI conditions. This system included 24 carbon fiber shielded PET modules which are positioned in between the coil-elements of a birdcage head-coil. In total 48 4-layer DOI detectors are included that gives 60 mm axial-FOV for PET imaging. Under all performance study the system worked quite well showing promise for near-future human brain study.

763

Plasma 9



Characterization of a new ultra-flexible, low profile RF receive coil technology.

Philip Rossman¹, Robert Stormont², Scott Lindsay², Fraser Robb², Dennis Savitskiy², David Stanley², John Huston¹, Timothy Kaufmann¹, and Kiaran McGee¹

¹Department of Radiology, Mayo Clinic, Rochester, MN, United States, ²GE Healthcare, Waukesha, WI

A new highly flexible RF coil design is described. Individual coil elements are constructed by means of a proprietary process that yields low reactance and low loss conductors while being lightweight, flexible, and durable. Phantom data indicate that for similar coil geometries, the coils provide equivalent SNR profiles but do not suffer from design limitations due to minimum coil overlap requirements of conventional copper coil elements. In vivo data demonstrate that these coils can be fabricated onto highly flexible and thin support materials that closely comply with anatomic contours in challenging imaging sites such as the c-spine.

764

Plasma 10



Resonance frequency detection of a stretchable RF receiver coil for MRI

Andreas Mehmam¹, Christian Vogt¹, Benjamin Sporrer², Matija Varga¹, Qiuting Huang², and Gerhard Troester¹

¹Electronics Laboratory, ETH Zurich, Zurich, Switzerland, ²Integrated Systems Laboratory, ETH Zurich, Switzerland

Wearable RF receiver coils change their resonance frequency when stretched or bent. We propose a system that detects this change in resonance frequency. The system is integrated on a wearable MRI receiver of 20 x 30mm². The change in resonance frequency can be detected in-field. The detection works by sweeping an excitation current through a frequency range and measuring the frequency response. The frequency response is transmitted via a glass fibre to an out-field signal processing unit. Measurements were conducted using a stretchable liquid metal coil on neoprene.

766

Plasma 12



Dielectric resonator antenna receive array at 7 Tesla using detunable ceramic resonators

Thomas Ruytenberg¹ and Andrew Webb¹

¹Radiology, Leiden University Medical Center, Leiden, Netherlands

A receive-only array of dielectric resonator antennas has been developed. A method for detuning the ceramic resonators is studied using simulations and measurements, after which a four-channel dielectric resonator antenna array is used for in vivo image acquisition of the ankle. Using this receive-only array allows for higher SNR and parallel imaging using SENSE.

767

Plasma 13



Top-Hat Dipole RF Coil with Large Field of View for 7 T Brain MR Imaging

Chang-Hyun Oh^{1,2,3,4}, Chulhyun Lee⁵, Suchit Kumar³, Jun-Sik Yoon¹, Ha-Kyu Jeong⁶, Jeong-Hee Kim², Young-Seung Jo^{1,5}, Jong-Min kim¹, Christian Bruns⁷, Tim Herrmann⁷, Johannes Bernarding⁷, and Zang-Hee Cho⁸

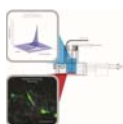
¹Department of Electronics and Information Technology, Korea University, Seoul, Korea, Republic of, ²Research Institute for Advanced Industrial Technology, Korea University, Sejong City, Korea, Republic of, ³Department of Biomicrosystem Technology, Korea University, Seoul, Korea, Republic of, ⁴ICT Convergence Technology for Health & Safety, Korea University, Sejong City, Korea, Republic of, ⁵Korea Basic Science Institute, Cheongju, Chungcheongbuk-do, Korea, Republic of, ⁶BIU Clinical Science MR, Philips Korea, Seoul, Korea, Republic of, ⁷Department for Biometrics und Medical Informatics, Otto-von-Guericke University, Magdeburg, Germany, ⁸Advanced Institutes of Convergence Technology, Seoul National University, Seoul, Korea, Republic of

In ultra-high-field brain MR imaging, the coverage for imaging with the optimized protocol is constrained not only by scan time, but also by the coil structure. Since presently available surface loop RF coils have limited field of view, it is very difficult to achieve the coverage from the top of the head to the end of the cervical vertebrae. Prior solution to this problem was to increase the number of elements. However, it increases the complexity of coil array design thus causing difficulties in construction of the coils. In this paper, an 8-channel top-hat dipole receive RF coil is proposed for the brain imaging at 7 Tesla MRI. By enabling the coil tuning with novel tuning methods for shorter RF coil lengths but still with reasonable uniformity and SNR for more imaging field of view compared with multi-element loop coils.

768



Plasma 14



Bioreactor for in vitro optical fluorescence and magnetic resonance spectroscopy

Benjamin L Cox^{1,2,3}, Joseph M Szulczewski^{3,4}, Kai D Ludwig¹, Erin B Adamson¹, Robert A Swader², Sarah A Erickson-Bhatt^{2,3,4}, Patricia J Keely⁴, Kevin W Eliceiri^{1,2,3,5}, and Sean B Fain^{1,6}

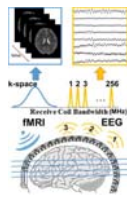
¹Medical Physics, University of Wisconsin - Madison, Madison, WI, United States, ²Medical Engineering, Morgridge Institute for Research, Madison, WI, United States, ³Laboratory for Optical and Computational Instrumentation (LOCI), University of Wisconsin - Madison, Madison, WI, United States, ⁴Cell and Regenerative Biology, University of Wisconsin - Madison, Madison, WI, United States, ⁵Biomedical Engineering, University of Wisconsin - Madison, Madison, WI, United States, ⁶Radiology, University of Wisconsin - Madison, Madison, WI, United States

The design and implementation of a novel bioreactor capable of facilitating both magnetic resonance spectroscopy (MRS) and optical fluorescence microscopy for complementary metabolic information is described. Fluorescence lifetime imaging (FLIM) of nicotinamide adenine dinucleotide (NADH) and hyperpolarized [¹⁻¹³C] pyruvic acid (PA) MRS of human breast cancer cells in a 3D collagen matrix is demonstrated. The system provides a novel test-bed for simulating cell-matrix and cell-cell interactions in a 3D microenvironment for investigating multi-scale cellular metabolism *in vitro*.

769



Plasma 15



Multimodal Imaging: MR-Compatible, Gradient Artifact free, Wireless recording system integrated with MR-scanner for Simultaneous EEG and fMRI acquisition

Ranjay Mandal¹, Nishant Babaria², Jiayue Cao¹, and Zhongming Liu^{1,2}

¹Biomedical Engineering, Purdue University, West Lafayette, IN, United States, ²Electrical and Computer Engineering, Purdue University, West Lafayette, IN, United States

The field of multimodal imaging has largely been propelled by two of the most widely used neuroimaging tools, fMRI and EEG, as the complementary nature of the two signals provides a unique avenue to evaluate the brain dynamics and its underlying neural circuitry. However, methodological challenges associated with simultaneous acquisition of EEG and fMRI impedes the method from achieving the full potential. To address these challenges, we present an MR-compatible, active recording system that utilizes surplus MR-hardware and inherent electromagnetic field to synchronize and wirelessly record gradient artifact free multichannel EEG signals and encode these Non-MR signals within the extended FOV of the MR image.

770

Plasma 11



Mary had a little Lamb: Scanner-recorded speech during MRI without gradient-induced sound

Jan Ole Pedersen^{1,2}, Christian Hanson, Rong Xue³, and Lars G. Hanson^{1,2}

¹Danish Research Centre for Magnetic Resonance, Centre for Functional and Diagnostic Imaging and Research, Copenhagen University Hospital, Kgs Lyngby, Denmark, ²Centre for Magnetic Resonance, DTU Elektro, Technical University of Denmark, Kgs Lyngby, Denmark, ³State Key Laboratory of Brain and Cognitive Science, Research, Institute of Biophysics, Chinese Academy of Sciences

During MRI, fast switching of imaging gradients generate loud noise of high intensity due to vibration of the gradient coils. The in-bore intercom used for patient communication is therefore typically turned off during scanning. This has implications for safety and image quality since patient speech and yells are not heard by the scanner operator. Using standard sequences, we demonstrate that sound can be recorded by MRI scanners and extracted from the scanners raw data, thereby enabling communication with patients for safety or experimental reasons.

Electronic Power Pitch Poster

Poster: Post-Processing & Motion

Exhibition Hall

Wednesday 14:45 - 15:45

771

Plasma 16



cBEaST: Cerebellar Brain Extraction based on Nonlocal Segmentation Technique – A comparison with state-of-the-art methods

Daniel Güllmar¹, Viktor Pfaffenroth^{2,3}, Rossitza Draganova², Xiang Feng¹, Jürgen R Reichenbach¹, Dagmar Timmann², and Andreas Deistung^{1,2}

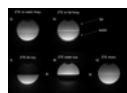
¹Medical Physics Group, Institute for Diagnostic and Interventional Radiology, Jena University Hospital – Friedrich Schiller-University, Jena, Germany, ²Section of Experimental Neurology, Department of Neurology, Essen University Hospital, Germany, ³Erwin L. Hahn Institute for Magnetic Resonance Imaging, University Duisburg-Essen, Essen, Germany

An automatic segmentation of the cerebellum is required to determine the cerebellar volume and for improving spatial normalization in voxel-based analysis approaches. While existing segmentation approaches typically work quite robust in healthy subjects, errors in segmentation increase with cerebellar atrophy and typically require manual corrections. We introduce a novel cerebellum segmentation approach, referred to as cBEaST, that relies on a dedicated multi-resolution segmentation library with manually edited cerebellar masks of both healthy and diseased subjects in combination with multi-atlas-propagation and segmentation as implemented in BEaST. Finally segmentation of the cerebellum with BEaST is compared with the alternative techniques SUIT and FreeSurfer.

772



Plasma 17



Signal-model-based water-fat separation in Zero Echo Time (ZTE) MRI

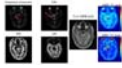
Romain Nicolas Froidevaux¹, Markus Weiger¹, Po-Jui LU², and Klaas Paul Pruessmann¹

¹University and ETH Zurich, Zürich, Switzerland, ²ETH Zurich, Zurich, Switzerland

The separation of water and fat in zero echo time (ZTE) imaging is challenging for several reasons: First, echo-based signal models are violated for fast-relaxing spins and require the use of long sequences. Second, frequency selective preparation pulses produce large SAR and are inefficient on short-T2 compounds. Finally the off-resonance induced phase vanishes at TE = 0. In this work, we introduce the principles of a technique that allows water-fat separation for a single ZTE acquisition and demonstrate its potential and limits with phantom and in-vitro experiments.

773

Plasma 18



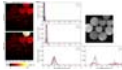
Suspicious Component Segmentation for Identifying Hippocampal Sclerosis Using Regularized Tissue-Fraction MR Fingerprinting
Kang Wang¹, Congyu Liao², Xiaozhi Cao², Zhixing Wang², Dengchang Wu¹, Hongjian He², Qiuping Ding², and Jianhui Zhong²

¹Department of Neurology, The First Affiliated Hospital, School of Medicine, Zhejiang University, Hangzhou, People's Republic of China, ²Center for Brain Imaging Science and Technology, Department of Biomedical Engineering, Zhejiang University, Hangzhou, People's Republic of China

A relaxometry-based tissue fraction segmentation using MR fingerprinting method was applied for identifying hippocampal sclerosis. The results demonstrated that tissue-fraction MR fingerprinting method could effectively segment multiple tissue components and mark the possible sclerosis regions, which is critical for clinical application including lesions diagnosis and multicomponent analysis.

774

Plasma 19



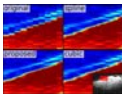
Improved Short-T2* Estimation with Bloch Equation-Modeled Concurrent Excitation and Relaxation
Ethan M Johnson¹, Kim Butts Pauly², and John M Pauly¹

¹Electrical Engineering, Stanford University, Stanford, CA, United States, ²Radiology, Stanford University, Stanford, CA, United States

Short-T2* magnetization (order of [0.1,1ms]) can relax appreciably during standard-rate excitation pulses, which can bias estimates of relaxation rates formed by fitting to observed signal decay. The effect can, however, be included in an updated model to improve T2* estimation for fast-relaxing signals. Here, a demonstration is presented.

775

Plasma 20



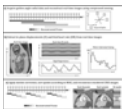
Edge preserving upsampling of image resolution in MRI
Marco Reiser¹ and Elias Kellner¹

¹Dep. of Radiology, Medical Physics, University Medical Center Freiburg, Freiburg, Germany

In this work we present a simple and efficient postprocessing method to isotropify the imaging resolution of MRI imagery. In MRI anisotropic voxel sizes are quite common due to several reasons. Typically the through-plane voxel size is higher than the in-plane resolution. We propose a simple technique to upsample to isotropic image resolution without introducing the typical block like artifacts known from conventional interpolation schemes.

776

Plasma 21



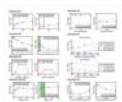
Motion-compensated reconstruction of fetal cardiac MRI using a golden-angle radial acquisition, retrospective gating, and compressed sensing
Christopher W. Roy^{1,2}, Mike Seed^{3,4}, and Christopher K. Macgowan^{1,2}

¹Medical Biophysics, University of Toronto, Toronto, ON, Canada, ²Physiology and Experimental Medicine, Hospital for Sick Children, Toronto, ON, Canada, ³Pediatric Cardiology, Hospital for Sick Children, ON, Canada, ⁴Pediatric and Diagnostic Imaging, University of Toronto, Toronto, ON, Canada

Fetal cardiac MRI requires high spatial and temporal resolution but is often limited by stochastic and periodic motion. To compensate for these sources of artifact, a radial golden-angle acquisition was used to acquire and reconstruct real-time fetal cardiac images. In-plane motion and fetal heart rate were then calculated from the real-time images and used to reconstruct reordered CINE images at high spatial and temporal resolution. Using this approach, motion-robust imaging of the fetal heart was successful in seven pregnant volunteers for both short-axis and long-axis multi-slice acquisitions.

777

Plasma 22



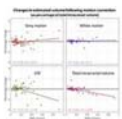
From Visualization to Quantification: Calibrating Motion Magnification by Amplified Magnetic Resonance Imaging
Wendy W Ni¹, Maged Goubran¹, Greg Zaharchuk¹, Michael Moseley¹, Kristen Yeom¹, and Samantha Holdsworth¹

¹Radiology, Stanford University, Stanford, CA, United States

The brain is constantly in motion. Changes in the cardio-ballistic motion of brain structures can provide invaluable information on natural processes and pathology. We have previously introduced a qualitative visualization technique, Amplified MRI (aMRI), to amplify subtle cardio-ballistic motion in the brain. Now we attempt to quantify the underlying motion through simulation-based characterization of the aMRI technique. By generating calibration curves for a range of motion parameters, we calculated the unamplified tissue displacement in two human subjects. The estimated displacements are higher than literature values. Nevertheless, our simulations are the first steps in benchmarking aMRI's potential as a quantitative technique.

778

Plasma 23



Assessing the effect of head-motion on tissue volume estimates
Daniel Gallichan^{1,2}

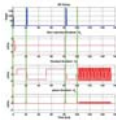
¹School of Engineering, Cardiff University, Cardiff, United Kingdom, ²EPFL- CIBM, Lausanne, Switzerland

We looked at data from 60 subjects undergoing 1mm resolution T1-weighted structural scans at 7T with 3D FatNavs allowing retrospective motion-correction. Motion parameters for 60 subjects were examined for general trends – and typical motion was dominated by translation in the z-direction and a small backwards rotation of the head. Quantitative estimates of tissue volumes were compared before and after motion-correction was applied, suggesting that total intracranial volume tends to be overestimated when the subject moves more – and that this is dominated by an overestimation of the CSF volume.

779

Plasma 24

Prospective motion correction on diffusion weighted imaging: improving data quality with four radio frequency and gradient pulses updates.
Danilo Maziero¹, Michael Herbst², and Thomas Ernst³



¹University of Hawaii, Honolulu, HI, United States, ²Department of Radiology, University Medical Center Freiburg, Freiburg, Germany, ³Department of Medicine, John A. Burns School of Medicine, University of Hawaii, Honolulu, HI, United States

Prospective Motion Correction (PMC) using fast camera-based tracking systems can dramatically increase DWI data quality and may have an important application in populations where movement is hard to prevent. Here we present images acquired with and without intra-sequence PMC from two subjects realizing fast head rotations up to 30°/s. Our results show that the DWI motion sensitivity can be reduced five-fold by applying 3 intra-sequence PMC updates (prior to each of the two refocusing RF pulse and prior to readout).

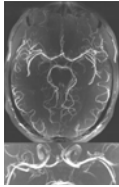
780



Plasma 25

Motion corrected high resolution time-of-flight angiography at 7T using Segmented FatNavs

Frédéric Gretschi¹ and Daniel Gallichan²



¹EPFL, Lausanne, Switzerland, ²School of Engineering, Cardiff, United Kingdom

We propose to insert Segmented FatNavs into a time-of-flight sequence, and use it as a multi-purpose module. It allows fat suppression, magnetization-transfer suppression of the tissue signal, and retrospective motion correction. Image quality was always enhanced after correction, even in cases of small motion, thereby making high-resolution brain angiography more reliable.

781



Plasma 26

Motion correction on a human PET/MR scanner: Clinical feasibility of a motion correction system in patients – an update report

Thomas Küstner^{1,2}, Christian Würsli³, Martin Schwartz^{2,4}, Hadi Fayad⁵, Thibaut Meriin⁵, Christopher Gilliam⁶, Thierry Blu⁶, Petros Martirosian⁴, Fritz Schick⁴, Bin Yang², Holger Schmidt¹, and Nina F. Schwenzer¹



¹Department of Radiology, University of Tuebingen, Tuebingen, Germany, ²Institute of Signal Processing and System Theory, University of Stuttgart, Stuttgart, Germany, ³University of Stanford, Palo Alto, CA, United States, ⁴Section on Experimental Radiology, University of Tuebingen, Tuebingen, Germany, ⁵LaTIM, INSERM, University of Bretagne, Brest, France, ⁶Department of Electronic Engineering, Chinese University of Hong Kong, Hong Kong, Hong Kong

The diagnostic accuracy of Positron-Emission-Tomography/Magnetic Resonance (PET/MR) is often reduced in regions affected by respiratory and cardiac motion. These motion-induced artifacts can be corrected by an MR-derived motion model (MM). Here, we improved the previously presented PET/MR motion correction system by two new sampling trajectories for the MR motion imaging and extend it by the usage of an additional Compressed Sensing reconstruction (BART), an optical-flow based registration (LAP) and the incorporation of motion correction into a listmode-based PET reconstruction (CASToR) which are all integrated into the Gadgetron-based reconstruction pipeline for a clinical feasible setup. In-vivo patient data substantiated the improvements.

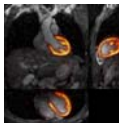
782



Plasma 27

Respiratory motion-corrected simultaneous cardiac PET and coronary MR angiography using a hybrid 3T PET-MR

Camila Munoz¹, Radhouene Neji^{1,2}, Gastao Cruz¹, Rene Botnar¹, and Claudia Prieto¹



¹Division of Imaging Sciences and Biomedical Engineering, King's College London, London, United Kingdom, ²MR Research Collaborations, Siemens Healthcare, Frimley, United Kingdom

Physiological motion remains a major challenge for cardiac PET-MR. Here we propose a framework for non-rigid respiratory motion-corrected simultaneous Coronary MR Angiography (CMRA) and cardiac PET. Motion estimated from low-resolution MR image navigators and from CMRA data itself is used for correcting CMRA and PET datasets to the same respiratory position. The proposed CMRA approach was validated in ten healthy subjects. Results from the PET-CMRA framework on three patients show that motion-corrected PET images have improved sharpness compared to uncorrected reconstructions, whereas motion-corrected CMRA images have improved coronary vessel length and sharpness compared to uncorrected and translational-corrected images.

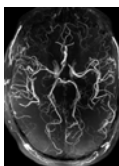
783



Plasma 28

Beyond the biological resolution limit: Prospectively motion corrected Time of Flight angiography at 7T

Hendrik Mattern¹, Alessandro Sciarra¹, Frank Godenschweger¹, Daniel Stucht¹, Falk Lüsebrink¹, and Oliver Speck^{1,2,3,4}



¹BMMR, Otto-von-Guericke-University, Magdeburg, Germany, ²German Center for Neurodegenerative Disease, Magdeburg, Germany, ³Center for Behavioral Brain Sciences, Magdeburg, Germany, ⁴Leibniz Institute for Neurobiology, Magdeburg, Germany

Subject motion limits the potential of high resolution Time of Flight (ToF) angiography at 7T, even small scale, involuntary movements can degrade the image quality. In this study, prospective motion correction was able to overcome the biological resolution limit in a healthy subject population (quality assessment with quantitative and qualitative metrics), and was used to acquire the highest *in vivo* ToF data set to date with an isotropic voxel size of 0.15mm³.

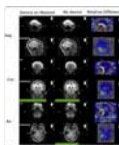
784



Plasma 29

Implementation of a 2.4 GHz wireless sensing platform for transmission of motion data from within a head coil at 3T.

Adam M.J. van Niekirk¹, Andre J. W. van der Kouwe^{1,2,3}, and Ernesta M. Meintjes¹

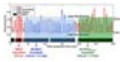


¹Division of Biomedical Engineering, Human Biology, University of Cape Town, Cape Town, South Africa, ²Athinoula A. Martinos Center, Massachusetts General Hospital, Charlestown, MA, United States, ³Radiology, Harvard Medical School, Boston, MA, United States

Prospective motion correction using external hardware can be compromised by poor marker attachment. In this work we introduce a new attachment site on the mastoid process of the subject. To achieve this, an active wireless marker is implemented that takes advantage of the versatility of an existing method (VectOrient). The effects of the device on the scanner's operation and *visa versa* are evaluated. The small 14x16mm² device shows good MRI compatibility. Any degradation in signal quality is localised and could be further reduced. The link quality is sufficient to stream patient motion parameters, quantifying patient pulse during MEMPRAGE and EPI pulse sequences.

785

Plasma 30



Respiratory Phase-Matched MR-based Attenuation Correction (MRAC) for Four-Dimensional (4D) PET in PET/MRI: A Feasibility Study
Jaewon Yang¹, Florian Wiesinger², Anne Menini², Jing Liu¹, Thomas A. Hope¹, Youngho Seo¹, and Peder E. Z. Larson¹

¹Radiology and Biomedical Imaging, UCSF, San Francisco, CA, United States, ²GE Global Research

PET/MRI is capable of simultaneous respiratory motion-resolved four-dimensional (4D) PET/4D MRI data acquisitions. Therefore, it is important to develop a clinically applicable method for respiratory phase-matched MR-based attenuation correction (MRAC) for accurate 4D PET quantification. This study proposed 4D MRAC protocols modifying the current MRAC protocol and evaluated their performance using a patient with liver metastases. For qualitative analysis, 4D MRAC improved phase-mismatch at the lung/liver interface substantially. For quantitative analysis, 4D MRAC improved PET quantification by 10-30% increase of PET-avid tumor uptake values, compared to static MRAC, specifically for the tumors located at the lung/liver interface.

Electronic Power Pitch Poster

Poster: Diffusion: Outside the Brain

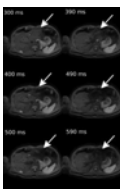
Exhibition Hall

Wednesday 17:15 - 18:15

Plasma 16

862

Plasma 1



Analysis of abdominal movement with Phase Optical Flow: Application to Diffusion imaging.

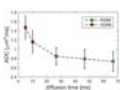
Stephan Hahn¹, Maxime Gérard¹, Damien Dasnoy-Sumell¹, Julie Absil², Olivier Debeir¹, and Thierry Metens²

¹Laboratories of Image, Signal processing and Acoustics, ULB, Brussels, Belgium, ²MRI Clinics&Radiology, Hôpital Erasme, Brussels, Belgium

We present a new method, the Phase Optical Flow, which provides an automatic determination of abdominal regional movements along the cardiac cycle and allows a real time determination of the optimal cardiac trigger time to be used in quantitative liver DWI. A phase based motion amplification was applied to real-time BTFE images acquired at 20 images/s. Then optical flow was used to derive the velocity vector field. The optimal cardiac time window was defined as the 100ms-period with minimal absolute vertical velocity. Validation was provided by liver DWI obtained at several cardiac trigger times.

863

Plasma 2



In vivo imaging of mean cell size and density of human breast tumors

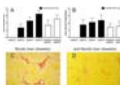
Hua Li^{1,2}, Lori R. Arlinghaus^{1,2}, A. Bapsi Chakravarthy³, Vandana G. Abramson², John C. Gore^{1,2}, and Junzhong Xu^{1,2}

¹Institute of Imaging Science, Vanderbilt University, Nashville, TN, United States, ²Department of Radiology and Radiological Sciences, Vanderbilt University, Nashville, TN, United States, ³Department of Radiation Oncology, Vanderbilt University, Nashville, TN, United States

We report a new MRI method termed IMPULSED (Imaging Microstructural Parameters Using Limited Spectrally Edited Diffusion) to quantitatively characterize mean cell size and density in solid tumors simultaneously and the first application of this method in breast cancer patients.

864

Plasma 3



Intravoxel incoherent motion MR imaging for staging liver fibrosis and monitoring anti-fibrotic response to losartan: an experimental study in rat model

Caiyuan Zhang¹, Yong Zhang², and Dengbin Wang¹

¹Radiology, Xinhua Hospital, Shanghai Jiao Tong University School of Medicine, Shanghai, People's Republic of China, ²MR Research China, GE Healthcare, Shanghai, China, Shanghai, People's Republic of China

To evaluate the feasibility of intravoxel incoherent motion (IVIM) MR imaging to stage liver fibrosis and its capability for monitoring anti-fibrotic response to treatment, we performed IVIM MR imaging for rats model induced by carbon tetrachloride and for rats treated with losartan. Our studies demonstrated that D^* is helpful to stage early and moderate fibrosis, and f is beneficial to discriminate advanced liver fibrosis and cirrhosis. In losartan treated rats, D^* and f showed statistical significance compared with CCl₄ alone. We concluded that perfusion parameters derived from IVIM have potential to monitor fibrosis progression and evaluate anti-fibrosis response to treatment.

865

Plasma 4



Diffusion-weighted MRI and coherent flow in the kidney

Andreas Max Weng¹, Fabian Hilbert¹, Henning Neubauer¹, Simon Veldhoen¹, Thorsten Alexander Bley¹, and Herbert Köstler¹

¹Department of Diagnostic and Interventional Radiology, University Hospital of Würzburg, Würzburg, Germany

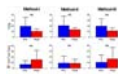
The IVIM model and typical DWI-evaluations assume flow in tissue to be incoherent. However, there is evidence that in some tissues flow might be coherent and thus, the DWI-signal might be influenced by the applied first gradient moment m_1 . A gradient scheme was implemented that allows applying different m_1 for a constant b -value. Moreover, the IVIM model was extended to also include coherent flow in the modeling process of DWI data. It was found that flow in the human kidney is, at least in part, coherent and that the proposed model is able to fit that data very robustly.

866

Plasma 5

An assessment of Intravoxel Incoherent Motion (IVIM) imaging in Detection of Acute Kidney Injury in Rodents

Keisuke Ishimatsu¹, Shanrong Zhang¹, Koji Sagiyama¹, Ming Chang Hu², Orson W Moe², and Masaya Takahashi¹

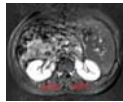


¹Advanced Imaging Research Center, UT Southwestern Medical Center, Dallas, TX, United States, ²Department of Internal Medicine / Charles and Jane Pak Center of Mineral Metabolism and Clinical Research, UT Southwestern Medical Center, Dallas, TX, United States

The objective is to investigate the concept of intravoxel incoherent motion (IVIM) for diffusion weight imaging (DWI) in the kidney. We first compared the variability of three methods for bi-exponential fitting applied to the five data sets of DWI obtained in a mouse kidney. Subsequently these three methods were compared with an arterial spin labeling (ASL) in detection of acute kidney injury (AKI) in a rat model. The IVIM imaging did not detect any changes in the AKI model although the ASL clearly demonstrated the reduction of the perfusion.

867

Plasma 6



Diffusion-Weighted MRI Identifies Viable Tissue in Wilms Tumour: Application for Subtype Analysis and Response to Chemotherapy

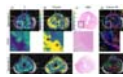
Harriet Rogers¹, Patrick Hales¹, Kathy Pritchard-Jones², and Christopher Clark¹

¹Developmental Imaging and Biophysics, Institute of Child Health, University College London, London, United Kingdom, ²Developmental Biology and Cancer, Institute of Child Health, University College London, London, United Kingdom

In Wilms Tumour (WT) Blastemal subtype has the worst prognosis. Diffusion MRI (DWI) can distinguish some histological subtypes. Gadolinium-contrast-injected T₁ MRI (T_{1gad}) identifies necrotic tissue. Gadolinium is contra-indicated in renal failure. 27 patients received DWI, 20/27 received T_{1gad}. DWI was fitted with Intravoxel Incoherent Motion providing Dmaps. Viable and necrotic regions identified on T_{1gad} were transferred to corresponding Dmaps. ROC analysis determined a D threshold separating necrotic and viable tissue. ANOVAs showed viable regions separated Blastemal from other subtypes, whole lesions could not. DWI separates necrotic and viable tissue in WT potentially identifying subtypes, assessing chemotherapy, guiding biopsies and surgery.

868

Plasma 7



Validation of VERDICT MRI using fresh and fixed prostate specimens with aligned histological slices

Colleen Bailey¹, Roger M Bourne², Bernard Siow^{3,4}, Edward W Johnston⁵, Hayley Pye^{6,7}, Susan Heavey^{6,7}, Thomy Mertzani¹, Hayley Whitaker⁸, Alexander Freeman⁸, Dominic Patel⁸, Greg Shaw^{6,7}, Ashwin Sridhar^{6,7}, Shonit Punwani⁹, David J Hawkes¹, Daniel C Alexander¹, and Eleftheria Panagiotaki¹

¹Centre for Medical Image Computing, University College London, London, United Kingdom, ²Discipline of Medical Radiation Sciences, University of Sydney, Sydney, Australia, ³Centre for Advanced Biomedical Imaging, University College London, London, United Kingdom, ⁴Imaging, Francis Crick Institute, London, United Kingdom, ⁵Centre for Medical Imaging, University College London, London, United Kingdom, ⁶Division of Surgery and Interventional Science, University College London, London, United Kingdom, ⁷Department of Urology, University College London Hospitals, London, United Kingdom, ⁸Department of Research Pathology, University College London, London, United Kingdom

This study provides the first step in validating the VERDICT diffusion model of tissue microstructure by examining the effects of fixation on tissue microstructure and comparing VERDICT parameter maps to histological features. Fresh and fixed parameter maps showed similar spatial trends: fixation decreased the extracellular volume fraction parameter and decreased the cell radius parameter slightly, consistent with water efflux. Intracellular volume fraction was lower in regions with lower cellularity, such as the peripheral zone, and directions of diffusion anisotropy corresponded with collagen and smooth muscle orientation patterns in the stroma.

869

Plasma 8



Diffusion-weighted MRI in the evaluation of posttherapeutic residual masses in lymphoma

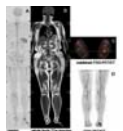
Siarhei Kharuzhyk¹, Edward Zhavrid², and Nina Sachivko²

¹Radiology, N.N. Alexandrov National Cancer Center, Minsk, Belarus, ²Chemotherapy, N.N. Alexandrov National Cancer Center, Minsk, Belarus

Residual masses do often present on posttreatment imaging in lymphoma. We conducted prospective study to evaluate diagnostic capabilities of CT, MRI and diffusion-weighted MRI (MRI-DWI) in differentiation residual tumors and non-active posttreatment masses in 40 lymphoma patients. MRI-DWI with visual analysis of apparent diffusion coefficient (ADC) maps was the most effective technique. Quantitative ADC analysis is a promising tool for differentiation of active and non-active residual masses in lymphoma.

870

Plasma 9



The clinical evaluation of combining DWIBS with whole body T1w imaging for diagnosing bone marrow involvement in lymphoma patients: a comparison with PET/CT

Mengtian Sun¹, Jingliang Cheng¹, Yun Meng¹, and Zhizheng Zhuo²

¹The First Affiliated Hospital of Zhengzhou University, 1st, Zhengzhou, People's Republic of China, ²Philips Healthcare, Beijing, People's Republic of China

This study aimed to evaluate the value of the combination of DWIBS (diffusion weighted imaging with background signal suppression) with whole body T1w imaging for diagnosing bone marrow involvement (BMI) in lymphoma patients, compared to PET/CT imaging. In the first part of this study, patients with newly diagnosed lymphoma were included and whole body DWIBS, T1w and PET/CT images were acquired for all 20 subjects. For the assessment of individual lesions, DWIBS with whole body T1w has advantages over DWIBS and has similar ability with PET/CT to detect BMI lesions.

871

Plasma 10



Intravoxel incoherent motion diffusion-weighted imaging for discriminating the pathological response to neoadjuvant chemoradiotherapy in locally advanced rectal cancer

Wen Lu¹, Yu xiaoping¹, and Zhang zhongping²

¹Hunan Cancer Hospital, Chang sha, People's Republic of China, ²GE Healthcare China, Beijing, People's Republic of China

In this study, we investigated the utility of IVIM-DWI in discriminating the pathological response to nCRT in locally advanced rectal cancer (LARC). We found that both the pre-nCRT and post-nCRT IVIM-DWI parametric values for LARC, together with their percentage changes, might benefit the evaluation of pathological response to nCRT, which suggest IVIM-DWI is potentially useful in discriminating pathological response for LARC patients.

872

Plasma 11



The value of diffusion kurtosis imaging in assessing pathological complete response to neoadjuvant chemoradiation therapy in rectal cancer: a comparison with conventional diffusion-weighted imaging

Fei-Xiang Hu¹, Tong Tong¹, Wei Tang¹, Yi-Qun Sun¹, Dang Wang¹, San-Jun Cai², Zhen Zhang³, Grimm Robert⁴, Xu Yan⁵, Cai-xia Fu⁶, and Wei-Jun Peng¹

¹Radiology, Fudan University Shanghai Cancer Center, Shanghai, People's Republic of China, ²Colorectal Surgery, Fudan University Shanghai Cancer Center, Shanghai, People's Republic of China, ³Radiotherapy, Fudan University Shanghai Cancer Center, Shanghai, People's Republic of China, ⁴MR Applications Predevelopment, Siemens Healthcare GmbH, Germany, ⁵MR Collaboration NE Asia, Siemens Healthcare, People's Republic of China, ⁶APPL, Siemens Shenzhen Magnetic Resonance Ltd., People's Republic of China

The aim of this study was to evaluate the performance of diffusion kurtosis imaging (DKI) in predicting pathological complete response (pCR) of locally advanced rectal cancer (LARC) to neoadjuvant chemoradiation therapy (CRT) before and at an early stage of the treatment, and in comparison to conventional diffusion-weighted imaging (DWI). Results showed that DKI outperformed conventional DWI in accurately differentiating between pCR and nonPCR patients who received neoadjuvant chemoradiation therapy both before and at an early stage of treatment.

873

Plasma 12



The application of whole lesion IVIM analysis using iZOOM DWI in the diagnosis of thyroid tumor

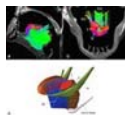
Yunlong Yue¹, Lili Zuo¹, Kaining Shi², Lee Jiang³, Jinsong Guo¹, and Yanfang Jin¹

¹Department of MR, Beijing Shijitan hospital of capital medical university, Beijing, People's Republic of China, ²Philips Healthcare (China), Beijing, People's Republic of China, ³Philips Healthcare (China), Suzhou, People's Republic of China

To explore the ability of IVIM parameters derived from iZoom DWI in differentiating malignant thyroid nodules from benign ones. 40 patients with 45 pathologically proven thyroid nodules were involved. iZOOM DWI with 2D RF was employed to decrease the distortion and carotid coil was used to increase the SNR. 3D ROI was drawn manually to cover the whole lesion. D and f values were significantly lower in malignant nodules than in benign nodules. According to ROC curve analysis IVIM almost reached the upper limit of the accuracy based on US.

874

Plasma 13



Diffusion Spectrum Imaging Tractography of the Human Tongue

Nahla M H Elsaid¹, Maureen Stone², Steven Roys¹, Rao P Gullapalli¹, Jerry L Prince³, and Jiachen Zhuo¹

¹Diagnostic Radiology, University of Maryland School of Medicine, Baltimore, MD, United States, ²Neural and Pain Sciences and Orthodontics, University of Maryland Dental School, Baltimore, MD, United States, ³Electrical and Computer Engineering, Johns Hopkins University, Baltimore, MD, United States

The human tongue is known to have a complex architecture of muscles. To fully understand how the muscle fibers are connected and how their relative position could affect the tongue functionality, diffusion weighted imaging is needed. Diffusion Spectrum Imaging (DSI) is able to characterize the fiber structure on a sub-voxel level including the fiber crossing or branching. As DSI sequences are usually time-consuming, in-vivo studies using DSI can be challenging. In this study, we present for the first time DSI of the post-mortem human tongue. and the associated tractography delineating the tongue muscle fibers. DSI has the ability to identify fiber crossings within the human tongue.

875

Plasma 14



Acquisition at maximum blood velocity overcomes the problem of the ill-posedness of the IVIM model: a demonstration with renal diffusion MRI

Bastien Milani¹, Jean-Baptiste Ledoux², and Menno Pruijm³

¹Nephrology, CHUV, Lausanne, Switzerland, ²Radiology, CHUV, ³Nephrology, CHUV

We explain why diffusion MRI should always be acquired when blood has maximum velocity in the organ of interest. We first give some theoretical arguments to support this hypothesis. We then demonstrate it with numerical experiments and with in-vivo experiments.

876

Plasma 15



Comparison of in-vivo Lung Morphometry Models from 3D Multiple b-value 3He Diffusion-Weighted MRI

Ho-Fung Chan¹, Juan Parra-Robles^{1,2}, Guilhem J Collier¹, and Jim M Wild¹

¹Academic Unit of Radiology, University of Sheffield, Sheffield, United Kingdom, ²Department of Bioengineering, Universidad Carlos III de Madrid, Madrid, Spain

The cylinder (CM) and stretched exponential (SEM) models have been proposed as a means of estimating lung alveolar microstructural length scales (L_m for CM and L_{mD} for SEM) from multiple b-value hyperpolarised gas DW-MRI. This work compares L_m and L_{mD} in healthy normals, idiopathic pulmonary fibrosis, and COPD patients. A correlation with a non-linear trend was observed between the L_m and L_{mD} parameters. This suggests that the two models have different operational ranges of length scale estimation accuracy due to inherent differences in their geometrical and mathematical assumptions.

Poster: MRS/MRSI Applications

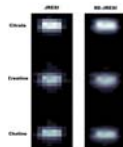
Exhibition Hall

Wednesday 17:15 - 18:15

877



Plasma 16



Resolution Enhanced accelerated Four Dimensional Echo Planar Spectroscopic Imaging: Application in Prostate Cancer

Zohaib Iqbal¹, Brian L. Burns¹, Rajakumar Nagarajan¹, Robert E. Reiter², Steven S. Raman¹, and M. Albert Thomas¹

¹Radiological Sciences, University of California - Los Angeles, Los Angeles, CA, United States, ²Urology, University of California - Los Angeles, Los Angeles, CA, United States

Prostate cancer (PCa) remains the most prevalent form of cancer in men. For diagnosis, Prostate-Specific Antigen (PSA) levels are most commonly used as a screening tool. Chemical shift imaging (CSI) methods can provide information on the biochemical concentrations of metabolites in different regions of the prostate. Here, we demonstrate a novel technique capable of improving the spatial and spectral resolution of the accelerated echo-planar J-resolved spectroscopic imaging (EP-JRESI) method, which obtains 2 spatial and 2 spectral dimensions in a single scan. This resolution enhanced EP-JRESI (RE-JRESI) method is evaluated in PCa patients and compared to the EP-JRESI results.

878

Plasma 17



Initial results of combined 1H and 31P spectroscopic imaging of the prostate at 7 Tesla

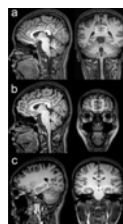
Bart WJ Philips¹, Mark van Uden¹, and Tom WJ Scheenen¹

¹Radiology and Nuclear Medicine, Radboud University Medical Centre Nijmegen, Nijmegen, Netherlands

Proton MR spectroscopy has proven to be a valuable tool in the evaluation and detection of prostate cancer by assessing metabolite ratios incorporating choline and citrate signals. The choline peak in the proton spectrum actually consists of several different peaks of choline containing compounds[2], of which some can be distinguished using 7 Tesla ³¹P spectroscopic imaging. In this work we present our first patient results of a method that combines ³¹P and ¹H within one measurement using a ³¹P Tx/Rx and ¹H Rx endorectal coil and we show its feasibility for correlating ³¹P and ¹H metabolite ratios.

879

Plasma 18



Reduced GABA levels correlate with cognitive impairment in relapsing-remitting multiple sclerosis

Guanmei Cao¹, Bin Zhao¹, Guangbin Wang¹, Weibo Chen², and Fei Gao¹

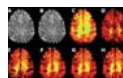
¹Shandong Medical Imaging Research Institute, Shandong University, Jinan, Shandong, People's Republic of China, ²Philips Healthcare, Shanghai, China, People's Republic of China

To investigate whether cognitive impairment in relapsing-remitting multiple sclerosis (RRMS) is associated with alterations in brain gamma-aminobutyric acid (GABA) levels, 31 RRMS patients and 26 healthy controls underwent 3T ¹H MRS and neuropsychologic assessment. GABA levels were quantified in the posterior cingulate cortex (PCC), the medial prefrontal cortex (mPFC) and left hippocampus (LHC). Patients showed reduced GABA+ in PCC and LHC, and reduced GABA+ levels correlated with cognitive function. This study demonstrates that abnormalities of the GABAergic system may be an important neurochemical mechanism of cognitive impairment in RRMS.

880



Plasma 19



Patch-based super-resolution of MRSI data in multiple sclerosis patients at 7 T

Saurabh Jain¹, Gilbert Hangel², Diana Sima^{1,3}, Wolfgang Bogner^{2,4}, Siegfried Trattnig^{2,4}, Sabine Van Huffel^{3,5}, Frederik Maes^{5,6}, and Dirk Smeets^{1,7}

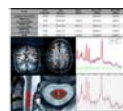
¹icometrix, R&D, Leuven, Belgium, ²High Field MR Centre, Medical University of Vienna, Vienna, Austria, ³Department of Electrical Engineering-ESAT, STADIUS Center for Dynamical Systems, Signal Processing and Data Analytics, KU Leuven, Leuven, Belgium, ⁴Christian Doppler Laboratory for Clinical Molecular MR Imaging, Vienna, Austria, ⁵Medical IT, iMinds, Leuven, Belgium, ⁶Department of Electrical Engineering-ESAT, PSI Medical Image Computing, KU Leuven, Leuven, Belgium, ⁷Biolmaging Lab, Universiteit Antwerpen, Antwerp, Belgium

The clinical application of brain MRSI is, upon several factors, limited by the comparatively low resolution that makes it difficult to resolve lesions. This work demonstrates the application of a patch-based super-resolution (PBSR) method that increases the spatial resolution of metabolite maps obtained from MRSI. The method is validated against conventional interpolation techniques in multiple sclerosis patient measurements. Our results clearly show the benefits of PBSR over other common interpolation techniques.

881



Plasma 20



Cervical spinal cord and brain MRS alterations in normal appearing white matter of multiple sclerosis (MS) patients at 3T

Patrik Oliver Wyss^{1,2,3,4}, Anke Henning^{1,2,5}, Andreas Hock^{1,6}, Andreas Lutterotti⁷, Roland Martin⁷, and Spyros Kollias⁴

¹Institute for Biomedical Engineering, University and ETH Zurich, Zurich, Switzerland, ²Max Planck Institute for Biological Cybernetics, Tuebingen, Germany, ³Swiss Paraplegic Centre, Nottwil, Switzerland, ⁴Institute of Neuroradiology, University Hospital Zurich, Zurich, Switzerland, ⁵Institute of Physics, Ernst-Moritz-Arndt University Greifswald, Greifswald, Germany, ⁶Department of Psychiatry, Psychotherapy and Psychosomatics Hospital of Psychiatry, University of Zurich, Zurich, Switzerland, ⁷Neuroimmunology and Multiple Sclerosis Research, Department of Neurology, University Hospital and University Zurich, Zurich, Switzerland

This investigation explores alterations of both cervical spinal cord and brain metabolite levels in normal appearing tissue in patients suffering from multiple sclerosis (MS). In the brain, a 2 dimensional J-resolved spectroscopy sequence and 2D prior-knowledge fitting is used and the metabolite cycling technique is applied to the cervical spinal cord at 3T. Relapsing-remitting MS (RRMS) and secondary progressive MS (SPMS) patients are included and alterations between brain and spinal cord metabolites are addressed.

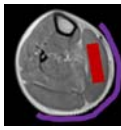
882

Plasma 21

¹H-NMR of carnosine combined with ³¹P-NMRS to better characterize skeletal muscle pH dysregulation in Duchenne muscular dystrophy

Harmen Reyngoudt^{1,2}, Suna Turk^{1,2}, and Pierre G. Carlier^{1,2}

¹NMR Laboratory, Institute of Myology, Paris, France, ²CEA, DRF, I2BM, MIRCen, Paris, France



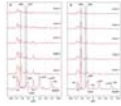
The finding of an alkaline P_i pool has been established with ^{31}P -NMRS in healthy resting skeletal muscle and the dystrophic muscle of GMRD dogs and DMD patients. The pH values corresponding to this P_i pool corresponds better with extracellular pH. Intracellular pH, however, can also be measured with 1H -NMRS, using carnosine. In a group of DMD patients, we observed that pH determined with ^{31}P -NMRS were systematically increased, whereas this was not always the case for pH based on the measurement of carnosine, revealing two groups in dystrophic muscle: (1) pH elevated with ^{31}P and 1H and (2) pH only elevated with ^{31}P .

883

Plasma 22

Apparent short transverse relaxation time of inorganic phosphate in breast cancer tissue at 7 tesla.

Wybe JM van der Kemp¹, Tijl A van der Velden¹, Alexander M Schmitz¹, Kenneth G Gilhuijs¹, Peter R Luijten¹, Dennis WJ Klomp¹, and Jannie P Wijnen¹



¹Department of Radiology, UMC Utrecht, Utrecht, Netherlands

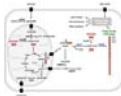
Here we show in a patient group with breast cancer an apparent shortening of the transverse relaxation time of the P_i signal at 7 tesla, as compared to healthy breast fibroglandular tissue and propose an underlying mechanism to explain this observation.

884

Plasma 23

Acetate metabolism towards fatty acids is down-regulated in IDH1 mutant glioma as shown by ^{13}C MRS

Chloé Najac¹, Marina Radoul¹, Pavithra Viswanath¹, Myriam M Chaumeil¹, and Sabrina M Ronen¹



¹Radiology and Biomedical Imaging, University of California San Francisco, San Francisco, CA, United States

IDH1 is the most prevalent driver mutation in lower-grade glioma and upgraded glioblastoma and is associated with additional metabolic reprogramming. Here, we investigated fatty acid biosynthesis and the role of acetate, which was recently recognized as a major fuel in primary glioblastoma. Labeling cells harboring either wild-type or mutant IDH1 with $[1,2-^{13}C]$ -acetate, we found a decrease in flux towards fatty acids in mutant IDH1 cells although the total fatty acid pools remained unchanged. Associated with cell biological assays, these results point to alternate sources for maintenance of fatty acid levels in IDH1 mutant cells.

885

Plasma 24

Automatic tissue-type classification of 1H -MRSI spectra in patients with glioblastoma

Nuno Pedrosa de Barros¹, Raphael Meier², Martin Pletscher¹, Urspeter Knecht¹, Mauricio Reyes², Roland Wiest¹, and Johannes Slotboom¹



¹SCAN / Neuroradiology, University Hospital Bern (Inselspital), Bern, Switzerland, ²Institute for Surgical Technology & Biomechanics, University of Bern, Bern, Switzerland

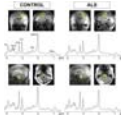
Clinical-routine MRSI-data analysis is commonly performed through the visual inspection of multiple metabolite and metabolite-ratio maps, and aims at *translating* the different spectroscopic patterns into known tissue-types, such as, necrosis, solid tumour, tumour-infiltration, normal-brain-tissue, etc. Such *translation/segmentation* requires solid expertise in MR-spectroscopy, which most clinicians do not have. Bad-quality-data, as well as frequency-dependant-selection-profiles further complicate proper interpretation of MRSI-data. Therefore, to facilitate the *clinical-use* of MRSI, we present an automatic MRSI-tissue-type segmentation algorithm, that includes automatic-quality-filtering and selection-profile-correction. The method was tested in glioblastoma and the tissue-types were compared against an MRI-based tumour-segmentation-method.

886

Plasma 25

High and Ultra-High Field Proton MR Spectroscopy in Early Amyotrophic Lateral Sclerosis

Ian Cheong¹, Malgorzata Marjanska, Dinesh Deelchand, Lynn Eberly, David Walk, and Gulin Oz



¹University of Minnesota Twin Cities, Minneapolis, MN, United States

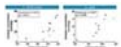
Amyotrophic lateral sclerosis (ALS) is a devastating disease of motor neurons with unknown etiology. Evidence suggests that the brain undergoes degenerative changes in ALS, particularly within areas of the descending motor pathway. Identifying robust and non-invasive biomarkers that are sensitive to neurodegeneration in ALS is essential for improving clinical trial design and assessment of treatment effectiveness. This study evaluated 1H -MRS-measured metabolite levels as biomarkers of disease severity. Ultra-high field (7 tesla) 1H -MRS revealed metabolic abnormalities in the motor cortex and brainstem of humans with ALS that are dependent on disease stage.

887

Plasma 26

Detection of in vivo biomarkers in fungal brain infection models and potential determination of cell viability.

Liesbeth Vanherp¹, Amy Hillen¹, Jennifer Poelmans¹, Katrien Lagrou², Greetje Vande Velde¹, and Uwe Himmelreich¹



¹Imaging and Pathology, University of Leuven, Leuven, Belgium, ²Laboratory of Clinical Bacteriology and Mycology, University of Leuven, Leuven, Belgium

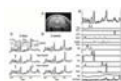
Animal models of cerebral infection by the pathogenic fungi *Cryptococcus neoformans* and *C. gattii* were developed and assessed longitudinally by using anatomical and diffusion MRI as well as MR spectroscopy. MR spectroscopy identified *in vivo* biomarkers for potential etiological diagnosis and more importantly for quantification of the fungal load in living animals. Our results have great potential to assist in the differential diagnosis of brain lesions in patients, whereby MR spectroscopy is a safer, non-invasive and rapid method in comparison to traditional invasive diagnostic methods such as CSF sampling or biopsies.

888

Plasma 27

Metabolic variability in a brief status epilepticus model

Jullie W Pan¹, Yijun Wu², Patrice Pearce³, Nihal de Lanerolle⁴, and Kevin Kelly⁵



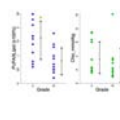
¹MRRC, University of Pittsburgh, Pittsburgh, PA, United States, ²Developmental Biology, Children's Hospital Pittsburgh, Pittsburgh, PA, ³Neurology, University of Pittsburgh, Pittsburgh, PA, ⁴Neurosurgery, Yale University, ⁵Allegheny Singer Research Institute, Pittsburgh, PA

This study uses short echo MR spectroscopy (TE 10ms) to study the metabolic changes seen in a status epilepticus kainate rodent model. Applied with a brief period (45min) of seizures, a hierarchical cluster analysis is performed on the spectroscopic changes measured 3days after the status injury. These data displayed a bimodal distribution characterizing two groups of animals, "more" or "less" injured. The classification persists into a repeat MRS measurement performed at 3wk, with the less injured group being able to recover; the more injured group did not recover well. Finally, this classification was consistent with Nissl based histological analysis.

889



Plasma 28



Polyunsaturated fatty acid (PUFA) is associated with tumour grading – An ex vivo study on whole breast tumours using multiple quantum coherence (MQC) MRS

Sai Man Cheung¹, Ehab Husain^{2,3}, Yazan Masannat^{3,4}, Klaus Wahle^{3,5}, Steven D Heys^{3,4}, and Jiabao He¹

¹Aberdeen Biomedical Imaging Centre, University of Aberdeen, Aberdeen, United Kingdom, ²Pathology Department, Aberdeen Royal Infirmary, Aberdeen, United Kingdom, ³School of Medicine, University of Aberdeen, Aberdeen, United Kingdom, ⁴Breast Unit, Aberdeen Royal Infirmary, Aberdeen, United Kingdom, ⁵Strathclyde Institute of Pharmacy and Biological Sciences, Glasgow, United Kingdom

Eicosanoids are derivatives of three different PUFA, vital in membrane formation and anti-inflammatory control. The presence of eicosanoids in adipose tissue and fibroblasts governs the release of signalling agents in breast, stimulating the invasion of breast cancer cells. Lipid composition has emerged as a potential predictor of breast cancer. However, current research focuses on the tumour initiation, while the understanding of lipid function in tumour progression remains sparse. We therefore hypothesise that there is a difference in PUFA concentration between grade II and III breast cancer. We applied MQC MRS for accurate PUFA measurement on freshly excised whole breast tumours.

890



Plasma 29



In-Vivo Regional detection of Gly in Human Brain: Implications in Glioma Patients at 3T

Vivek Tiwari¹, Zhongxu An¹, Sandeep Kumar Ganji¹, and Changho Choi¹

¹Advanced Imaging Research Center, UT Southwestern Medical Center, Dallas, TX, United States

Glycine, an inhibitory-neurotransmitter and a co-agonist of N-Methyl-D-aspartate, has been implicated in rapid cancer cell-proliferation and is elevated in high-grade gliomas than low-grade. Gly concentrations range from 0.5-1.0 M in normal brain and exhibits regional-variation. Given such a low in-vivo concentration of Gly, potential overlap from ml and regional-variation, here we have developed a novel Gly-optimized single-voxel-localized triple-refocusing scheme for precise co-detection of Gly and ml in Gray-matter (GM)-rich Medial-Occipital (MO) and White-matter (WM) rich Left-Parietal (LP) healthy-brain region, and further extended to measure glycine level in glioma patients.

891

Plasma 30



Differential diagnosis of Hepatic metabolites between non-alcoholic steatohepatitis and simple steatosis in humans and a murine model using a 1H MR spectroscopy study with long TE

Tae-Hoon Kim¹, Hong Young Jun¹, Chang-Won Jeong¹, Jong-Hyun Ryu¹, Kou Gyeom Kim¹, and Kwon-Ha Yoon²

¹Radiology, Imaging Science Research Center, Iksan, Korea, Republic of, ²Radiology, Wonkwang University School of Medicine, Iksan, Korea, Republic of

Liver biopsy is the gold standard for diagnosing non-alcoholic fatty liver disease (NAFLD) but with practical constraints. MR spectroscopy (MRS) allows in vivo assessment of hepatocellular metabolism and has shown potential for biochemical differentiation in diffuse liver disease. Recent 13C-MRS demonstrated that alanine and lactate levels in inflammatory liver injury were increased compared to those in normal liver, and these changes were positively correlated with liver enzyme levels. However, the clinical use of 13C-MRS technique is limited because it necessitates 13C-resonance specific hardwares and softwares for data acquisition. This study used long TE 1H-MRS to monitor changes of hepatocellular metabolites in NAFLD.

Electronic Power Pitch Poster

Poster: Breakthrough Methods & Applications in Cancer Imaging

Exhibition Hall

Thursday 9:15 - 10:15

977

Plasma 1



High resolution imaging of the optic chiasm at 7T MRI improves lesion detection and tumour delineation compared to 3T

Guido van Haren¹, Lorna Grech-Fonk^{2,3}, Marco Versteegen⁴, Wouter Teeuwisse², Teresa Ferreira¹, Irene Notting³, Wouter van Furth⁴, Alberto Pereira⁵, Gregorius Luyten³, Andrew Webb², and Jan-Willem Beenakker^{2,3}

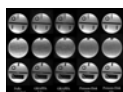
¹Radiology, LUMC, Leiden, Netherlands, ²Radiology, CJ Gorter center for high field MRI, LUMC, Leiden, Netherlands, ³Ophthalmology, LUMC, Leiden, Netherlands, ⁴Neurosurgery, LUMC, Leiden, Netherlands, ⁵Endocrinology, LUMC, Leiden, Netherlands

The limited resolution of 3Tesla MRI often leads to missed lesions or ambiguities in the tumour environment for patients with a pituitary macro-adenoma. In this study we developed a robust high-resolution 7Tesla MRI-protocol of the optico-chiasmatic system and evaluated its clinical value. The 7T MR-images reveal tiny lesions in the optic nerve or chiasm which are not visible at 3T. These lesions could explain the vision loss for 3 of the 7 evaluated patients and gave the physician new treatment possibilities. Overall, this study shows the great clinical opportunities of 7Tesla MRI for patients with pituitary macro-adenoma or other neuro-ophthalmic conditions.

Plasma 2

Accelerated 3D bSSFP Imaging for Treatment Planning on an MRI-Guided Radiotherapy System

Yu Gao^{1,2}, Ziwu Zhou¹, Fei Han¹, Percy Lee^{2,3}, Daniel Low^{2,3}, Peng Hu^{1,2}, and Yingli Yang^{2,3}



¹Radiology, University of California, Los Angeles, Los Angeles, CA, United States, ²Physics and Biology in Medicine IDP, University of California, Los Angeles, Los Angeles, CA, United States, ³Radiation Oncology, University of California, Los Angeles, Los Angeles, CA, United States

The purpose of this work is to introduce a compressed sensing and parallel imaging combined technique to reduce the acquisition time for planning MR. We implemented a variable-density Poisson-Disk under-sampled acquisition along with L1-ESPIRiT reconstruction technique on an MRI-guided radiotherapy system. Phantom study showed that our technique had superior image quality over the conventional GRAPPA approach. Patient and volunteer study demonstrated that comparable images can be acquired with half of the original time. In addition, the proposed technique was able to achieve high resolution imaging where the GRAPPA approach failed due to high noise level.



Plasma 3



Feasibility of magnetic resonance colonography for an immune check-point inhibitor in orthotopic colorectal rechallenge tumor models
Jinil Kim¹, Yoon Seok Choi², Dong-Cheol Woo¹, Chul-Woong Woo¹, Sang Tae Kim¹, Jae Im Kwon¹, and Kyung Won Kim³

¹Asan Institute for Life Sciences, ASAN Medical Center, Seoul, Korea, Republic of, ²Medical research institute, Gangneung Asan Hospital, Gangneung, Korea, Republic of, ³Department of Radiology, ASAN Medical Center, Seoul, Korea, Republic of

In the immunotherapy research field, establishing appropriate preclinical model is very important to evaluate the complex immune reaction. Orthotopic tumor model is more physiologic than ectopic tumor model, however its use may be limited due to difficulty in evaluating deep-seated tumors, especially in the colorectum having a complex anatomy. MR colonography (MRC) is a new technique in preclinical trial, which uses Fluorinert, a negative contrast agent, to fill the colorectum. Our study demonstrated that MRC is quite feasible to evaluate colorectal tumors and metastatic foci in orthotopic colorectal tumor model, which can be useful in immunotherapy drug development.

Plasma 4



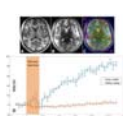
Multi-modal and multi-scale measurement of metabolism *in vivo* in a breast cancer model

Benjamin L Cox^{1,2,3}, Joseph M Szulczewski^{3,4}, David R Inman⁴, Erin B Adamson¹, Kai D Ludwig¹, Justin J Jeffery⁵, Stephen A Graves¹, Alison B Roth¹, David B Mummy^{1,6}, Patricia J Keely⁴, Kevin W Eliceiri^{1,2,3,5,6}, and Sean B Fain^{1,7}

¹Medical Physics, University of Wisconsin - Madison, Madison, WI, United States, ²Medical Engineering, Morgridge Institute for Research, Madison, WI, United States, ³Laboratory for Optical and Computational Instrumentation (LOCI), University of Wisconsin - Madison, Madison, WI, United States, ⁴Cell and Regenerative Biology, University of Wisconsin - Madison, Madison, WI, United States, ⁵UW Carbone Cancer Center, Madison, WI, United States, ⁶Biomedical Engineering, University of Wisconsin - Madison, Madison, WI, United States, ⁷Radiology, University of Wisconsin - Madison, Madison, WI, United States

Performing MRI, PET/CT, and optical imaging at the cellular scale *in vivo* provides highly complementary information as a powerful tool to study cancer metabolism. Recent development of implanted optical windows allows for optical imaging *in vivo*. Here, we demonstrate multi-modal and multi-scale imaging of tumor progression in a mouse model of breast cancer by performing optical imaging through an implanted window, and whole-body MRI and PET/CT in a single day. The challenge of PET-MR registration is also addressed using dual-PET-MR fiducial markers embedded in a custom-imaging tray.

Plasma 5



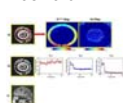
Dynamic Glucose Enhanced MRI - A prospective study in healthy volunteers and glioblastoma patients

Daniel Paech¹, Patrick Schuenke², Christina Koehler¹, Johannes Windschuh², Sibumundiyanapurath³, Sebastian Bickelhaupt¹, Philipp Bäumer¹, David Bonekamp¹, Martin Bendszus⁴, Wolfgang Wick³, Peter Bachert², Mark E. Ladd², Heinz-Peter Schlemmer¹, Moritz Zaiss⁵, and Alexander Radbruch¹

¹Radiology, German Cancer Research Center, Heidelberg, Germany, ²Medical Physics in Radiology, German Cancer Research Center, Heidelberg, Germany, ³Neurology, University Hospital Heidelberg, Heidelberg, ⁴Neuroradiology, University Hospital Heidelberg, Heidelberg, ⁵Max-Planck-Institut Tübingen, Tübingen, Germany

Glucose is the main energy source of cancer cells to proliferate and survive. Recently, promising results to assess changes in cellular metabolism using natural unlabeled D-glucose as biodegradable MRI contrast agent, have been reported employing Chemical Exchange Saturation Transfer (CEST) and Chemical Exchange sensitive Spin-Lock (CESL) imaging. In this work, the CESL-based dynamic glucose enhanced (DGE) contrast was investigated in healthy volunteers and a homogenous cohort of newly diagnosed untreated glioblastoma patients at 7 Tesla. DGE MRI allowed for sensitive visualization of physiological glucose uptake in the healthy human brain and pathophysiologically increased glucose enhancement of brain tumors.

Plasma 6



3D printed Breast DCE-MRI phantom to mimic structure and pharmacokinetics

Nithin N Vajuvalli¹, Chethan Kumar M¹, Amaresha Shridhar Konar^{1,2}, Shivaprasad Ashok Chikop¹, Darshan Shivaramu Keelara¹, Ashwini Kumnoor¹, Ramesh Venkatesan², and Sairam Geethanath¹

¹Medical Imaging Research Centre, Dayananda Sagar Institution, Bangalore, India, ²Wipro GE healthcare, Bangalore, India

DCE MRI plays a critical role in routine clinical breast examination. Current work focuses on the development of Breast DCE MRI phantom using a 3D printer to mimic poor and well perfused regions. The phantom developed was controlled through user entered K^{trans} values entered in a GUI which interfaced with a peristaltic pump to control flow rates. The K_{ep} parameters was controlled through the 3D model geometry. Prospective MR images of the phantom were acquired on a 1.5T scanner using the TRICKS sequence; and pharmacokinetic maps based on Tofts model were computed and quantified.

Plasma 7



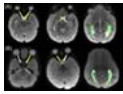
Recurrent Neural Network on DCE-MRI in Prostate Cancer

Xia Li¹, Vivek Vaidya², Sandeep Gupta¹, Rakesh Mullick², Oguz Akin³, and Dattesh Shanbhag²

DCE-MRI has become an important protocol in mpMRI analysis of prostate cancer and it has been quantified typically using pharmacokinetic modelling and the estimated parameters are then used with other approaches (machine learning or deep learning (DL)) to characterize/discriminate tumor tissue against healthy tissue. However, it is not clear if applying DL to the DCE-MRI time series directly is beneficial for prostate cancer detection. Hence, we propose a DL based method to differentiate prostate tumor from healthy tissues at the voxel level using raw arbitrary signal DCE time-series itself. Overall, DL based tumor characterization provided similar detectability for prostate tumor when compared to K^{trans} and V_e maps. We also evaluated differences in tumor characterization when contrast agent concentration time-curves were used instead of arbitrary signal curves and found them to provide similar detectability.

984

Plasma 8



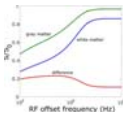
In vivo assessment of tumour invasion of the visual pathway in optic pathway glioma patients using multi-shell diffusion tensor MRI
Patrick W Hales¹, Victoria Smith², Patricia O'Hare³, Kshitij Mankad⁴, Felice d'Arco⁴, Jessica Cooper⁴, Ramneek Kaur¹, Kim Phipps³, Darren Hargrave³, and Christopher A Clark¹

¹Developmental Imaging & Biophysics Section, University College London, London, United Kingdom, ²Ophthalmology Department, Great Ormond Street Children's Hospital, London, United Kingdom, ³Haematology and Oncology Department, Great Ormond Street Children's Hospital, London, United Kingdom, ⁴Radiology Department, Great Ormond Street Children's Hospital, London, United Kingdom

Optic pathway glioma (OPG) is a childhood tumour of the visual pathway. Some OPG patients remain stable, whereas others experience rapid visual decline; however, conventional MRI cannot stratify these patients. We used multi-shell DTI to measure tumour invasion of the optic pathway in 23 OPG patients, in conjunction with visual assessment. A strong correlation was found between fractional anisotropy in the optic nerves and optic radiations, and visual acuity ($p=0.00092$ and $p=0.008$ respectively). Our study demonstrates that multi-shell diffusion-MRI offers increased sensitivity over conventional MRI in detecting white matter integrity and function in the visual pathway of OPG patients.

985

Plasma 9



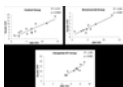
Pipeline for longitudinal assessment of patient-derived mouse xenografts using 3D magnetization transfer-weighted MRI
Kimberly L. Desmond¹, David Bakhshinyan², Maleeha Qazi², Parvez Vora², Chirayu Chokshi², Sheila K. Singh², and Nicholas A. Bock¹

¹Psychology, Neuroscience and Behaviour, McMaster University, Hamilton, ON, Canada, ²McMaster Stem Cell and Cancer Research Institute, McMaster University, Hamilton, ON, Canada

A pipeline was developed, driven by 3D magnetization transfer-weighted images acquired without contrast agent, to automatically assess mouse models of patient-derived tumours against an atlas of control NOD-SCID mice, for the purposes of longitudinal, high-throughput screening of mice for response to cancer therapy and recurrence.

986

Plasma 10



Tumor Interstitial Fluid Pressure and Hydraulic Conductivity Estimates by DCE-MRI in a Rat Model of Cerebral Tumor

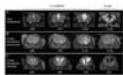
Rasha Elmghirbi^{1,2}, Nagaraja N. Tavarekere³, Stephen L. Brown⁴, Swayamprava Panda¹, Kelly A. Keenan³, Glauber Cabral¹, Hassan Bagher-Ebadian^{2,4}, and James R. Ewing^{1,2}

¹Neurology, Henry Ford Hospital, Detroit, MI, United States, ²Physics, Oakland University, Rochester Hills, MI, United States, ³Neurosurgery, Henry Ford Hospital, Detroit, MI, United States, ⁴Radiation Oncology, Henry Ford Hospital, Detroit, MI, United States

An elevated tumor interstitial fluid pressure (TIFP) is a critical element for assessing therapeutic response. This study demonstrates the use of DCE-MRI to estimate TIFP, and validates that estimate by an invasive method in a rat glioblastoma model, with and without treatment interventions. Significant positive correlations between MRI-derived TIFP estimates and invasive measures of TIFP were found in all groups (e.g., for untreated group, $R^2=0.76$, $p<0.0001$). These findings validate an MRI-estimated TIFP as a noninvasive measure of TIFP in embedded cerebral tumors, and suggest that it may be a useful tool in assessing tumor response to therapy.

987

Plasma 11



A preclinical MRI study investigating the impact of the local microenvironment on the progression of diffuse intrinsic pontine glioma in patient-derived xenografts

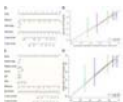
Mariama Fofana¹, Jessica KR Boulton¹, Maria Vinci¹, Valeria Molinari¹, Kathryn Taylor¹, Sergey Popov¹, Alan Mackay¹, Chris Jones¹, and Simon P Robinson¹

¹The Institute of Cancer Research, London, United Kingdom

Diffuse intrinsic pontine glioma (DIPG) is a devastating childhood brain tumour with very poor outcome. The local brain microenvironment appears to play an important role in the tumorigenesis of DIPG, and is currently underinvestigated. Infratentorial and hemispheric tumour growth patterns of orthotopic DIPG xenografts were assessed longitudinally by anatomical MRI, and confirmed by immunohistochemical analysis. ADC, T_1 and T_2 were higher in infratentorial tumours than hemispheric tumours, corresponding to a higher degree of tumour-associated oedema observed histologically.

988

Plasma 12



Multi-parametric MRI Radiomics for Pre-treatment Prediction of the Progression-Free Survival in Advanced Nasopharyngeal Carcinoma

Bin Zhang¹

¹Guangdong General hospital, Guangzhou, People's Republic of China

To our knowledge, this is the first MRI-based radiomics study to predicting survival of tumor. The results of our study show that multiparametric MRI-based radiomics nomogram significantly improves the 7th edition of AJCC TNM staging system and clinical data in predicting individualized progression-free survival (PFS) in advanced NPC (stage III-IVb). In fact, the radiomics nomogram built in our study could integrate all prognostic biomarkers/signatures that have been published in this area to improve its predictive performance. Besides, for the first time, our radiomics heatmaps showed positive associations between radiomics signature features with overall stage, T-stage and negative associations between radiomics signature features with N-stage. Our radiomics study provides some different insights into the mechanism of hematogenous and lymphatic metastasis of NPC.

989

Plasma 13

MR Elastography and Perfusion MRI for the Early Assessment of Treatment Response in Soft Tissue Sarcomas



Kay Pepin¹, Roger Grimm², Soudabeh Kargar³, Sarah James¹, Matthew Howe², Karen Fritchie⁴, Matthew Frick², Doris Wenger², Richard Ehman², Nadia Laack¹, Michael Herman¹, and Deanna Pafundi¹

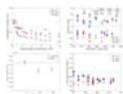
¹Radiation Oncology, Mayo Clinic, Rochester, MN, United States, ²Radiology, Mayo Clinic, Rochester, MN, United States, ³Mayo Graduate School, Mayo Clinic, Rochester, MN, United States, ⁴Pathology, Mayo Clinic, Rochester, MN, United States

Advanced imaging is a critical component in the development of patient-specific and novel treatment strategies, and the non-invasive evaluation of early response in sarcomas. Our central hypothesis is that changes in sarcoma stiffness quantified with MRE and perfusion with DCE-MRI throughout therapy can predict response. Soft tissue sarcomas are a rare malignancy arising in a wide range of anatomic locations. Anatomy-specific imaging protocols were developed to evaluate soft tissue sarcomas in 9 patients. In 3 patients, we investigated the feasibility to assess response to radiation therapy and observed a decrease in parameters related to tumor stiffness and perfusion metrics.

990

Plasma 14

Quantitative Imaging for Radiotherapy on an MR-Linac Scanner



Folkert Koetsveld¹, Leon C. ter Beek², Petra J. van Houdt¹, Laurens D. van Buuren¹, and Ulke A. van der Heide¹

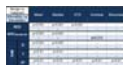
¹Radiotherapy, Netherlands Cancer Institute, Amsterdam, Netherlands, ²Radiology, Netherlands Cancer Institute, Amsterdam, Netherlands

The MR-Linac integrates an MR-scanner with a radiotherapy treatment machine. Patients undergoing radiotherapy treatment will be imaged daily on the MR-Linac. We investigated the suitability of the MR-Linac as a platform for quantitative imaging. Daily quantitative imaging can be used for imaging biomarker discovery, and give information on tumor treatment response. We did phantom studies of four quantitative MRI techniques: T2 mapping, dynamic contrast enhanced imaging, T1 mapping and diffusion weighted imaging to determine the accuracy of these techniques on the MR-Linac. We tested the repeatability of T2 mapping on a volunteer.

991

Plasma 15

Support vector machine for breast cancer classification using DWI histogram features: preliminary study



Igor Vidić¹, Liv Egnell¹, Jose R. Teruel², Torill E. Sjøbak³, Neil P. Jerome³, Agnes Østlie⁴, Hans E. Fjøsne^{5,6}, Tone F. Bathen³, and Pål Erik Goa¹

¹Department of Physics, Norwegian University of Science and Technology (NTNU), Trondheim, Norway, ²Department of Radiology, University of California, La Jolla, CA, United States, ³Department of Circulation and Medical Imaging, Norwegian University of Science and Technology (NTNU), Trondheim, Norway, ⁴Clinic of Radiology and Nuclear Medicine, St. Olavs University Hospital, Trondheim, Norway, ⁵Department of Cancer Research and Molecular Medicine, Norwegian University of Science and Technology (NTNU), Trondheim, Norway, ⁶Department of Surgery, St. Olavs University Hospital, Trondheim, Norway

In this work we use the machine learning method support vector machine (SVM) to classify malignant and benign tumors, as well as ER+HER2- and ER+HER2+. As feature we use histogram properties of DWI-models (RED, ADC, IVIM) parameters as features. Our study showed that SVM classifiers using combinations of features from different models have predictive power in both analyses, also it performed better than SVM using combination of parameters obtained only from one of the models. The results are encouraging because SVM with DWI parameters can potentially hinder unnecessary biopsies.

Electronic Power Pitch Poster

Poster: Contrast Mechanisms: New Horizons

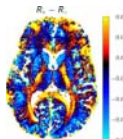
Exhibition Hall

Thursday 9:15 - 10:15

992

Plasma 16

On the decay of SSFP configurations



Damien Nguyen^{1,2}, Rahel Heule^{1,2}, Carl Ganter³, and Oliver Bieri^{1,2}

¹Radiological Physics, University of Basel Hospital, Basel, Switzerland, ²Department of Biomedical Engineering, University of Basel, Basel, Switzerland, ³Department of Diagnostic Radiology, Klinikum rechts der Isar, Technical University Munich, Munich, Germany

In this work, we explore the decay of negative and positive steady state configurations as a mean to assess the tissue microstructure. Steady state configurations are retrieved up to a high order from an exhaustive sampling of the frequency response profile of low-angle balanced SSFP scans. Subsequently, the decay of configurations (termed DECO) is analyzed using a single-pole matrix pencil analysis yielding positive and negative DECO images. Any asymmetry in the configuration decay is directly linked to asymmetric frequency content within a voxel and is captured in the DECO difference image.

Plasma 17

Asymmetries of the balanced SSFP profile allow to probe microstructure anisotropy at 9.4 Tesla



Philipp Ehse^{1,2}, Mario Gilberto Báez-Yáñez^{2,3}, Michael Erb¹, and Klaus Scheffler^{1,2}



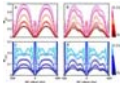
¹Biomedical Magnetic Resonance, University of Tübingen, Tübingen, Germany, ²Dept. of High-Field Magnetic Resonance, Max Planck Institute for Biological Cybernetics, Tübingen, Germany, ³Graduate Training Centre of Neuroscience, University of Tübingen, Tübingen, Germany

The bSSFP signal profile exhibits tissue-dependent asymmetries that can be used as a novel contrast mechanism and have been hypothesized to relate to the tissue microenvironment. In this work, we investigate this effect at ultra high-field using phase-cycled bSSFP at an isotropic resolution of 1.2 mm. As in the original publication, we also observe strong asymmetries in white matter and a comparison to DTI data reveals that the largest asymmetries occur in white matter tracts oriented orthogonal to the main magnetic field.

994

Plasma 18

Quantitative modeling of exchange in bSSFPX

Shu Zhang¹, Robert E Lenkinski^{1,2}, and Elena Vinogradov^{1,2}

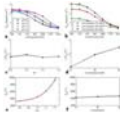
¹Department of Radiology, UT Southwestern Medical Center, Dallas, TX, United States, ²Advanced Imaging Research Center, UT Southwestern Medical Center, Dallas, TX, United States

bSSFP was shown to be sensitive to exchange and is explored as an alternative way for CEST/ $T_{1\rho}$ experiments (the bSSFPX method). In this abstract, an analytical solution is derived for the magnetization behavior in the bSSFPX. The solution describes the transient signal fluctuations for short saturation times. The solution is verified by comparing it to full, step-wise computation of Bloch-McConnell Equations. Overall, this solution is in good agreement with Bloch-McConnell Equations and follows the transient signal oscillations well. Work is in progress to use this solution to quantify exchange rates experimentally.

995

Plasma 19

Spin-lock imaging of exogenous exchange-based contrast agents to assess tissue pH

Zhongliang Zu¹, Hua Li¹, Xiaoyu Jiang¹, and John C Gore¹

¹Vanderbilt University, Nashville, TN, United States

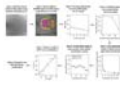
We measured spin-lock relaxation rates as a function of locking field to quantify tissue pH and the concentration of an exogenous X-ray contrast agent, iohexol, based on chemical exchange effects. Results show that spin-lock imaging can be used to detect exchange-based agents and the effects of tissue acidification.

996



Plasma 20

Quantification of trans-endothelial water exchange and vessel geometry using contrast-enhanced MRI and alterations in a transgenic rat model of Alzheimer's disease

Ben Dickie¹, Hervé Boutin^{1,2}, Jose Ulloa^{3,4}, Laura M Parkes¹, and Geoff JM Parker³

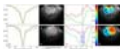
¹Division of Neuroscience and Experimental Psychology, University of Manchester, Manchester, United Kingdom, ²The Wolfson Molecular Imaging Centre, University of Manchester, Manchester, United Kingdom, ³Division of Informatics, Imaging and Data Sciences, University of Manchester, Manchester, United Kingdom, ⁴Bioxydyn, Manchester

MRI measurements of cerebrovascular function and structure are important for understanding neurodegenerative disease mechanisms. In this study, a novel contrast-enhanced multi-flip angle multi-echo (MFAME) MRI technique capable of simultaneously quantifying vessel permeability surface area product to water (PS_w), blood water population fraction (p_b), and contrast agent r_2^* is presented, and applied to a transgenic rat model of Alzheimer's disease (TgF344-AD). Transgenic rats exhibit higher p_b and lower PS_w in the hippocampus compared to wild-types, suggesting MFAME MRI may be sensitive to regional pathologic microvascular alterations in this model.

997

Plasma 21

CEST-weighted MRI at 21.1 T: application to glioma and ischemic rat model

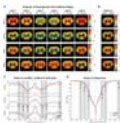
Tangi Roussel^{1,2}, Jens T. Rosenberg³, Samuel C. Grant^{3,4}, and Lucio Frydman²

¹NeuroSpin, Commissariat à l'Energie Atomique et aux Energies Alternatives, Gif-sur-Yvette, France, ²Department of Chemical Physics, Weizmann Institute of Science, Rehovot, Israel, ³National High Magnetic Field Laboratory, Florida State University, Tallahassee, FL, United States, ⁴Department of Chemical & Biomedical Engineering, The Florida State University, Tallahassee, FL, United States

This study explores and demonstrates the opportunities opened by ultrahigh fields for in vivo CEST-weighted imaging. CEST-weighted fast spin-echo imaging was performed on two neurological models: hypoxic ischemic and glioblastoma. A remarkably strong CEST contrast ($\approx 15\%$) was observed for the tumors at 3.32 ppm originating mainly from an APT increase and a strong decrease in NOE and MT. Ischemic lesions were still more robustly detected with standard T_2 -weighted images than with CEST. Potential explanations and dependence with high magnetic field are discussed.

998

Plasma 22

Offset-Saturation-Induced (osi-) Variations in Multiexponential T_2 at 16.4T: A New Dimension for Probing White Matter ContrastTeresa Serradas Duarte¹ and Noam Shemesh¹

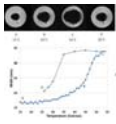
¹Champalimaud Neuroscience Programme, Champalimaud Centre for the Unknown, Lisbon, Portugal

Whether Magnetization Transfer could affect Multiexponential T_2 (MET_2) Relaxometry remains poorly explored. Here, the effects of irradiation at different offset frequencies on the MET_2 components were evaluated as novel contrast mechanisms for white matter in the rat spinal cord at 16.4T. MET_2 coefficients were found to shift with off-resonance saturation, showing unique tract-specific signatures across the irradiation frequency. Offset-saturation-induced (osi-) MET_2 Relaxometry maps show strong contrasts between microstructurally-distinct rat spinal cord tracts. The potential of exploiting the osi- MET_2 shift phenomenon to increase white matter contrast is discussed.

999

Plasma 23

Magneto-Caloric Materials as Tunable and Switchable Labels for MRI



Mladen Barbic¹, Tim D Harris¹, Stephen Dodd², H Douglas Morris³, Alan P Koretsky², Barbara Marcheschi⁴, Alan Huston⁴, and Neil R Dilley⁵

¹Applied Physics and Instrumentation Group, HHMI-Janelia Research Campus, Ashburn, VA, United States, ²Laboratory of Functional and Molecular Imaging, NIH/NINDS, Bethesda, MD, United States, ³NIH Mouse Imaging Facility, NIH/NINDS, Bethesda, MD, United States, ⁴Code 5611, Optical Sciences Division, Naval Research Laboratory, Washington, DC, United States, ⁵Quantum Design, Inc., San Diego, CA, United States

We present the case for the use of magneto-caloric materials as tunable and switchable labels for MRI. Sharp magnetic phase transitions these materials have at typical physiological temperatures and in the presence of the large DC magnetic field values associated with MRI machines make them uniquely suitable for the development of novel MRI contrast agents. We present physical and MRI measurements of a prototypical magneto-caloric material Iron-Rhodium (FeRh) that clearly demonstrate the MR image contrast changes due to the temperature tunable magnetic state of the material in the MRI compatible magnetic field range and physiologically relevant temperature range.

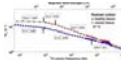
1000



Plasma 24

The T₁-Dispersion Curve as a Biomarker of Colorectal Cancer

Vasileios Zampetoulas¹, Lionel M. Broche¹, Graeme I. Murray², and David J. Lurie¹



¹Aberdeen Biomedical Imaging Centre, School of Medicine, Medical Sciences & Nutrition, University of Aberdeen, AB25 2ZD, Scotland, United Kingdom, ²Department of Pathology, University of Aberdeen, AB25 2ZD, Scotland, United Kingdom

A graph of T₁ versus applied magnetic field, obtained via Fast Field-Cycling (FFC) NMR relaxometry, can be used as a diagnostic tool thanks to the information it provides about molecular dynamics. In this work, FFC NMR relaxometry, extended to magnetic fields below 17 μT, was used to investigate new biomarkers of colorectal cancer. The acquired results indicated that there were significant differences in the molecular motions with correlation times 0.1-10 ms and 0.5-1.4 μs between the healthy and cancer tissues examined, showing great potential for diagnosis, staging and monitoring response to treatment.

1001

Plasma 25

Detecting regional changes in brain tissue quantitative T₁ values due to hydration status

Sofia Chavez^{1,2}



¹Centre for Addiction and Mental Health (CAMH), Toronto, ON, Canada, ²Psychiatry, University of Toronto, Toronto, ON, Canada

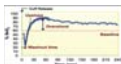
Volumetric/morphometric changes in brain structures are often investigated as markers for disease or drug-induced effects. Brain tissue has been shown to shrink during mild dehydration which is not typically controlled for in MRI studies thus potentially confounding the results. Quantitative T₁ is expected to change in response to changes in water content of tissue. Here, we show for the first time, that T₁ maps, generated as we suggest, can capture regional water shifts that result from changes in hydration status. These can be used to control for water shifts in volumetric/morphometric studies and may aid in the interpretation of results.

1002

Plasma 26

In vivo whole-blood T₂ versus HbO₂ calibration by modulating blood oxygenation level in the femoral vein through intermittent cuff occlusion

Michael C Langham¹, Ana E Rodríguez-Soto¹, Nadav Schwartz², and Felix W Wehrli¹



¹Radiology, University of Pennsylvania, Philadelphia, PA, United States, ²Obstetrics and Gynecology, University of Pennsylvania, Philadelphia, PA, United States

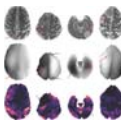
The relationship between whole-blood T₂ and blood hemoglobin oxygen saturation (HbO₂) can be modeled as $\frac{1}{T_2} = \frac{1}{T_{20}} + K(1 - HbO_2)^2$, where K and T₂₀ are determined empirically in vitro. The feasibility of estimating K and T₂₀ in vivo is investigated with T₂-prepared bSSFP at 1.5T in the superficial femoral vein (SFV) with intermittent cuff occlusion. In this manner a range of HbO₂ were achieved allowing quantification of venous oxygen saturation via MR susceptometry, a method that had been validated rigorously against blood gas analysis. Initial result (K=19.6Hz, T₂₀=185ms) is lower than the literature value (24.6Hz, 254ms) but not unexpected because transient bSSFP signal is acquired while disturbing the T₂-prepared magnetization.

1003

Plasma 27

Visualizing local mechanical properties of agar phantoms and meningioma patients using magnetic resonance rheology

Sebastian Theilenberg¹, Jakob Bindl¹, Anna-Lisa Kofahl¹, Carsten Urbach¹, and Karl Maier¹



¹Helmholtz-Institut für Strahlen- und Kernphysik, University of Bonn, Bonn, Germany

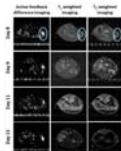
Magnetic resonance rheology is a novel method to create an imaging contrast based on the mechanical properties of brain tissue. It is based on a short fall of the head that creates a broadband excitation of the tissue. The resulting deflections of the tissue elements are depicted using motion sensitive phase imaging. This contribution presents measurements on agar phantoms as well as four meningioma patients to show the feasibility of the method to depict local alterations of the mechanical properties of the investigated material.

1004

Plasma 28

Early Cancer Detection Using Paramagnetic Liposome by a Novel Contrast Mechanism with Active-feedback Magnetic Resonance Imaging

Sayoni Ray¹, Chao-Hsiung Hsu², Zhao Li¹, Fang-Chu Lin¹, Ying-Chih Lin², and Yung-Ya Lin¹

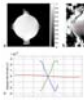


¹DEPARTMENT OF CHEMISTRY AND BIOCHEMISTRY, University Of California, Los Angeles, Los Angeles, CA, United States, ²Department of Chemistry, National Taiwan University, Taiwan

The detection of early tumors requires creating the contrast between healthy and tumor tissues that share a common morphology, making it difficult to distinguish them by relaxation-based MRI technique. Here we have exploited the small magnetic differences between the healthy and tumor tissues to develop a detection technique of early tumors using theranostic nanoparticle paramagnetic (Gd) liposome along with continuous wave (CW) irradiation in the presence of the feedback magnetic field from an active-feedback electronic device for *in vivo* subcutaneous glioblastoma multiforme mouse models and obtained significantly superior contrast compared to the conventional MRI technique, in agreement with spin-dynamics simulations.

1005

Plasma 29



Analysis of magnetohydrodynamic effects in current injection induced magnetic flux density images at very high magnetic fields

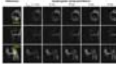
Atul S Minhas¹, Munish Chauhan², and Rosalind J Sadleir²

¹Centre for Pre-clinical Imaging, Department of Cellular and Molecular Physiology, University of Liverpool, Liverpool, United Kingdom, ²School of Biological and Health Systems Engineering, Arizona State University, Tempe, AZ, United States

Magnetic resonance imaging based electrical conductivity imaging of biological tissues could be highly challenging at magnetic fields of the order of 18.8T. We could see significant magnetohydrodynamic (MHD) effects in low viscosity materials at such fields. In this study, we investigated these effects using saline and agarose phantoms and explained the MHD mechanism using a fluid flow model coupled with electromagnetic field equations. Experimental and simulation results showed a correlation between the higher magnetic field and velocity. This relation changed from exponential to linear as the viscosity of material increased. The velocity was negligible for highly viscous materials such as agarose.

1006

Plasma 30



Quadrupolar jump-and-return sequence for sodium knee MRI at 7 tesla

Jae Seung Lee¹, Ding Xia¹, and Ravinder Regatte¹

¹Radiology, New York University, New York, NY, United States

Glycosaminoglycans (GAGs) is an important biomarker for the diseases related to the degradation of cartilage tissues. The GAG content in cartilage tissue is known to be well correlated with the sodium concentration. In addition, the collagenous extracellular matrices of cartilage tissues provide sodium ions with ordered environments. Recently, the so-called quadrupolar jump-and-return (QJR) sequence has been developed, which can selectively detect sodium ions in ordered environments. In this work, we demonstrate the feasibility of the QJR sequence for *in vivo* knee MRI by assessing its performance on the contrast modification to cartilage tissues and fluid.

Electronic Power Pitch Poster

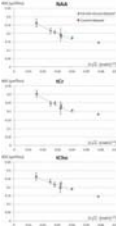
Poster: Cutting Edge Diffusion

Exhibition Hall

Thursday 14:00 - 15:00

1082

Plasma 1



Approaching free intracellular diffusion by diffusion-weighted MRS at ultra-short time scales: initial results in the rodent brain using a 1.5 T/m gradient

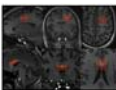
Clémence Ligneul¹, Marco Palombo¹, Julien Flament², and Julien Valette¹

¹Molecular Imaging Research Center (MIRcen), Commissariat à l'Energie Atomique, Fontenay-aux-Roses, France, ²UMS 27, INSERM, Fontenay-aux-Roses, France

At ultra-short time scales, intracellular metabolites are expected to experience less restriction, so that their apparent diffusion coefficient (ADC) as measured by diffusion-weighted MRS should approach the free intracellular diffusivity in a manner which depends on small microstructural features. In this work we use a unique gradient insert capable of reaching 1.5 T/m to measure metabolite ADC in the rat brain up to 665 Hz using oscillating gradients (corresponding to 0.21-ms diffusion time in the Mitra limit), in order to approach and estimate free intracellular diffusion.

1083

Plasma 2



Accurate estimation of intra-axonal diffusivity and anisotropy of NAA in humans at 7T

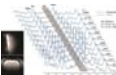
Henrik Lundell¹, Carson Ingo², Tim Bjørn Dyrby^{1,3}, and Itamar Ronen⁴

¹Danish Research Centre for Magnetic Resonance, Centre for Functional and Diagnostic Imaging and Research, Copenhagen University Hospital Hvidovre, Copenhagen, Denmark, ²Department of Physical Therapy and Human Movement Sciences, Northwestern University, Chicago, IL, United States, ³Department of Applied Mathematics and Computer Science, Technical University of Denmark, Kongens Lyngby, Denmark, ⁴C. J. Gorter Center for High Field MRI, Department of Radiology, Leiden University Medical Center, Leiden, Denmark

Diffusion weighted spectroscopy offers a unique probe for tissue microstructure and recent studies demonstrate NAA diffusivity as an independent marker of axonal health. In this study we address the problem of macroscopic dispersion of fiber directions and suggest the use of high angular gradient resolution and powder averaging as an experimentally inexpensive and accurate way to solve this problem. We explore the limits of this approach in simulations and in experiments on humans at 7T.

1084

Plasma 3



Glutamate diffusion at high b-values in the rat brain *in vivo* under light and deep anesthesia conditions

Xi Chen¹, Siddhartha Muktan Tamang¹, Fei Du¹, and Dost Ongur¹

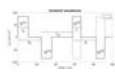
¹McLean Hospital, Belmont, MA, United States

Magnetic resonance techniques are developed to measure brain glutamate (Glu) concentrations but still not able to detect synaptic Glu release. In the currently study, in vivo diffusion-weighted MRS using low to very high b-values was performed on rat brain prefrontal cortex under both light and deep anesthesia conditions. Significant Glu diffusion and concentration changes were observed under different anesthesia levels in the absence of similar changes in NAA or creatine. The slower diffusion and lower concentration under deep anesthesia may reflect more Glu packed into synaptic vesicles with reduced mobility and NMR visibility.

1085



Plasma 4



Bias in the apparent exchange rate measurements: insight from numerical simulations

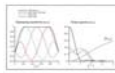
Patricia Ulloa¹, Vincent Methot¹, and Martin A. Koch¹

¹University of Lübeck, Lübeck, Germany

Using double diffusion encoding it is possible to acquire microstructural and water exchange information. Here, simulations are used to study how restriction effects influence apparent exchange measurements. The simulations indicate that at the chosen experimental parameters the restriction effect can be considerable for large pores and small mixing times, τ_m . In typical exchange rate experiments using clinical MR systems with $\tau_m > 40$ ms, the restriction effect can probably be neglected if pores are small.

1086

Plasma 5



Microscopic anisotropy with spectrally modulated q-space trajectory encoding

Henrik Lundell¹, Markus Nilsson², Tim Bjørn Dyrby^{1,3}, Geoff JM Parker^{4,5}, Penny L Hubbard Cristinacce⁴, Fenglei Zhou⁴, Daniel Topgaard⁶, and Samo Lasic^{1,7}

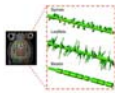
¹Danish Research Centre for Magnetic Resonance, Centre for Functional and Diagnostic Imaging and Research, Copenhagen University Hospital Hvidovre, Hvidovre, Denmark, ²Clinical Sciences Lund, Radiology, Lund University, Lund, Sweden, ³4. Department of Applied Mathematics and Computer Science, Technical University of Denmark, Kongens Lyngby, Denmark, ⁴Centre for Imaging Sciences, The University of Manchester, Manchester, United Kingdom, ⁵Bioxydyn Limited, Manchester, United Kingdom, ⁶Division of Physical Chemistry, Department of Chemistry, Lund University, Lund, Sweden, ⁷CR Development AB, Lund, Sweden

Multi-dimensional diffusion encoding can, in contrast to conventional diffusion encoding, disambiguate between isotropic and anisotropic diffusional variance in multicompartments systems. This is done by varying the shape of the encoding tensor, i.e. going from measuring one projection of the diffusion tensors to measuring the trace of the diffusion tensors. Additional morphological features, such as the sizes of cells, are reflected in the diffusion spectrum. In this study we combine encoding tensors with varying spectral content and shape. This augmented protocol demonstrates distinctively different levels of microscopic fractional anisotropy (μ FA) and time-dependent diffusion in phantoms and in white matter, cerebral cortex, and cerebellar cortex in a fixed monkey brain.

1087



Plasma 6



Can we detect the effect of spines, leaflets and beads on the diffusion of brain intracellular metabolites? A confrontation between high b-values and high-frequencies diffusion-weighted MRS in the mouse brain in vivo.

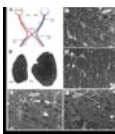
Marco Palombo¹, Clemence Ligneul¹, Edwin Hernandez-Garzon¹, and Julien Valette¹

¹Molecular Imaging Research Center (MIRCen), Commissariat à l'Energie Atomique, Fontenay-aux-Roses, France

Prior models used to clarify which aspects of tissue microstructure mostly affect intracellular diffusion and corresponding diffusion-weighted magnetic resonance signal have focused on relatively simple geometrical descriptions of the cellular microenvironment (spheres, randomly oriented cylinders, etc...), neglecting finer morphological details which may have an important role. Neuritis may exhibit beading; some types of neurons present high density of spines; and astrocytes and macroglial cells processes present leaflets, which may all slow impact the diffusion process. Here we use numerical simulations to interpret metabolites diffusion-weighted MRS data in the mouse brain in terms of such fine secondary structures.

1088

Plasma 7



Diffusion MRI of axonal degeneration in areas of fiber crossing: Histological correspondence.

Luis Concha¹, Jorge Larriva-Sahd¹, Gilberto Rojas-Vite¹, Ramsés Noguez-Imm¹, Ricardo Coronado-Leija², Alonso Ramírez-Manzanares², and José Luis Marroquín²

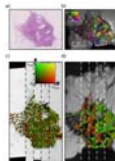
¹Institute of Neurobiology, Universidad Nacional Autónoma de México, Queretaro, Mexico, ²Computer Science, Centro de Investigación en Matemáticas, Guanajuato, Mexico

The tensor model has been widely used to infer characteristics of white matter through diffusion MRI. Unfortunately, this model does not provide reliable information about crossing fiber regions. Several models have been proposed that seem to overcome the limitations of the tensor. However, biological interpretations of such models are limited by the lack of histological conformation. Using an animal model of axonal degeneration, we compare histology to data derived from two approaches (CSD and multi-tensor), in an effort to provide validation of metrics that can bring substantial and clinically useful information about crossing fiber regions.

1089



Plasma 8



Diffusion anisotropy in breast cancer tissue corresponds to spatial patterns of collagen alignment from structure tensor analysis of histology

Colleen Bailey¹, Francesco Grussu², Bernard Siow^{3,4}, Thomy Mertzaniidou¹, John H Hipwell¹, Julie Owen⁵, Patrycja Gazinska⁵, Sarah E Pinder⁵, Daniel C Alexander¹, David J Hawkes¹, and Eleftheria Panagiotaki¹

¹Centre for Medical Image Computing, University College London, London, United Kingdom, ²Institute of Neurology, University College London, London, United Kingdom, ³Centre for Advanced Biomedical Imaging, University College London, London, United Kingdom, ⁴Imaging, Francis Crick Institute, London, United Kingdom, ⁵Breast Research Pathology, King's College London and Guy's Hospital, London, United Kingdom

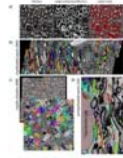
Directional and anisotropy measures from a diffusion model composed of VERDICT compartments were compared with directional and anisotropy measures from structure tensor analysis of registered histology images. A significant positive correlation was found between the direction of the Zeppelin component of the diffusion model (assumed to represent the extracellular space) and the predominant direction of the structure tensor from the stroma, where the primary feature is aligned collagen. The correlation of anisotropy measures was weak, which may be due to difficulties in detecting alignment in regions with densely-packed collagen, which have nearly uniform intensity on H&E staining.

1090



Plasma 9

[A 3D electron microscopy segmentation pipeline for hyper-realistic diffusion simulations](#)
Michiel Kleinnijenhuis¹, Errin Johnson², Jeroen Mollink^{1,3}, Saad Jbabdi¹, and Karla Miller¹



¹Oxford Centre for Functional MRI of the Brain, University of Oxford, Oxford, United Kingdom, ²Sir William Dunn School of Pathology, University of Oxford, Oxford, United Kingdom, ³Department of Anatomy, Donders Institute for Brain, Cognition & Behaviour, Radboud University Medical Center, Nijmegen, Netherlands

Simulations of the diffusion signal can shed light on how the MR signal is generated from particular tissue microstructure. In our approach we use microscopy data to generate a realistic ground truth for investigating diffusion properties. We have developed a method to automatically segment large volumes of 3D electron microscopy data into individual axons for diffusion simulations. From these segmentations, we can also derive benchmark tissue microstructure characteristics such as axonal diameter, g-ratio and other compartment properties.

1091

Plasma 10



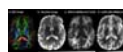
[Rotationally invariant mapping of microstructural and orientational neuronal tissue parameters in human brain](#)
Dmitry S Novikov¹, Jelle Veraart¹, Ileana O Jelescu¹, and Els Fieremans¹

¹Radiology, NYU School of Medicine, New York, NY, United States

We develop a general framework for estimating orientational and microstructural parameters of neurites. By employing a set of rotational invariants, we analytically reveal the nontrivial topology of the parameter estimation landscape, showing that multiple branches of parameters describe the measurement almost equally well, with only one of them corresponding to the biophysical reality. A comprehensive acquisition shows that the branch choice differs for white and for gray matter. We reveal hidden degeneracies in MRI parameter estimation for neuronal tissue, provide microstructural and orientational maps in the whole brain without constraints or priors, and assess commonly used parameter constraints.

1092

Plasma 11



[Isotropic Diffusion Weighted MRI \(IDWI\) – a novel, efficient clinical method for quantifying orientationally-averaged features of water diffusion in tissues](#)

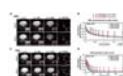
Alexandru Vlad Avram¹, Joelle Sarlis², Elizabeth Hutchinson³, and Peter Basser³

¹NIBIB, National Institutes of Health, Bethesda, MD, United States, ²NINDS, National Institutes of Health, Bethesda, MD, United States, ³NICHD, National Institutes of Health, Bethesda, MD, United States

We propose a novel, efficient diffusion method, called isotropic diffusion weighted MRI (IDWI), for measuring orientationally-averaged properties of tissue water diffusion, free from modulations due to anisotropy. Using efficient diffusion gradient sampling schemes, IDWI rapidly and accurately quantifies the mean apparent diffusion coefficient (mADC) over a wide range of b-values, along with other important rotation-invariant intrinsic microstructural parameters, such as the mean t-kurtosis. The ability to efficiently and effectively remove modulations due to anisotropy in images with high-b values may improve existing diffusion MRI techniques and spur the development and clinical translation of new methods with improved biological specificity.

1093

Plasma 12



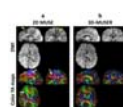
[Diffusion MRI differentiated acute inflammation from axonal injury but missed axonal loss](#)
Tsen-Hsuan (Abby) Lin¹, Michael Wallendorf², Peng Sun¹, and Sheng-Kwei Song^{1,3,4}

¹Radiology, Washington University School of Medicine, St. Louis, MO, United States, ²Biostatistics, Washington University School of Medicine, St. Louis, MO, United States, ³The Hope Center for Neurological Disorders, Washington University School of Medicine, St. Louis, MO, United States, ⁴Biomedical Engineering, Washington University in St. Louis, St. Louis, MO

Diffusion MRI with higher b-values and custom-designed diffusion schemes are critical to identify subtle and coexisting pathology in CNS. In the current study, we employed single-axial high-b diffusion-weighted imaging (DWI) and low-b diffusion basis spectrum imaging (DBSI) to assess mouse optic nerve crush acutely. The results suggested coexisting CNS pathology affected apparent diffusion coefficient (ADC), and low-b DBSI was able to reflect axon and myelin integrity as well as inflammatory edema and cellularity even before histological detection. DBSI-detected axon volume correlated with axonal loss negatively, suggesting cytotoxic-edema-associated axonal swelling might mask axonal loss acutely.

1094

Plasma 13



[Three-Dimensional Multiplexed Sensitivity Encoding and Reconstruction \(3D-MUSER\): 3D Phase Correction for 3D Multi-shot DWI](#)
Hing-Chiu Chang¹, Edward S. Hui^{1,2}, Xiaoxi Liu¹, Pui-Wai Chiu¹, and Nan-kuei Chen^{3,4}

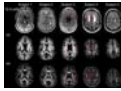
¹Department of Diagnostic Radiology, The University of Hong Kong, Hong Kong, Hong Kong, ²The State Key Laboratory of Brain and Cognitive Sciences, The University of Hong Kong, Hong Kong, ³Department of Biomedical Engineering, University of Arizona, Tucson, AZ, United States, ⁴Brain Imaging and Analysis Center, Duke University Medical Center, Durham, NC, United States

3D interleaved DW-EPI with 2D multiplexed sensitivity encoding has been shown useful in achieving submillimeter DTI. Similar to other 3D DTI techniques, 2D phase variation is only considered in eliminating aliasing artifacts, thereby limiting feasible slab thickness. 3D phase correction is a potential strategy to significantly improve the image quality and feasible slab thickness of 3D DTI. To enable 3D phase correction, we develop a new reconstruction algorithm, and implement an EVI-based navigator echo for direct 3D phase measurement. Quantitative results show that the proposed algorithm can effectively eliminate aliasing artifacts and signal corruptions due to 3D inter-shot phase variations.

1095



Plasma 14



Visualizing Axonal Damage in Multiple Sclerosis Using Double Diffusion Encoding MRI in a Clinical Setting

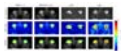
Grant Kaijuin Yang^{1,2}, Qiyan Tian^{1,2}, Christoph Leuze², Max Wintermark², and Jennifer McNab²

¹Electrical Engineering, Stanford University, Stanford, CA, United States, ²Radiology, Stanford University, Stanford, CA, United States

Double diffusion encoding (DDE) measurements of microscopic anisotropy show promise as a method of assessing neurodegeneration. Unfortunately, DDE has yet to be demonstrated in a clinical setting due to constraints in SNR and scan time. Here, we used an optimized gradient orientation scheme to show the first DDE measurements of microscopic anisotropy in multiple sclerosis (MS) patients. Five MS patients were scanned using a DDE sequence optimized to run in five minutes. The microscopic anisotropy maps show improved visualization of axonal damage compared to fractional anisotropy (FA) and may provide additional insight into changes in tissue microstructure.

1096

Plasma 15



Accelerated Diffusion-Sensitized MR Imaging of the Eye and Orbit at 3.0 T and 7.0 T free of Geometric Distortions Using a Combined RARE-EPI Acquisition Technique

Katharina Paul¹, Helmar Waiczies², André Kuehne², Till Huelnhagen¹, Eva Oberacker¹, Oliver Stachs³, and Thoralf Niendorf^{1,2,4}

¹Berlin Ultrahigh Field Facility (B.U.F.F.), Max Delbrueck Center for Molecular Medicine in the Helmholtz Association, Berlin, Germany,

²MRI.TOOLS GmbH, Berlin, Germany, ³Department of Ophthalmology, University of Rostock, Rostock, Germany, ⁴Experimental and Clinical Research Center (ECRC), a joint cooperation between the Charité Medical Faculty and the Max Delbrueck Center for Molecular Medicine in the Helmholtz Association, Berlin, Germany

Diffusion-weighted imaging of the eye and orbit is an emerging MRI application to provide guidance during diagnostic assessment and treatment of ophthalmological diseases. RARE based diffusion-sensitized imaging (ms-RARE) provides images free of geometric distortions. Yet imaging speed, RF power deposition and artifacts by involuntary eye motion remain a concern. Combined acquisition techniques (CAT) merging RARE and EPI within one echo train offer the possibility to shorten acquisition times and relax specific absorption rate constraints. This study examines the applicability of RARE-EPI CAT for diffusion-sensitized imaging of the eye and orbit free of geometric distortions at 3.0 T and 7.0 T.

Electronic Power Pitch Poster

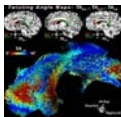
Poster: Emerging Neuroimaging Techniques

Exhibition Hall

Thursday 14:00 - 15:00

1097

Plasma 16



Characterization of White Matter Tortuosity using High-Resolution gSlider-SMS Diffusion Imaging

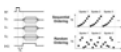
Choukri Mekkaoui¹, Marcel P Jackowski², Kawin Setsompop¹, Qiuyun Fan¹, Ned A Ohringer¹, William J Kostis³, Timothy G Reese¹, Alexandra J Golby⁴, and Susie Y Huang¹

¹Harvard Medical School - Massachusetts General Hospital, Boston, MA, United States, ²University of São Paulo, São Paulo, Brazil, ³Rutgers Robert Wood Johnson Medical School, New Brunswick, NJ, United States, ⁴Brigham and Women's Hospital, Harvard Medical, Boston, MA, United States

Conventional tractography excludes acute directional changes. We define these acute changes as tortuosity and use it to characterize gray-white matter boundaries, as well as quantify deformation and remodeling in pathologic states. Five healthy volunteers and a brain tumor patient were scanned using the gSlider-SMS technique. Diffusion data was processed to create 3D contiguous ribbons that characterize tortuosity. Twisting angles of the 3D ribbons were compared within and between subjects, and were visually and statistically consistent. This highly informative tractographic method could be applied to evaluate tumor infiltration and adjacent brain compression, or traumatic brain injury.

1098

Plasma 17



In Vivo Characterization of an Ultrashort-T2 Component in the Brain Reveals a Chemical Shift

Peder Eric Zufall Larson¹, Tanguy Boucneau², Shuyu Tang¹, Misung Han¹, Peng Cao¹, and Roland G Henry³

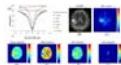
¹Radiology and Biomedical Imaging, University of California - San Francisco, San Francisco, CA, United States, ²Ecole normale supérieure de Cachan, Paris, France, ³Neurology, University of California - San Francisco, San Francisco, CA, United States

A new approach for direct measurements of myelin content is to image an sub-millisecond T2 component in the brain, likely associated with myelin membrane protons. This study characterized this ultrashort-T2 component across the whole brain using a novel relaxometry approach at ultrashort echo times (UTEs). This component had an estimated T2* ~ 0.6-1.0 ms at 3T and ~0.2-0.4 ms at 7T, as well as an approximately -3.2 ppm frequency shift from water that has never been measured before in vivo. This verifies that the ultrashort-T2 component primarily arises from methylene protons, as in the myelin phospholipid membranes.

1099



Plasma 18



Improved Differentiation of Low- and High-Grade Gliomas by APT Contrast Fitted from Z-Spectrum

Jiaxuan Zhang^{1,2}, Rongwen Tain^{1,3}, Xiaohong Joe Zhou^{1,4}, Wenzhen Zhu², and Kejia Cai^{1,5}

¹Center for MR Research, University of Illinois at Chicago, Chicago, IL, United States, ²Department of Radiology, Tongji Hospital, Huazhong

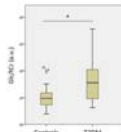
University of Science and Technology, Wuhan, People's Republic of China, ³Department of Radiology, University of Illinois at Chicago, Chicago, IL, United States, ⁴Departments of Radiology, Neurosurgery, and Bioengineering, University of Illinois at Chicago, Chicago, IL, United States,

⁵Departments of Radiology and Bioengineering, University of Illinois at Chicago, Chicago, IL, United States

Preoperative grading is important for treatment planning in glioma patients. Amide proton transfer (APT)-weighted imaging is helpful in grading since it reflects metabolic changes associated with mobile proteins and peptides. However, the conventional APT based on asymmetrical analysis receives contaminations from semi-solid magnetization transfer asymmetry and nuclear overhauser enhancement effects. Multi-component Z-spectral fitting for the separated quantification of APT can help to remove those contaminations. In this study, we performed such fitting on Z-spectral data from glioma patients. We found that fitted APT provided higher power in differentiating low- and high- grade gliomas compared to the conventional APT quantification.

1100

Plasma 19



3T 1H PRESS (TE 68 ms) reveals elevated cerebral glucose in patients with diabetes mellitus type 2, which is associated with fasting blood glucose

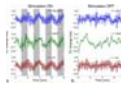
Frank C.G. van Bussel¹, Tamar M van Veenendaal¹, Miranda T Schram², Coen D.A. Stehouwer², Walter H Backes¹, and Jacobus F.A. Jansen¹

¹Radiology, Maastricht University Medical Center, Maastricht, Netherlands, ²Internal Medicine, Maastricht University Medical Center, Maastricht, Netherlands

A standard 1H PRESS sequence, with a TE of 68 ms, acquired at 3T is applied to investigate differences in cerebral glucose concentrations in type 2 diabetes mellitus (T2DM) compared with controls with normal glucose metabolism. Subjects with T2DM (n=38) display an increased cerebral glucose level compared to controls (n=38). These levels are also associated with two blood glucose measures, fasting blood glucose (FBG) and glycated hemoglobin (HbA1c).

1101

Plasma 20



Towards opto-fMRS: Ultra high field MRS measurement of T2* changes due to optogenetic stimulation

Jamie Near^{1,2}, Dan Madularu^{1,2}, Jennifer Robinson³, Chathura Kumaragamage⁴, Axel Mathieu², Sylvain Williams^{1,2}, M Natasha Rajah^{1,2}, and Uzay Emir⁵

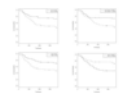
¹Department of Psychiatry, McGill University, Montreal, QC, Canada, ²Centre d'Imagerie Cérébrale, Douglas Mental Health University Institute, Montreal, QC, Canada, ³Integrated Program in Neuroscience, McGill University, Montreal, QC, Canada, ⁴Biomedical Engineering, McGill University, Montreal, QC, Canada, ⁵Nuffield Department of Clinical Neurosciences, University of Oxford, Oxford, United Kingdom

Combining optogenetics with fMRI/fMRS (opto-fMRI/opto-fMRS) offers the unique potential to study the whole brain functional or neurochemical effects of stimulating specific neuronal populations within a given brain region. In this study, we investigated the BOLD functional changes and neurochemical changes resulting from optogenetic stimulation of glutamatergic or GABAergic neurons in the medial septum. Stimulation of both glutamatergic and GABAergic neurons in the medial septum resulted in prominent bold activation within the hippocampus, and in other regions. This study represents a unique imaging investigation into the functional response to stimulation of multiple distinct neuronal populations within a single brain region.

1102



Plasma 21



Glycine, a marker of survival in paediatric brain tumours measured with non-invasive Magnetic Resonance Spectroscopy: A five-year survival analysis.

Ben Babourina-Brooks¹, Sarah Kohe¹, Simrandip K Gill¹, Martin Wilson², Lesley Macpherson³, Nigel P Davies⁴, and Andrew C Peet^{1,3}

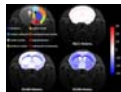
¹University of Birmingham, Birmingham, United Kingdom, ²Birmingham University Imaging Centre, University of Birmingham, Birmingham, United Kingdom, ³Birmingham Children's Hospital NHS Foundation Trust, Birmingham, United Kingdom, ⁴Imaging & Medical Physics, University Hospitals Birmingham NHS Foundation Trust, Birmingham, United Kingdom

Brain tumours have a high mortality rate and are the most common solid tumour of childhood. MRS is a non-invasive imaging technique that measures tumour metabolites which can provide prognostic information to aid clinical management. The metabolite glycine is associated with proliferation and tumorigenesis through the one-carbon metabolic cycle. Glycine concentration has been shown to increase with tumour grade using short echo time MRS at 1.5T, however has not been assessed as a survival marker. This study investigates glycine as a marker of survival in paediatric brain tumours and assesses its added value compared to other established metabolite survival markers.

1103



Plasma 22



About the complementarity of gluCEST and 1H-MRS for the study of neurodegenerative diseases using animal models

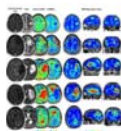
Jérémy Pépin¹, Clémence Ligneul¹, Julien Valette¹, Emmanuel Brouillet¹, and Julien Flament^{1,2}

¹Molecular Imaging Research Center (MIRCe), Commissariat à l'Energie Atomique (CEA), Fontenay-aux-Roses, France, ²UMS27, INSERM, Fontenay-aux-Roses, France

Animal models of neurodegenerative diseases are useful tools to investigate neurodegenerative diseases. However, there is often a wide variety of described models for a same pathology, each model exhibiting its own characteristics. In this work, we used two mouse models of Huntington's disease exhibiting very different alterations. Using a protocol combining gluCEST imaging and 1H-MRS, we showed that, while gluCEST may evidence alterations in unexpected brain regions, it may also be blind to disease process in certain situations where glutamate levels are preserved. This highlights the complementarity of both methods to identify relevant biomarkers of the pathology.

1104

Plasma 23



A "Glycolytic Index" for quantifying abnormal metabolism in human gliomas using multi-echo amine chemical exchange saturation transfer spin- and-gradient echo echoplanar imaging (ME-aCEST-SAGE-EPI) at 3T

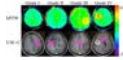
Robert J Harris¹, Kevin Leu, Timothy F Cloughesy, Whitney B Pope, Phioanh L Nghiemphu, Albert Lai, Linda M Liau, and Benjamin M Ellingson²

¹University of California Los Angeles, Los Angeles, CA, United States, ²Radiological Sciences, University of California Los Angeles, Los Angeles, CA, United States

Abnormal metabolism is a hallmark of cancer. The current study demonstrates use of a novel imaging technique for fast, simultaneous pH- and hypoxia-weighted images using multi-echo amine chemical exchange saturation transfer spin-and-gradient-echo echoplanar imaging (ME-aCEST-SAGE-EPI). From these data, we demonstrate use of a "glycolytic index", quantified as the ratio of relative acidity to metabolic rate of oxygen, in estimating metabolically active tumor tissue in 15 patients with gliomas. The glycolytic index showed unique heterogeneous metabolic contrast within the tumor region, and was able to easily stratify tumor from healthy tissue when compared with other imaging techniques.

1105

Plasma 24



Qualitative and quantitative analysis of amide proton transfer-weighted MR images at 3 Tesla of adult gliomas

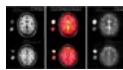
Xianlong Wang¹, Hao Yu², Shanshan Jiang², Yu Wang³, Yanyu Wang², Ge Zhang⁴, Chunxiu Jiang², Guodong Song⁵, Yi Zhang⁶, Hye-Young Heo⁶, Jinyuan Zhou⁶, and Zhibo Wen²

¹Radiology, Zhujiang Hospital of Southern Medical University, Guangzhou, People's Republic of China, ²Radiology, Zhujiang Hospital of Southern Medical University, ³Pathology, Zhujiang Hospital of Southern Medical University, ⁴Radiology, Hainan General Hospital, ⁵Radiology, Beijing Hospital, ⁶Radiology, Johns Hopkins University

We evaluated the reliability and clinical value of amide proton transfer-weighted (APTW) MR imaging at 3 Tesla in adult gliomas. Fifty-seven patients with primary gliomas were recruited and scanned. Two radiologists evaluated the location and size of the APTW hyperintensity and enhancing areas, and measured the tumor and contralateral normal-appearing white matter (CNAWM) APTW values. The correlation between relative APTW (rAPTW) values and pathologic grades was calculated. Results showed APTW analysis had good reliability. APTW images almost showed the same compared with T1-weighted contrast-enhancing (T1W+C) images. The tumor rAPTW values had a strong positive correlation with pathologic grades.

1106

Plasma 25



Cerebral Sodium (²³Na) Magnetic Resonance Imaging in Patients with Migraine

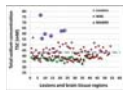
Melissa M Ong¹, Alexander Schmidt¹, Simon Konstandin², Justus Benrath³, Mathias Meyer¹, Lothar R Schad⁴, Stefan O Schoenberg¹, and Stefan Haneder^{1,5}

¹Institute of Clinical Radiology and Nuclear Medicine, University Medical Center Mannheim, University of Heidelberg, Mannheim, Germany, ²University of Bremen, MR-Imaging and Spectroscopy, Faculty 01 (Physics/Electrical Engineering), Bremen, Germany, ³Clinic for Anaesthesiology and Operative Intensive Care, University Medical Center Mannheim, University of Heidelberg, Mannheim, Germany, ⁴Computer Assisted Clinical Medicine, University Medical Center Mannheim, University of Heidelberg, Mannheim, Germany, ⁵Institute of Diagnostic and Interventional Radiology, University Hospital Cologne, Cologne, Germany

To evaluate sodium concentrations in subgroups of patients with clinically manifest migraine, 12 patients underwent a cerebral ²³Na-magnetic resonance imaging examination using a dual-tuned (²³Na/¹H), dedicated head-coil. ²³Na-sequences were reconstructed according to a T1 MP-RAGE, allowing direct cross-referencing of predetermined regions-of-interest (ROI). Significant differences in sodium concentrations could be observed for the white matter and anterior cerebrospinal fluid in patients with and without accompanying aura (p<0.05). These data suggest, that cerebral sodium concentrations may have the potential to differentiate between different subgroups of migraine.

1107

Plasma 26



Differentiating subtypes of multiple sclerosis lesions using sodium MR imaging

Yulin Ge¹, Yongxian Qian, Jean-Christophe Brisset, and Fernando E Boada

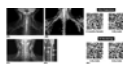
¹New York University School of Medicine, New York, NY, United States

Although conventional 1H MRI is commonly used for diagnosis and monitoring disease progression in multiple sclerosis (MS), it is not specific to pathology and cell vitality, and is limited in differentiating underlying pathology in MS lesions. In this study, using sodium (²³Na) MRI, we demonstrated several subtypes of MS lesions with different sodium concentration changes, which may represent various stages of demyelination and axonal injury. Such information that is not available on conventional imaging may have value in characterize early versus chronic inactive lesions in MS.

1108



Plasma 27



Imaging of the Brachial Plexus using a 3D Dixon-TSE Pulse Sequence with Blood Vessel and CSF Signal Suppression: Preliminary Experience in Children

Barbara Cervantes¹, Amber L. Pokorney², Jan S. Kirschke³, Patricia Cornejo², Jeffrey H. Miller², Dimitrios C. Karampinos¹, and Houchun Harry Hu²

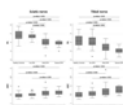
¹Department of Diagnostic and Interventional Radiology, Klinikum rechts der Isar, Technische Universitat Munchen, Munich, Germany, ²Department of Radiology, Phoenix Children's Hospital, Phoenix, AZ, United States, ³Department of Neuroradiology, Klinikum rechts der Isar, Technische Universitat Munchen, Munich, Germany

We demonstrate the clinical feasibility and utility of a 3D Dixon TSE sequence in imaging the brachial plexus nerves in children. The employed high spatial resolution MR Neurography (MRN) technique utilizes a refocusing flip angle train to maximize nerve signal and to suppress cerebrospinal fluid signal. Additionally, a T2-preparation with motion-sensitizing gradients was employed to suppress flowing blood signal and Dixon-based chemical-shift water-fat imaging was used to suppress fat signal in the head, neck, and chest. We illustrate this MRN technique in delineating the brachial plexus nerves and associated pathological conditions in 25 pediatric patients (age range: 6 months-21 years).

1109



Plasma 28



Diffusion-Tensor-Imaging MR-Neurography for the detection of polyneuropathy in Type 1 diabetes

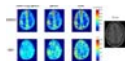
Michael Vaeggemose¹, Mirko Pham², Steffen Ringgaard³, Hatice Tankisi⁴, Niels Ejksjaer¹, Sabine Heiland⁵, Per L. Poulsen⁶, and Henning Andersen¹

¹Dept. of Neurology, Aarhus University Hospital, Aarhus C, Denmark, ²Dept. of Neuroradiology, Würzburg University Hospital, Würzburg, Germany, ³MR Research Centre, Aarhus University Hospital, Aarhus N, Denmark, ⁴Dept. of Neurophysiology, Aarhus University Hospital, Aarhus C, Denmark, ⁵Heidelberg University Hospital, Heidelberg, Germany, ⁶Dept. of Endocrinology, Aarhus University Hospital, Aarhus C, Denmark

Diabetic peripheral neuropathy (DPN) is an irreversible complication that often remains undiagnosed until advanced stages. Thus, to prevent progression of DPN, early diagnosis is important emphasizing the need for more sensitive diagnostic techniques. Diagnosis is based on a neurological examination, nerve conduction studies, and quantitative sensory testing. Magnetic-resonance-neurography (MRN) enables microstructural nerve fascicle imaging of peripheral neuropathies (1–4). In a previous study on patients with severe DPN we found that diffusion-tensor-imaging (DTI) is a reproducible method in detection of DPN (5). Furthermore, DTI-MRN provided a more accurate group separation than by changes based on T2 or proton-density contrast.

1110

Plasma 29



Optimal quantitative mapping of Cerebral Metabolic Rate of Oxygen (CMRO₂) by combining quantitative susceptibility mapping (QSM)-based method and quantitative BOLD (qBOLD)

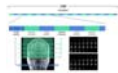
Junghun Cho¹, Youngwook Kee², Pascal Spincemaille², Thanh Nguyen², Jingwei Zhang¹, and Yi Wang^{1,2}

¹Cornell University, Ithaca, NY, United States, ²Weill Cornell Medical College, New York, NY, United States

Current two CMRO₂ mapping methods, QSM-based method and qBOLD, suffer from the issues in their own model assumptions, such as blood flow challenge and linear relationship assumption between cerebral blood volume (CBV) and flow (CBF) in QSM-based method and the high sensitivity to noise and recent one-compartment assumption in qBOLD. We combined these two models with regularization based on that vein blood volume fraction and vein oxygenation are shared, which removes the challenge and linear assumption in QSM method and alleviates the high noise sensitivity and one-compartment assumption issue in qBOLD. The proposed model provided more uniform OEF and CMRO₂.

1111

Plasma 30



Asynchronous Local Analysis of simultaneous BOLD ASL Multislice Acquisition (ALABAMA): Toward Whole-Brain Noninvasive Estimation of Resting-State Neuronal-Vascular Coupling

Vincent Schmithorst¹, Vince Lee¹, and Ashok Panigrahy¹

¹Radiology, Children's Hospital of Pittsburgh of UPMC, Pittsburgh, PA, United States

A method (ALABAMA) for regional estimation of the coupling between R₂^{*} fluctuations and log signal intensity (S₀) (related to R₂^{*}-CBF coupling via a calibration factor) during the resting state is proposed. The method incorporates pseudo-continuous ASL (pCASL) labeling together with simultaneous multi-slice (SMS) and double-echo EPI acquisition for fast temporal resolution. The sequence yields robust positive $\Delta R_2^* - \Delta \ln S_0$ correlations in most resting-state networks, which may then be used to estimate resting-state neuronal-vascular coupling (NVC) with an additional calibration scan. However, negative correlations were found in posterior DMN and central executive network (CEN) regions, possibly reflective of altered flow-metabolism relationships.